Title
Nonlinear vibrational spectroscopy of surfactants at liquid interfaces

Author
Miranda, P.B.

Publication Date
1998-12-14

LBNL-42635

ERNEST ORLANDO LAWRENCE
BERKELEY NATIONAL LABORATORY

Nonlinear Vibrational Spectroscopy of Surfactants at Liquid Interfaces

Paulo B. Miranda

Materials Sciences Division

December 1998

Ph.D. Thesis

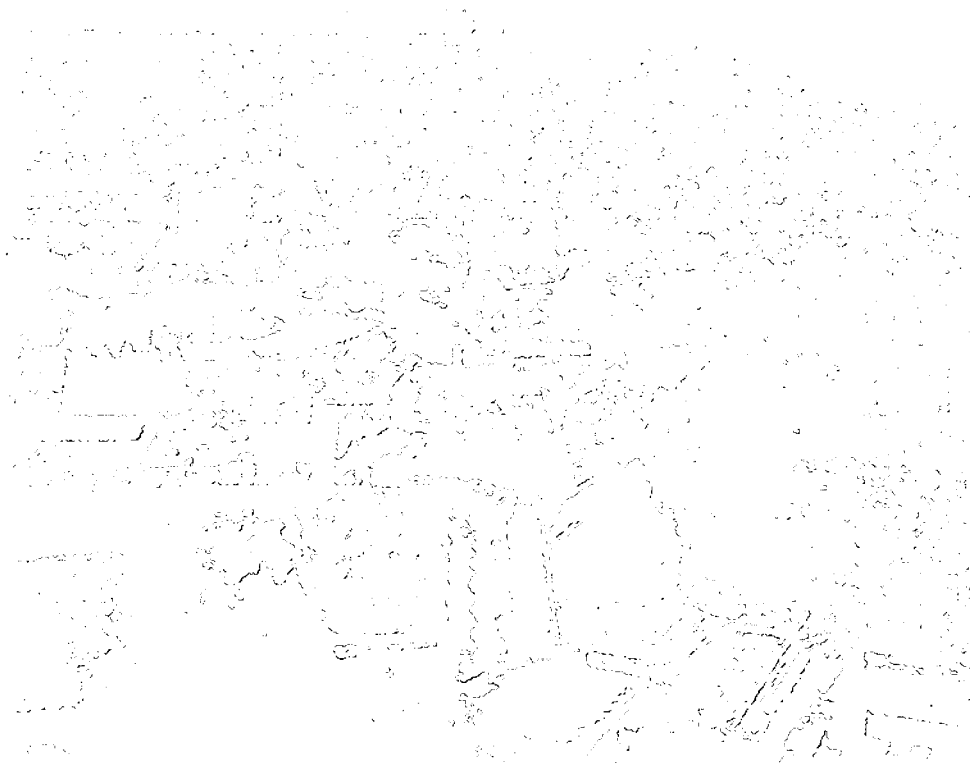

DISCLAIMER

LBNL-42635

Nonlinear Vibrational Spectroscopy of Surfactants at Liquid Interfaces

Paulo Barbeitas Miranda
Ph.D. Thesis

Department of Physics
University of California, Berkeley

and

Materials Sciences Division
Ernest Orlando Lawrence Berkeley National Laboratory
University of California
Berkeley, CA 94720

December 1998

This work was supported by the Director, Office of Energy Research, Office of Basic Energy Sciences, Materials Sciences Division, of the U.S. Department of Energy under Contract No. DE-AC03-76SF00098.

Nonlinear Vibrational Spectroscopy of Surfactants at Liquid Interfaces

by

Paulo Barbeitas Miranda

B.S. (Pontifícia Universidade Católica-RJ, Brazil) 1991
M. A. (University of California, Berkeley) 1994

A dissertation submitted in partial satisfaction of the

requirements for the degree of

Doctor of Philosophy

in

Physics

in the

GRADUATE DIVISION

of the

UNIVERSITY OF CALIFORNIA, BERKELEY

Committee in charge:

Professor Yuen R. Shen, Chair
Professor Daniel S. Chemla
Professor Herbert L. Strauss

Fall 1998

Abstract

Nonlinear Vibrational Spectroscopy of Surfactants at Liquid Interfaces

by

Paulo Barbeitas Miranda

Doctor of Philosophy in Physics

University of California, Berkeley

Professor Yuen Ron Shen, Chair

Surfactants are widely used to modify physical and chemical properties of interfaces. They play an important role in many technological problems. Surfactant monolayers are also of great scientific interest because they are two-dimensional systems that may exhibit a very rich phase transition behavior and can also be considered as a model system for biological interfaces.

In this Thesis, we use a second-order nonlinear optical technique (Sum-Frequency Generation - SFG) to obtain vibrational spectra of surfactant monolayers at liquid/vapor and solid/liquid interfaces. The technique has several advantages: it is intrinsically surface-specific, can be applied to buried interfaces, has submonolayer sensitivity and is remarkably sensitive to the conformational order of surfactant monolayers.

The first part of the Thesis is concerned with surfactant monolayers at the air/water interface (Langmuir films). Surface crystallization of an alcohol Langmuir film and of liquid alkanes are studied and their phase transition behaviors are found to be of different nature, although driven by similar intermolecular interactions. The effect of crystalline order of Langmuir monolayers on the interfacial water structure is also

investigated. It is shown that water forms a well-ordered hydrogen-bonded network underneath an alcohol monolayer, in contrast to a fatty acid monolayer which induces a more disordered structure. In the latter case, ionization of the monolayer becomes more significant with increase of the water pH value, leading to an electric-field-induced ordering of interfacial water molecules. We also show that the orientation and conformation of fairly complicated molecules in a Langmuir monolayer can be completely mapped out using a combination of SFG and second harmonic generation (SHG). For a quantitative analysis of molecular orientation at an interface, local-field corrections must be included.

The second part is a study of self-assembled surfactant monolayers at the solid/liquid interface. It is shown that the conformation of a monolayer adsorbed onto a solid substrate and immersed in a liquid is highly dependent on the monolayer surface density and on the nature of intermolecular interactions in the liquid. Fully packed monolayers are well ordered in any environment due to strong surfactant-surfactant interactions and limited liquid penetration into the monolayer. In contrast, loosely packed monolayers are very sensitive to the liquid environment. Non-polar liquids cause a mild increase in the surfactant conformational disorder. Polar liquids induce more disorder and hydrogen-bonding liquids produce highly disordered conformations due to the hydrophobic effect. When immersed in alkanes, under certain conditions the surfactant chains may become highly ordered due to their interaction with the liquid molecules (chain-chain interaction). In the case of long-chain alcohols, competition between the hydrophobic effect and chain-chain interaction is observed.

Acknowledgments

The results presented in this Thesis are largely fruit of other people's work. To them, I want to express my sincere gratitude. First of all, my advisor Prof. Ron Shen cannot be thanked enough. He has dedicated many hours to teaching and guiding me. From him I learned not only physics but also how to become a researcher. He has been a constant source of help, encouragement and challenge. I will never forget the many times I went to his office puzzled by our results, and he filled me with hope and sharp insights. Many other times I went there proud of some small accomplishment in the research, and he challenged me to get a more complete physical picture, to have a deeper understanding of the problems and to express myself in a clearer way. He has set a great example and challenging standards for efficiency, clarity of thinking and expression that I hope to be able to follow throughout my career.

The next person of great influence on me during my Ph.D was a fellow student and mentor, Quan Du. He thought me how to get things done in the laboratory and to have a critical attitude against other peoples' conjectures. He was also a constant source of challenge to get things done more efficiently and correctly. From him I also learned a lot about cleaning and sample preparation. I am afraid I did not learn everything I should have learned from him.

Other contemporary graduate students and post-docs were also great source of help, support and friendship. Among them, George Sefler gave major contributions to the results of Chapters 3 and 4. Unfortunately we were classmates for only 2 years, before he moved to another department. His help and friendship were certainly missed. The work

contained in Chapter 6 was fruit of an exciting collaboration with Hiroyuki Saijo and Valérie Pflumio. Hiro was the expert chemist from whom I learned most of what I know about surfactants and monolayer preparation. We had great fun together purifying the surfactants he synthesized! Valérie was not only a great help in performing the experiments, but she also helped me learn about polymers and the hydrophobic effect. The work of Chapter 5 was a collaboration with two other students, Xiaowei Zhuang and Doseok Kim. Xiaowei was the real driving force behind it, with her combination of intellect, humor and optimism. She is another great example I hope to follow in the future. Doseok also thought me a lot about nonlinear optics and we had a lot of fun finalizing the OPA setup and building the SFG detection arm.

In addition to those mentioned above, I also benefited from many interesting discussions on life and science with other students, post-docs and visitors. I also borrowed equipment and advice from many of them. I will not be able to name them all, but special thanks goes to Lorenzo Marrucci, Dieter Wilk, Chris Mullin, Dieter Johannsmann, Rodney Chin, Paul Cremer, Xiaofeng Jin, Shen Ye, Minyao Mao, Christian Raduege, Eric Anglaret, Ralf Muenster, Joachim Diener, Xincai Su, Wolfgang Beck and Steve Baldelli. To the new talented students in the group, Seok-Cheol Hong, Xing Wei and John McGuire, I wish them good luck and a successful career. I was supposed to train Xing, but I am afraid I learned more from him than he from me...

I am also indebted to many others for crucial support. I have witnessed three generations of group secretaries: Barbara Gordon, Barbara Iwai and Barbara Srulowitz. I sincerely thank them for their administrative support. Anne Takizawa, Mercy Wang and Donna Sakima, of the Physics Department administrative staff, were extremely important

in the beginning of my Ph.D program, helping me to get settled in Berkeley. They have also been a constant help with administrative issues since then. To the workers in the Machine and Electronics Shop, my sincere gratitude for your immediate assistance in building or fixing equipment, especially to Andy Bocato, George Weber, LeVern Garner and John Davis.

I gratefully acknowledge financial support during the first four years of my Ph.D research by a graduate fellowship from the Brazilian Research Council (CNPQ).

During these long years of hard work, my wife Fernanda has been my source of love, friendship and support. She helped me become a more sociable person and provided us the necessary distractions to keep our social life in good health. She also gave us Amanda, the sunshine of our lives for the last fifteen months. They have my unconditional love.

Finally, the love, support and education I received from my parents during my youth were the foundation of the person I am now. To them, my deepest gratitude. I dedicate this Thesis to my father, Luiz C. M. Miranda. He was my first teacher, from whom I learned to appreciate science and nature.

Table of Contents

Chapter 1. Introduction

In modern science and technology, liquid interfaces are certainly as important as solid surfaces and interfaces. They play a key role in many problems that are intimately connected to our daily life, spanning from physics, chemistry, materials science, and engineering to life science, environment science, and others. For example, the air/water interface is directly involved with environment problems such as acid rain and water pollution.[1] Liquid/liquid interfaces are essential for many biological systems[2,3] while liquid/solid interfaces are highly relevant to such important processes as cleaning, wetting, adhesion, lubrication, etching, corrosion, electrochemical reactions, and oil recovery.[4,5]

The physical and chemical properties of interfaces can be readily modified by adsorption of foreign species. A general class of such adsorbates is the amphiphilic organic molecule. These molecules have two main building blocks: one polar, hydrophilic part called the "head-group" which interacts strongly with water or other hydrophilic materials, and a hydrophobic part, usually consisting of one or more hydrocarbon (or fluorocarbon) chains, or "tails", which interact only weakly with hydrophilic materials. They therefore readily adsorb at an interface between hydrophilic and hydrophobic media to minimize the interfacial free energy. For this reason, these molecules are said to be "surface active" and usually referred to as surfactants.

Surfactant monolayers adsorbed onto solid surfaces may serve as lubricants or corrosion inhibitors,[4,6] or they may be used to modify in a controlled way the surface chemistry of a substrate,[7] with important applications ranging from biology[8] to

microfabrication technology.[9] Surfactant adsorption at the solid/liquid interface has many industrial applications.[6] In the mining industry for example, they are widely used in mineral separation by the flotation method:[4,10] surfactants adsorbed at mineral/aqueous solution interface can modify the wetting behavior of the mineral surface. Foam is generated in a suspension of ground ore in the surfactant solution, and the mineral particles get trapped at the liquid/vapor interface of foam bubbles, leading to effective mineral separation. Surfactant adsorption onto the surface of colloidal particles may affect the colloid stability by modifying interparticle interactions.[11] They are therefore widely used as paint additives or in the cosmetic industry.[6,12] Finally, the properties of surfactant solutions makes them ubiquitous in our daily life as household products such as detergents, fabric softeners, hair conditioners, etc.[5,6] Surfactants at liquid/liquid interfaces are responsible for emulsification[4] and are also considered models for biological systems like cell membranes.[2,3,11] Insoluble surfactant monolayers at the liquid/vapor interface are called Langmuir films. They are model two-dimensional systems that exhibit a very rich phase transition behavior.[13,14] They can also be transferred to solid substrates by the Langmuir-Blodgett technique to form high quality multilayer films with many applications such as sensors[15] or optoelectronic materials.[16]

Because of their extreme importance, the interfacial properties of surfactant systems have been extensively investigated in the literature. Most previous work was, however, concerned with thermodynamic quantities such as adsorption isotherms, [10,17-22] contact angles[18,20,23,24] (wetting measurements), adsorption energies[17,21,22] and surface potentials. [10,17-21] They have provided some insights to the adsorption mechanisms and the structure of adsorbed films. However, these measurements can offer only limited

information about the microscopic structure of the adsorbed surfactant layer. Recently, other techniques that can provide directly more information about the molecular-level structure of surfactant monolayers have been used. For example, neutron reflection,[25-27] X-Ray diffraction,[13,14,28] X-Ray photoelectron spectroscopy,[29] nuclear magnetic resonance,[30,31] infrared spectroscopy,[32-35] surface-enhanced Raman spectroscopy,[36-38] scanning tunneling microscopy,[39,40] atomic force microscopy[41] and the surface force apparatus[39,42-44] have been adopted to study the structure of monolayers or bilayers of many different surfactants. However, most existing surface techniques that employ particle (electron, ion, or atom) scattering or emission require a sample situated in high vacuum and, therefore, are not suitable for use on vapor/liquid interfaces or buried liquid interfaces. On the other hand, optical techniques such as attenuated total reflection spectroscopy,[45] infrared and Raman spectroscopy,[32-35] and ellipsometry[46] have wider applicability, but are not intrinsically surface-specific to allow probing surface molecules with good discrimination against contributions from the bulk. Although all the above techniques start to reveal more detailed microscopic information about surfactants at liquid interfaces, little is still known about the molecular orientation and conformation of adsorbed surfactants. On the theoretical side, however, following recent advances in computer calculations, the field of numerical simulation of surfactants at liquid interfaces has been blooming.[47,48] Comparisons between simulations and experiments are likely to bring significant advances in this field.

In this Thesis we describe our studies of surfactant monolayers at both solid/liquid and liquid/vapor interfaces using the nonlinear optical technique of sum-frequency generation (SFG).[49] As will be described in Chapter 2, this technique allows us to obtain

vibrational spectra of interfaces with negligible contribution from bulk molecules and has the advantages of giving more direct information about conformation of hydrocarbon chains (see Chapter 2). Since the study of surfactant conformation will be the main theme of this Thesis, we shall now explain what we mean by that.

All surfactants studied herein have a polar head-group and one or two hydrophobic alkyl chains attached to it. Figure 1 shows the structure of an alkyl chain in its lowest energy configuration. The chain is composed of n CH_2 groups interconnected by tetrahedral bonds in a planar zigzag configuration and terminated by a CH_3 group. Each bond joining two adjacent CH_2 groups has a torsional potential of the form shown schematically in Figure 2. We see that there is an absolute minimum for a torsional angle equal to zero, corresponding to the adjacent CH_2 groups pointing in opposite directions. If all bonds are in this potential minimum, the resulting molecular configuration will be the one shown in Figure 1 and it is called the *all-trans* conformation. However, if one of the bonds is in a secondary minimum at approximately $\pm$ 120°, the bond is said to be in a *gauche*$^{\pm}$ conformation, the plus sign referring to the + 120° torsion. This will break the planar symmetry of the chain shown in Figure 1 so that it will now project out of the plane of the page beyond the gauche bond. Figure 3 shows space-filling models for an all-trans chain and one that contains one gauche bond near the middle of the chain. In this Thesis, we will sometimes use the loose nomenclature of "straight chain" for an all-trans chain and "gauche defect" for a bond in a gauche conformation. It should be noted from Figure 2 that the energy difference between a trans and gauche conformation is comparable to k_BT at room temperature, and therefore under normal conditions (e.g., in liquid alkanes) the chain conformation may contain several thermally populated gauche

defects. Finally, we should mention that the above description is only an approximation (known as the Rotational Isomeric State model[50]), and in fact the torsional angle about any bond can assume any value, with highest probabilities around the energy minima, of course. A more realistic description of the chain conformation should include fluctuations of the torsional angle about the trans and gauche minima that can be as large as ± 20°.[50] Also, as a first approximation one can consider each bond conformation as independent of the adjacent ones, but in practice a few conformations (gauche$^+$-gauche$^-$) are highly unlikely due to steric interactions.[50]

This Thesis is organized as follows. In Chapter 2 we will describe the basic theory of SFG at interfaces and how it can be used as a surface vibrational spectroscopy technique. Only the essential points for understanding our data analysis will be discussed and emphasis will be on a few of the unique features of the technique in the context of surface vibrational spectroscopy. It will be concluded with a brief section on the experimental implementation of SFG vibrational spectroscopy.

Chapter 3 will discuss our investigations of surface phase transitions. The surface crystallization of an alcohol monolayer at the air/water interface is compared to the surface freezing transition of liquid alkanes. Phase transitions in Langmuir films have been well studied for a long time using surface tension and surface potential measurements.[51] However, only recently grazing-angle X-ray diffraction has provided unambiguous evidence for crystalline order in the monolayers.[13,14,28] However, molecular information about the liquid phase of these monolayers is not as complete. The surface freezing transition at the surface of liquid alkanes was recently discovered by surface tension and X-ray reflectivity measurements.[52,53] It was found that at a few degrees above

the melting point of several long-chain alkanes, there was a crystalline monolayer "floating" on the liquid surface. Again, much less information was available about the surface structure well above the melting point of the alkane, when the surface was liquid-like. Clearly, the underlying driving force for the surface crystallization in both cases is the same: the strong van der Waals attractions between long, parallel alkyl chains. What we found was that, despite the similarities in the phase transition mechanism, the chain conformation and orientation in the liquid phase were very different for the alkane and alcohol monolayers. In all cases, the chains are on average oriented along the surface normal. The chains at the alkane surface are quite disordered in the liquid phase and become considerably more ordered, with much less gauche conformations in the surface crystalline phase. In contrast, the alcohol chains are nearly all-trans both below and above the transition temperature (with only a small surface density change at the phase transition) because the alcohol head-groups are now interacting with the water substrate leading to a more ordered upright arrangement of molecules.

As the crystalline alcohol monolayer interacts with the water surface, one may expect to have an enhanced order in the surface water molecules due to an epitaxial interaction with the ordered alcohol head-groups. This has indeed been suggested by Leiserowitz *et. al.* who showed that water droplets covered by a crystalline alcohol monolayer have an ice nucleation temperature much higher than those covered by a fatty acid monolayer.[54,55] This was attributed to a good lattice matching between the alcohol monolayer and the ice structure. In Chapter 4 we will discuss the vibrational spectra of surface water molecules covered by an alcohol or fatty acid monolayer. The vibrational frequency of the OH stretch mode for a water molecule is very sensitive to hydrogen

bonding.[56] Therefore, the vibrational spectra of ice and water are quite different due to the stronger and more ordered hydrogen-bonding network of water molecules in ice as compared to water. As suggested by the ice nucleation experiments, we find the network of water underneath an alcohol monolayer resembling the ice structure. In contrast, the water structure underneath a fatty acid monolayer is considerably disordered. However, in the latter case the monolayer head-groups can be ionized by a sufficiently high water pH value, yielding a charged monolayer that produces a strong electric field at the interface. This surface field is able to orient water molecules at the interface into an ordered, ice-like hydrogen-bonded structure. This is consistent with the notion that strong electric fields are able to induce ice nucleation.[57]

Chapter 5 continues our study of Langmuir films. There, the focus will be on the quantitative determination of molecular orientation at interfaces. It will be shown that using the second-order nonlinear optical processes of SFG and second harmonic generation (SHG) it is possible to completely map out the orientation and conformation of surface molecules. However, in order to have the deduced molecular conformation in agreement with the expected one, we must include in the data analysis local-field corrections at the interface.

Chapter 6 will be concerned with conformation of self-assembled surfactant monolayers adsorbed at solid/liquid interfaces. These monolayers are spontaneously formed by surfactant adsorption onto a solid substrate and have found innumerous applications in current technology.[58] We have studied surfactant conformations for monolayers at the fused quartz/air interface and various fused quartz/liquid interfaces. It was found that if the monolayers have high surface coverage (i.e., fully packed

monolayers) with area per surfactant chain around 20 to 25 $Å^2$/chain, the chains are nearly all-trans and this conformation hardly changes upon immersion of the monolayer into any liquid environment. However, if the monolayer is more loosely packed with surface coverage equivalent to ~ 35 $Å^2$/chain or lower, the surfactant alkyl chains at the solid/air interface are considerably more disordered than the fully packed monolayers, due to a reduction in the interchain van der Waals interaction (chain-chain interaction). The difference becomes more pronounced when the monolayers are immersed in a liquid. We found that depending on the relative strength of the intermolecular interactions between liquid and alkyl chain and the interactions among liquid molecules, the chain conformation could vary significantly. From the vibrational spectra we deduced that it could appear as an ordered, all-trans conformation when immersed in long enough liquid alkanes, or as a highly disordered conformation with a large enough number of gauche defects to give a more compact molecular configuration, when the monolayer was immersed in hydrogen-bonding liquids. The latter case can be understood as a manifestation of the hydrophobic effect, the main driving force behind protein folding and the formation of micelles or other aggregates in surfactant solutions.[59]

Finally, Chapter 7 will summarize the main results and comment on the advantages and obstacles of SFG spectroscopy in the study of surfactants at liquid interfaces.

References

(1) T. N. Veziroglu, ed., *Environmental Problems and Solutions: Greenhouse Effect, Acid Rain, Pollution*, Hemisphere, New York (1990).

(2) R. B. Gennis, *Biomembranes: molecular structure and function*, Springer-Verlag, New York (1989).

(3) J. H. Fendler, *Membrane Mimetic Chemistry*, Wiley-Interscience, New York (1982).

(4) A. W. Adamson, *The Physical Chemistry of Surfaces*, 5th ed., Wiley-Interscience, New York (1990).

(5) R. Sharma, ed., *Surfactant Adsorption and Surface Solubilization*, ACS Symposium Series **615**, American Chemical Society, Washington, DC (1995).

(6) Karsa, D. R., ed. *Industrial Applications of Surfactants II*, The Royal Society of Chemistry, Cambridge, UK (1990).

(7) J. D. Swalen *et. at.*, *Langmuir* **3**, 932 (1987).

(8) C. S. Chen, M. Mrksich, S. Huang, G. M. Whitesides and D. E. Ingber, *Science* **276**, 1425 (1997).

(9) Y. Xia and G. M. Whitesides, *Angew. Chem. Int. Ed.* **37**, 550 (1998).

(10) D. W. Fuerstenau and R. Herrera-Urbina, in *Cationic Surfactants, Physical Chemistry,* p. 407, D. N. Rubingh and P. M. Holland, eds, Surfactant Sci. Ser. **37**, M. Dekker, New York (1991).

(11) J. N. Israelachvili, *Intermolecular and Surface Forces*, 2nd ed., Academic Press, London (1992).

(12) W. M. Lienfield, in *Cationic Surfactants*, p. 9, E. Jungermann, ed., Surfactant Sci.

Ser. **4**, M. Dekker, New York (1970)

(13) B.; Lin, M. C. Shih, T. M. Bohanon, G. E. Ice and P. Dutta, *Phys. Rev. Lett.* **65**, 191 (1990).

(14) R. M. Kenn, C. Böhm, A. M. Bibo, I. R. Peterson, H. Möhwald, J. Als-Nielsen and K. Kjaer, *J. Phys. Chem.* **95**, 2092 (1991).

(15) D. H. Charych, J. O. Nagy, W. Spevak and M. D. Bednarski, *Science* **261**, 585 (1993).

(16) G. Roberts, *Langmuir-Blodgett Films*, Plenum, New York, (1990).

(17) J.L. Trompette, J. Zajac, E. Keh, and S. Partyka, *Langmuir* **10**, 812 (1994).

(18) B. T. Ingram and R. H. Ottewill, in *Cationic Surfactants, Physical Chemistry,* p. 87, D. N. Rubingh and P. M. Holland, eds, Surfactant Sci. Ser. **37**, M. Dekker, New York (1991).

(19) P. Wängnerud and G. Olofsson, *J. Colloid Interface Sci.* **153**, 392 (1992).

(20) Z. M. Zorin, N. V. Churaev, N. E. Esipova, I. P. Sergeeva, V. D. Sobolev and E. K. Gasanov, *J. Colloid Interface Sci.* **152**, 170 (1992).

(21) S. Partyka, M. Lindheimer and B. Faucompre, *Colloids Surf. A* **76**, 267, (1993).

(22) P. Wängnerud, D. Berling and G. Olofsson, *J. Colloid Interface Sci.* **169**, 365 (1995).

(23) Z. M. Zorin, V. P. Romanov and N. V. Churaev, *Colloid Polymer Sci.* **267**, 968 (1979).

(24) W. A. Zisman, in *Contact Angle, Wettability and Adhesion*, F. M. Fowkes, ed., Advances in Chemistry **43**, p. 1, American Chemical Society, Washington, DC

(1964).

(25) W. R. Birch, M. A. Knewtson, S. Garoff, R. M. Suter and S. Satija, *Colloids Surf. A* **89**, 145 (1994).

(26) A. R. Rennie, E. M. Lee, E. A. Simister and R. K. Thomas, *Langmuir* **6**, 1031 (1990).

(27) J. Penfold *et. al.*, *J. Chem. Soc. Faraday Trans.* **93**, 3899 (1997).

(28) J. Als-Nielsen, D. Jacquemain, K. Kjaer, F. Leveiller, M. Lahav and L. Leiserowitz, *Phys. Rep.* **246**, 251 (1994).

(29) Y. L. Chen, S. Chen, C. Frank and J. Israelachvili, *J. Colloid Interface Sci.* **153**, 244 (1992).

(30) E. Söderlind and P. Stilbs, *Langmuir* **9**, 1678 (1993).

(31) E. Söderlind and P. Stilbs, *Langmuir* **9**, 2024 (1993).

(32) L. C. Sander, J. C. Callis and L. R. Field, *Anal. Chem.* **55**, 1068 (1983).

(33) Y. I. Rabinovich, D. A. Guzonas and R.-H. Yoon, *J. Colloid Interface Sci.* **155**, 221 (1993).

(34) R. G. Nuzzo, L. H. Dubois and D. L. Allara, *J. Am. Chem. Soc.* **112**, 558 (1990).

(35) R. Mendelsohn, J. W. Brauner and A. Gericke, *Annu. Rev. Phys. Chem.* **46**, 305 (1995).

(36) A. L. Dendramis, E. W. Schwinn and R. P. Sperline, *Surf. Sci.* **134**, 675 (1983).

(37) S. Sun, R. L. Birke and J. R. Lombardi, *J. Phys. Chem.* **94**, 2005 (1990).

(38) K. Suga, M. Bradley and J. F. Rusling, *Langmuir* **9**, 3063 (1993).

(39) G. E. Poirier and E. D. Pylant, *Science* **272**, 1145 (1996).

(40) L. A. Bumm, J. J. Arnold, M. T. Cygan, T. D. Dunbar, T. P. Burgin, L. Jones II, D. L. Allara, J. M. Tour and P. S. Weiss, *Science* **271**, 1705 (1996).

(41) Y. Tsao, S. X. Yang, D. F. Evans and H. Wennerström, *Langmuir* **7**, 3154 (1991).

(42) Y. L. E. Chen, M. L. Gee, C. A. Helm, J. N. Israelachvili and P. M. McGuiggan, *J. Phys. Chem.* **93**, 7057 (1989).

(43) J. L. Parker, V. V. Yaminsky and P. M. Claesson, *J. Phys. Chem.* **97**, 7706 (1993).

(44) M. W. Rutland and J. L. Parker, *Langmuir* **10**, 1110 (1994).

(45) M. Mrksich, G. B. Sigal and G. M. Whitesides, *Langmuir* **11**, 4383 (1995).

(46) F. Tiberg, *J. Chem. Soc. Faraday Trans.* **92**, 531 (1996).

(47) K. J. Schweighofer, U. Essmann and M. Berkowitz, *J. Phys. Chem. B* **101**, 3793 (1997).

(48) M. L. Klein, *J. Chem. Soc. Faraday Trans.* **88**, 1701 (1992).

(49) P. B. Miranda and Y. R. Shen, *J. Phys. Chem. B* (submitted).

(50) P. J. Flory, *Statistical Mechanics of Chain Molecules*, Interscience, New York (1969).

(51) G. L. Gaines, Jr., *Insoluble Monolayers at Liquid-Gas Interfaces*, Interscience, New York (1966).

(52) X. Z. Wu, B. M. Ocko, E. B. Sirota, S. K. Sinha, M. Deutsch, B. H. Cao and M. W. Kim, *Science* **261**, 1018 (1993).

(53) X. Z. Wu, E. B. Sirota, S. K. Sinha, B. M. Ocko and M. Deutsch, *Phys. Rev. Lett.* **70**, 958 (1993).

(54) M. Gavish, R. Popovitz-Biro, M. Lahav and L. Leiserowitz, *Science* **250**, 973

(1990).

(55) R. Popovitz-Biro, J. L. Wang, J. Majewski, E. Shavit, L. Leiserowitz and M. Lahav, *J. Am. Chem. Soc.* **116**, 1179 (1994).

(56) G. A. Jeffrey, *An Introduction to Hydrogen Bonding*, Oxford University Press, New York (1997).

(57) P. V. Hobbs, *Ice Physics*, Clarendon Press, Oxford, UK (1974).

(58) G. M. Whitesides, *Scientific American* **273**, 146 (1995).

(59) C. Tanford, *The Hydrophobic Effect: formation of micelles and biological membranes*, 2nd ed., J. Wiley, New York (1980).

Figure Captions

Figure 1. Schematic representation of the generic structure of a surfactant molecule. The alkyl chain is 5 carbons long in this case ($R(CH_2)_4CH_3$). R is the polar head-group. Adapted from Ref. 50.

Figure 2. Potential energy for rotation about a C – C bond of an alkyl chain. $j = 0$ corresponds to the trans conformation, with CH_2 groups pointing in opposite directions. The horizontal dashed line corresponds to k_BT at room temperature. Adapted from Ref. 50.

Figure 3. Space-filling model of an alkane in (a) the all-trans conformation and (b) in a conformation containing one gauche defect near the middle of the chain.

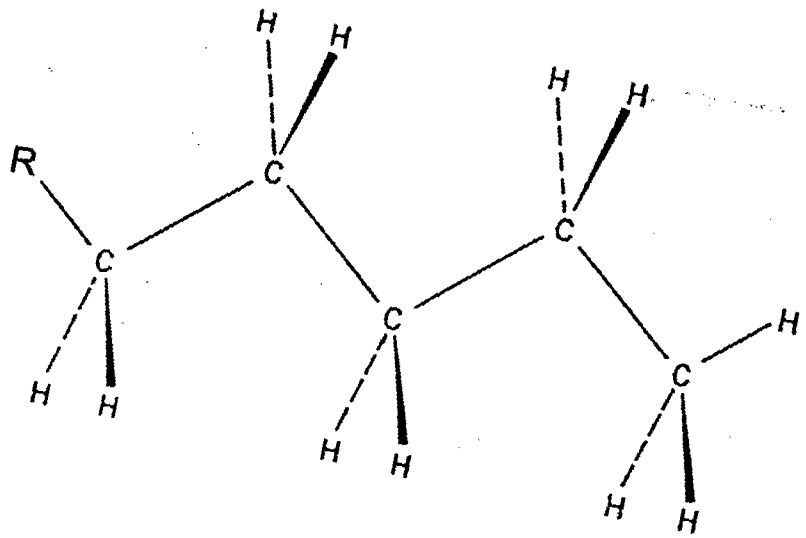

Figure 1

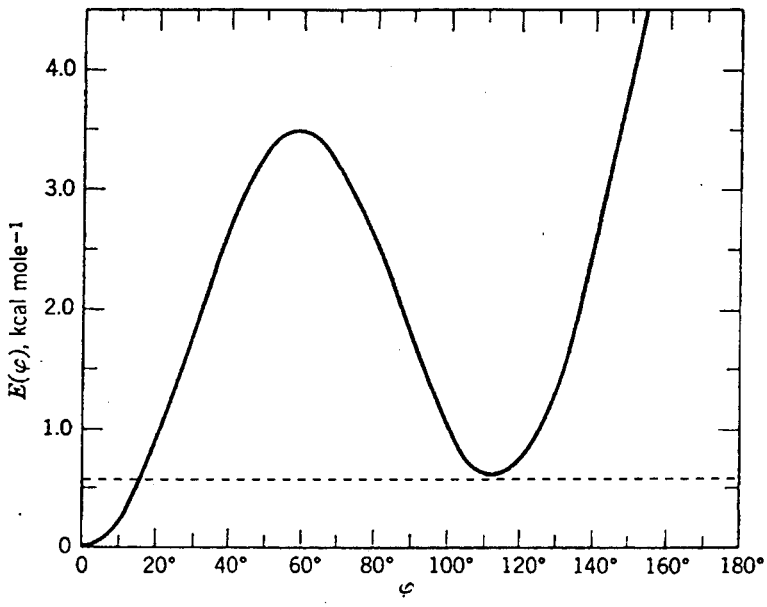

Figure 2

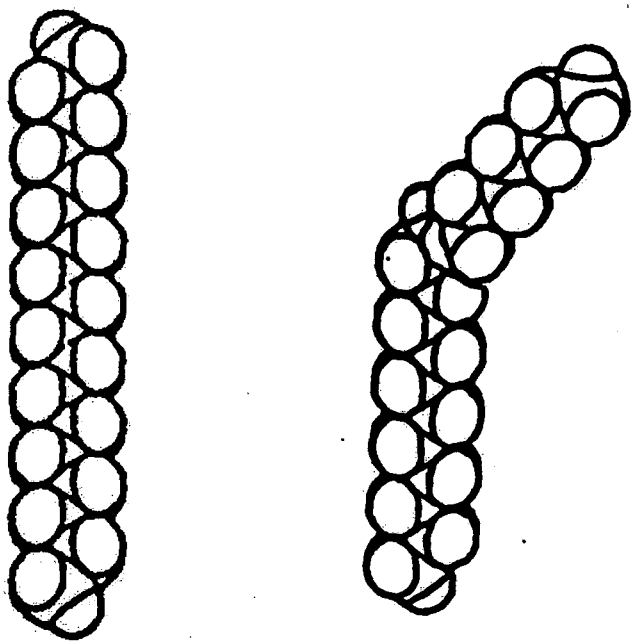

Figure 3

Chapter 2. Surface Vibrational Spectroscopy by SFG

A. Background

As mentioned in Chapter 1, most conventional surface science techniques that employ particle scattering or emission are not generally applicable to liquid or buried interfaces. In such cases, surface studies usually rely on optical probes like ellipsometry, X-Ray scattering and spectroscopic techniques such as infrared (IR), Raman or ultraviolet-visible (UV-VIS) spectroscopy. Many of them are, however, not intrinsically surface-specific and therefore are unable to discriminate contributions from surface and the bulk of materials. In some cases, difference spectroscopy or modulation techniques may be able to enhance surface specificity of a technique.

Second-order nonlinear optical processes such as second harmonic generation (SHG) and sum-frequency generation (SFG) are forbidden in media with inversion symmetry,[1] as we will show below. At an interface between centrosymmetric media, however, inversion symmetry is broken and these processes become allowed. This is the reason behind their intrinsic surface specificity.

The development of these processes into effective surface probes started in the early 80's with the investigation of SHG from metal surfaces.[2] Since then SHG became a powerful surface analytical tool, with capability of application in surface electronic spectroscopy. Infrared-visible SFG as a vibrational spectroscopic technique was first demonstrated in 1987. Because of its unique capabilities in surface vibrational spectroscopy, it has also grown considerably in popularity, although much less than SHG.

This is true partly because it is relatively new compared to SHG and also because of its more complicated experimental arrangement.

We will now describe the basic theory of SFG at interface as a vibrational spectroscopy tool. Only the points essential to the understanding of the data analysis and interpretation in this Thesis will be presented. For a more detailed account, the reader is referred to the literature.[1-5]

B. Basic Theory

We generally consider an interfacial system as a three-layer system composed of two centrosymmetric media 1 and 2 and an interfacial layer *i* (see Figure 1). The interfacial layer can be either a bare interface or an interface with a layer of adsorbates. For example, in the case of a Langmuir film, medium 1 is air and medium 2 water, and the interfacial layer *i* is a surfactant monolayer adsorbed on water. Under the irradiation of two optical fields $\mathbf{E}_1(\mathbf{r},t) = \mathbf{E}_1 e^{i(\mathbf{k}_1\cdot\mathbf{r}-\omega_1 t)} + c.c.$ and $\mathbf{E}_2(\mathbf{r},t) = \mathbf{E}_2 e^{i(\mathbf{k}_2\cdot\mathbf{r}-\omega_2 t)} + c.c.$ with frequencies and wavevectors ω_1, $\mathbf{k}_1$ and ω_2, $\mathbf{k}_2$ respectively, the generated effective second-order nonlinear polarization $\mathbf{P}_{eff}^{(2)}(\omega = \omega_1 + \omega_2)$ can be expressed as a multipole expansion[6,7]

$$\mathbf{P}_{eff}^{(2)}(\omega = \omega_1 + \omega_2) = \mathbf{P}^{(2)}(\omega) - \nabla\cdot\mathbf{Q}^{(2)}(\omega) + \frac{c}{i\omega}\nabla\times\mathbf{M}^{(2)}(\omega) + \cdots \qquad (2.1)$$

where the first, second and third terms on the right-hand side are the contributions to the second-order polarization due to electric dipole, electric quadrupole and magnetic dipole, respectively. At the interface, the optical fields have a large spatial variation. If we keep

only terms to the first order in the spatial derivatives, $\mathbf{P}^{(2)}$, $\mathbf{Q}^{(2)}$ and $\mathbf{M}^{(2)}$ can be expressed as

$$\mathbf{P}^{(2)}(\omega) = \chi^{D}:\mathbf{E}_1(\omega_1)\mathbf{E}_2(\omega_2) + \chi^{P_1}:\nabla\mathbf{E}_1(\omega_1)\mathbf{E}_2(\omega_2) + \chi^{P_2}:\mathbf{E}_1(\omega_1)\nabla\mathbf{E}_2(\omega_2)$$

$$\mathbf{Q}^{(2)}(\omega) = \chi^{Q}:\mathbf{E}_1(\omega_1)\mathbf{E}_2(\omega_2) \qquad (2.2).$$

$$\mathbf{M}^{(2)}(\omega) = \chi^{M}:\mathbf{E}_1(\omega_1)\mathbf{E}_2(\omega_2)$$

In Eqs. (2.2), χ's are tensors describing the material response. If a medium has inversion symmetry, the tensors χ above should be invariant upon the inversion operation, whereas $\mathbf{P}_{eff}^{(2)}$, $\mathbf{E}_i$ and ∇ are vectors and therefore change sign upon inversion. From this we see immediately that the term proportional to χ^D (the local electric dipole contribution) should vanish. All other terms may be nonvanishing even in media with inversion symmetry. At the interface, however, the inversion symmetry is necessarily broken and the electric dipole contribution may also become nonvanishing. Since the electric dipole contribution is the lowest order in the expansion, it is expected to be the dominant one. If this is the case, the nonlinear polarization $\mathbf{P}_{eff}^{(2)}$ will be dominated by the interface. It will then radiate optical fields at frequency $\omega = \omega_1 + \omega_2$ into media 1 and 2. Nevertheless, the other higher order terms in Eq. (2.1) may be in general non-negligible. In this case the surface specificity of second-order processes is lost or greatly reduced. Considerable effort has been devoted to devise a general method to separate interfacial and bulk contributions to SFG.[8] The result is, however, not conclusive. Without sufficient knowledge of the field profile at the interface and molecular parameters, one may have to resort to experimental checks to prove that the signal generated by surface SHG or SFG is dominated by interfacial contributions.[9]

One experimental approach that can be generally used to do this is to modify in some way the interface between two media. If after the surface modification the detected second-order signal is hardly changed, the bulk contributions are overwhelming any surface electric dipole contribution. Fortunately the opposite is quite often observed: the nonlinear signal is strongly dependent on surface conditions, showing that indeed the dipole contribution is dominant.[10-12] For all interfaces studied in this Thesis, and for liquid interfaces in general, the dipole contribution is dominant and the SHG and SFG techniques are highly surface-specific. This will be explicitly demonstrated in Chapter 3 for the case of liquid alkane interfaces.

If the higher-order contributions in Eq. (2.1) can be neglected, the effective second-order nonlinear polarization will be confined to the interfacial layer *i* and will be given by

$$\mathbf{P}^{(2)}(\omega = \omega_1 + \omega_2) = \chi^{(2)}_{eff}(\omega = \omega_1 + \omega_2) : \mathbf{E}_1(\omega_1)\mathbf{E}_2(\omega_2) \tag{2.3}$$

where $\chi^{(2)}_{eff}(\omega = \omega_1 + \omega_2)$ is the effective electric dipole nonlinear susceptibility of the interface, and we have dropped the superscript D in χ for simplicity. For IR-visible SFG, ω_1 is in the visible range and ω_2 in the IR range. For SHG, $\omega_1=\omega_2$ and $\mathbf{E}_1=\mathbf{E}_2$. This interfacial polarization sheet is then a source of radiation for SFG and SHG into media 1 and 2. It radiates two coherent beams at frequency ω in the reflected and transmitted directions (see Figure 1). The output angle of the sum-frequency beam is given by phase matching in the surface plane:

$$\mathbf{k}_{1//} + \mathbf{k}_{2//} = \mathbf{k}_{//} \tag{2.4}$$

where $\mathbf{k}_{i//}$ is the component of the wavevector $\mathbf{k}_i$ parallel to the surface plane. For the geometry shown in Figure 1 it can be expressed as

$$\omega_1 n_1(\omega_1)\sin\beta_1 + \omega_2 n_1(\omega_2)\sin\beta_2 = \omega n_1(\omega)\sin\beta \tag{2.5}$$

where n_i (Ω) is the refractive index of medium *i* at frequency Ω and β_i is the incidence angle of the field at frequency ω_i. One can then substitute the polarization given by Eq. (2.3) in the wave equation to obtain the radiated sum-frequency field. The sum-frequency intensity in the reflected direction is given by[2-4]

$$I(\omega) = \frac{8\pi^3\omega^2 \sec^2\beta}{c^3 n_1(\omega)n_1(\omega_1)n_1(\omega_2)}\left|\chi^{(2)}_{eff}\right|^2 I_1(\omega_1)I_2(\omega_2) \tag{2.6}$$

where $I(\Omega)$ is the intensity of the field at frequency Ω. The effective nonlinear susceptibility $\chi^{(2)}_{eff}$ takes the form

$$\chi^{(2)}_{eff} = [\hat{\mathbf{e}}(\omega)\cdot\mathbf{L}(\omega)]\cdot\chi^{(2)}:[\mathbf{L}(\omega_1)\cdot\hat{\mathbf{e}}(\omega_1)][\mathbf{L}(\omega_2)\cdot\hat{\mathbf{e}}(\omega_2)] \tag{2.7}$$

with $\hat{\mathbf{e}}(\Omega)$ being the unit polarization vector and $\mathbf{L}(\Omega)$ the Fresnel factor for the field at frequency Ω. The Fresnel factor $\mathbf{L}(\Omega)$ is a diagonal tensor whose elements are the Fresnel transmission coefficients that relate the cartesian components of the field in the interfacial layer to the input field components.

In general, $\chi^{(2)}$ has 27 independent elements. However, we can use the symmetry of the interface to reduce the number of nonvanishing independent elements. In the case of an azimuthally isotropic interface, there are only four independent nonvanishing elements in $\chi^{(2)}$. With the lab coordinates chosen such that z is along the interface normal and x in the incidence plane as shown in Figure 1, they are $\chi_{xxz} = \chi_{yyz}$, $\chi_{xzx} = \chi_{yzy}$, $\chi_{zxx} = \chi_{zyy}$ and χ_{zzz}. These four elements can be deduced by measuring SFG with four different input and output polarization combinations, namely, SSP (referring to S-polarized sum-

frequency field, S-polarized $\mathbf{E}_1$, and P-polarized $\mathbf{E}_2$, respectively), SPS, PSS and PPP. The effective nonlinear susceptibilities under these four polarization combinations can be expressed as

$$\chi^{(2)}_{eff,SSP} = L_{yy}(\omega)L_{yy}(\omega_1)L_{zz}(\omega_2)\sin\beta_2\ \chi_{yyz}$$

$$\chi^{(2)}_{eff,SPS} = L_{yy}(\omega)L_{zz}(\omega_1)L_{yy}(\omega_2)\sin\beta_1\ \chi_{yzy}$$

$$\chi^{(2)}_{eff,PSS} = L_{zz}(\omega)L_{yy}(\omega_1)L_{yy}(\omega_2)\sin\beta\ \chi_{zyy} \tag{2.8}$$

$$\begin{aligned}\chi^{(2)}_{eff,PPP} = &-L_{xx}(\omega)L_{xx}(\omega_1)L_{zz}(\omega_2)\cos\beta\cos\beta_1\sin\beta_2\ \chi_{xxz}\\ &-L_{xx}(\omega)L_{zz}(\omega_1)L_{xx}(\omega_2)\cos\beta\sin\beta_1\cos\beta_2\ \chi_{xzx}\\ &+L_{zz}(\omega)L_{xx}(\omega_1)L_{xx}(\omega_2)\sin\beta\cos\beta_1\cos\beta_2\ \chi_{zxx}\\ &+L_{zz}(\omega)L_{zz}(\omega_1)L_{zz}(\omega_2)\sin\beta\sin\beta_1\sin\beta_2\ \chi_{zzz}\end{aligned}$$

where $L_{xx}(\Omega)$, $L_{yy}(\Omega)$ and $L_{zz}(\Omega)$ are the diagonal elements of $\mathbf{L}(\Omega)$, given by

$$L_{xx}(\Omega) = \frac{2n_1(\Omega)\cos\gamma}{n_1(\Omega)\cos\gamma + n_2(\Omega)\cos\beta} \tag{2.9}$$

$$L_{yy}(\Omega) = \frac{2n_1(\Omega)\cos\beta}{n_1(\Omega)\cos\beta + n_2(\Omega)\cos\gamma} \tag{2.10}$$

$$L_{zz}(\Omega) = \frac{2n_2(\Omega)\cos\beta}{n_1(\Omega)\cos\gamma + n_2(\Omega)\cos\beta}\left(\frac{n_1(\Omega)}{n'(\Omega)}\right)^2 \tag{2.11}.$$

In the above equations, $n'(\Omega)$ is the refractive index of the interfacial layer, β is the incidence angle of the beam in consideration and γ is the refracted angle ($n_1(\Omega)\sin\beta = n_2(\Omega)\sin\gamma$). Since the interfacial layer is only one (or a few) monolayer thick, its refractive index can be different from that of its own bulk material and difficult to measure.[13] It is therefore the usual practice that $n'(\Omega)$ is chosen to be equal to either

$n_1(\Omega)$, $n_2(\Omega)$ or the bulk refractive index of the material at the interface. However, as noticed previously[14-16] and shown later in Chapter 5, the determination of molecular orientation is quite sensitive to the value of $n'(\Omega)$, and choosing $n'(\Omega)$ to be equal to $n_1(\Omega)$ or $n_2(\Omega)$ is not always a good approximation.

In Chapter 5 we will use both SHG and SFG to determine molecular orientation in a Langmuir film. For this reason we now present the necessary modifications to Eq. (2.8) for the case of SHG. In this case, the last two sub-indices of χ_{ijk} are interchangeable,[17] since the input fields are the same. Thus there are only three nonvanishing independent χ-elements, $\chi_{xxz} = \chi_{yyz} = \chi_{xzx} = \chi_{yzy}$, $\chi_{zxx} = \chi_{zyy}$ and χ_{zzz}. They can be deduced from measurement with three different input and output polarization combinations, PS, SM and PP. Here the first and second letters denote the output and input polarization, respectively, and M refers to the polarization midway between S and P. From Eq. (2.7) the effective nonlinear susceptibilities take the forms

$$\chi^{(2)}_{eff,PS} = L_{zz}(\omega)(L_{yy}(\omega_1))^2 \sin\beta\, \chi_{zyy}$$

$$\chi^{(2)}_{eff,SM} = L_{yy}(\omega) L_{zz}(\omega_1) L_{yy}(\omega_1) \sin\beta_1\, \chi_{yzy} \qquad (2.12).$$

$$\begin{aligned}\chi^{(2)}_{eff,PP} = &+L_{zz}(\omega)(L_{xx}(\omega_1))^2 \sin\beta \cos^2\beta_1\, \chi_{zxx} \\ &-2L_{xx}(\omega) L_{zz}(\omega_1) L_{xx}(\omega_1) \cos\beta \sin\beta_1 \cos\beta_1\, \chi_{xzx} \\ &+L_{zz}(\omega)(L_{zz}(\omega_1))^2 \sin\beta \sin^2\beta_1\, \chi_{zzz}\end{aligned}$$

In the case where the interface is composed of molecules, as in all examples discussed in this Thesis, $\chi^{(2)}$ is related to the molecular hyperpolarizability $\alpha^{(2)}$ by the coordinate transformation

$$\chi^{(2)}_{ijk} = N_s\, l_{ii}(\omega)\, l_{jj}(\omega_1)\, l_{kk}(\omega_2) \sum_{\xi,\eta,\zeta} \left\langle (\hat{\mathbf{i}}\cdot\hat{\xi})(\hat{\mathbf{j}}\cdot\hat{\eta})(\hat{\mathbf{k}}\cdot\hat{\zeta}) \right\rangle \alpha^{(2)}_{\xi\eta\zeta} \qquad (2.13)$$

where N_s is the surface density of molecules, $(\boldsymbol{i},\boldsymbol{j},\boldsymbol{k})$ and (ξ,η,ζ) are unit vectors along the lab and molecular coordinates, respectively, and $\boldsymbol{l}$ is a tensor describing the microscopic local-field correction and the angular brackets denote an average over the molecular orientational distribution. For molecules in the bulk, we can use the Lorentz local-field correction $\boldsymbol{l} = \frac{1}{3}(\varepsilon+2)\cdot\mathbf{I}$, where $\mathbf{I}$ is the identity tensor and ε is the bulk dielectric constant.[1] In this case $\boldsymbol{l}$ can be neglected if we renormalize $\alpha^{(2)}$ as $(\frac{1}{3}(\varepsilon+2))^3\alpha^{(2)}$. However, at an interface the local-field correction is anisotropic and less well known.[18] As will be discussed in Chapter 5, for the determination of molecular orientation at an interface the effect of $\boldsymbol{l}(\Omega)$ can be lumped into the refractive index $n'(\Omega)$ in Eq. (2.11). We can then omit l_{ii}, l_{jj}, and l_{kk} in Eq. (2.13) and write

$$\chi^{(2)}_{ijk} = N_s \sum_{\xi,\eta,\zeta} \left\langle (\hat{\mathbf{i}}\cdot\hat{\xi})(\hat{\mathbf{j}}\cdot\hat{\eta})(\hat{\mathbf{k}}\cdot\hat{\zeta}) \right\rangle \alpha^{(2)}_{\xi\eta\zeta} \qquad (2.14).$$

To obtain information about the interfacial system from its second-order response, we must examine the microscopic expressions for $\alpha^{(2)}$. They can be calculated by standard second-order perturbation theory.[19] From the microscopic expressions one sees that if one of the frequencies ω, ω_1 or ω_2 coincides with a vibrational or electronic transition, energy denominators become small and resonant enhancement of $\alpha^{(2)}$ is expected. In the case of IR-visible SFG we are concerned with vibrational resonances of the surface molecules. With the IR frequency (ω_2) near a vibrational transition from ground to first exited vibrational level, $\alpha^{(2)}$ and $\chi^{(2)}$ can be written as[20,21]

$$\alpha^{(2)} = \alpha_{NR}^{(2)} + \sum_q \frac{\alpha_q}{\omega_2 - \omega_q + i\Gamma_q} \tag{2.15}$$

$$\chi^{(2)} = \chi_{NR}^{(2)} + \sum_q \frac{\chi_q}{\omega_2 - \omega_q + i\Gamma_q} \tag{2.16}$$

where the subscript NR refers to a nonresonant contribution due to all other resonances away from the IR range in consideration, and α_q (χ_q), ω_q, and Γ_q denote the strength, resonant frequency and damping constant of the q^{th} vibrational mode, respectively. The strength of each resonance α_q can be expressed in the usual notation of Raman and IR spectroscopy as

$$\alpha_{q,\xi\eta\zeta} = \frac{1}{2\omega_q} \frac{\partial \alpha_{\xi\eta}^{(1)}}{\partial Q} \frac{\partial \mu_\zeta}{\partial Q} \Delta\rho_q \tag{2.17}$$

where $\frac{\partial \alpha_{\xi\eta}^{(1)}}{\partial Q}$ and $\frac{\partial \mu_\zeta}{\partial Q}$ are the Raman polarizability derivative and IR dipole moment derivative for the normal mode Q, respectively, and $\Delta\rho_q$ is the population difference between ground and excited vibrational states for the q^{th} mode. Eqs. (2.15) to (2.17) have important consequences. First of all, the resonant enhancement of $\alpha^{(2)}$ as an infrared laser is scanned over vibrational resonances gives the surface vibrational spectrum. Since the SFG signal is proportional to $|\chi^{(2)}|^2$, we see from Eq. (2.16) that the resonant features in an SFG spectrum are due to an interference between the resonant and nonresonant contributions. The nonresonant background may be complex, in general, although it should become real if ω and ω_1 are away from resonances in any medium. This interference leads to a more complicated lineshape than in the case of usual IR and Raman spectroscopy. A few examples are schematically illustrated in Figure 2 for

various values of χ_q and χ_{NR}. Therefore, in general one has to extract parameters such as resonant frequencies, linewidths and mode strengths by fitting the spectrum to a theoretical expression for $\chi^{(2)}$ such as Eq. (2.16). We will comment on curve fitting in Chapter 5. Another consequence of Eq. (2.17) is that a vibrational mode must be both IR and Raman active to be observable in the SFG spectrum. This is equivalent to the requirement that a molecule must not have an inversion center to have nonvanishing $\alpha^{(2)}$.[22] Finally, if both ω and ω_1 are away from electronic resonances, $\frac{\partial \alpha^{(1)}_{\xi\eta}}{\partial Q}$ is symmetric upon interchange of indices ξ and η,[22] so that the first two indices of $\chi^{(2)}_{ijk}$ are interchangeable.

Each mode may be associated with a particular moiety on the molecule.[22] If $(\chi_q)_{ijk}$ can be obtained from the resonant feature in the SFG spectrum, and $(\alpha_q)_{\xi\eta\zeta}$ is known, then according to Eq. (2.14) the average orientation of the selected moiety may be deduced. This will be discussed in more detail in Chapter 5. However, for the sake of a concrete example we will now present a simple model that yields the nonvanishing $(\alpha_q)_{\xi\eta\zeta}$ elements for the symmetric stretch vibration of CH_3 and CH_2 groups of an alkyl chain and describe how information about the orientation of a CH_3 group can be obtained by measuring $(\chi_q)_{ijk}$.

We begin assuming that both ω and ω_1 are far away from electronic resonances. We assume a simple bond aditivity model: each CH bond has a dipole moment derivative μ_o along the bond direction (c-axis) and a cylindrically symmetric Raman polarizability derivative tensor α_o whose nonvanishing elements are $\alpha_{cc} = \alpha_o$ and $\alpha_{aa} = \alpha_{bb} = R \cdot \alpha_o$. The

parameter R describes how anisotropic the polarizability derivative of a single CH bond is and can be taken from theoretical calculations[23] (R = 0.14) or determined from Raman spectra of polymethylene[24] (R = 0.18). The $\frac{\partial \alpha_{\xi\eta}^{(1)}}{\partial Q}$ elements for the CH_3 and CH_2 groups are then determined by adding the contributions from all CH bonds. Similarly, $\frac{\partial \mu_\zeta}{\partial Q}$ for each group is determined by adding the contribution of individual bonds. Finally $\alpha_{q,\xi\eta\zeta}$ is determined by Eq. (2.17).

For the CH_3 group with C_{3V} symmetry, we take the symmetry axis as ζ, and ξ is such that one CH bond is in the $\xi\zeta$ plane. For the symmetric stretch mode the normal coordinate is $Q = \frac{1}{\sqrt{3}}(r_1 + r_2 + r_3)$, where r_i is C-H bond distance for the i^{th} H atom. We then have

$$\frac{\partial \mu}{\partial Q} = \frac{\partial \mu}{\partial r_1}\frac{\partial r_1}{\partial Q} + \frac{\partial \mu}{\partial r_2}\frac{\partial r_2}{\partial Q} + \frac{\partial \mu}{\partial r_3}\frac{\partial r_3}{\partial Q} = \frac{1}{\sqrt{3}}(3\mu_o \cos\delta)\hat{\zeta} = \frac{1}{\sqrt{3}}\mu_o\hat{\zeta} \qquad (2.18)$$

where δ is the angle between a CH bond and the ζ axis ($\cos\delta = 1/3$) and μ_o is the dipole moment derivative for a single CH bond. For the polarizability derivative we note that with C_{3V} symmetry its nonvanishing elements are $\frac{\partial \alpha_{\xi\xi}}{\partial Q}$, $\frac{\partial \alpha_{\eta\eta}}{\partial Q}$ and $\frac{\partial \alpha_{\zeta\zeta}}{\partial Q}$. They are calculated as follows

$$\begin{aligned}\frac{\partial \alpha_{\zeta\zeta}}{\partial Q} &= \frac{\partial \alpha_{\zeta\zeta}}{\partial r_1}\frac{\partial r_1}{\partial Q} + \frac{\partial \alpha_{\zeta\zeta}}{\partial r_2}\frac{\partial r_2}{\partial Q} + \frac{\partial \alpha_{\zeta\zeta}}{\partial r_3}\frac{\partial r_3}{\partial Q} \\ &= \frac{1}{\sqrt{3}}(3\alpha_o \cos^2\delta + 3R\alpha_o \sin^2\delta) = \frac{1}{3\sqrt{3}}(1+8R)\alpha_o\end{aligned} \qquad (2.19)$$

and similarly for the other elements,

$$\frac{\partial \alpha_{\xi\xi}}{\partial Q} = \frac{\partial \alpha_{\eta\eta}}{\partial Q} = \frac{1}{3\sqrt{3}}(4+5R)\,\alpha_o \qquad (2.20).$$

Substituting Eqs. (2.18) to (2.20) in Eq. (2.17) we get the following relations between the nonvanishing $\alpha^{(2)}$ elements for the CH_3 symmetric stretch

$$\alpha^{(2)}_{\xi\xi\zeta} = \alpha^{(2)}_{\eta\eta\zeta} = r\,\alpha^{(2)}_{\zeta\zeta\zeta} = \left(\frac{4+5R}{9}\right)\frac{\alpha_o \mu_o}{2\omega_q}\Delta\rho_q \quad \text{, with} \quad r = \frac{4+5R}{1+8R} \qquad (2.21).$$

We can repeat the same procedure to calculate $\alpha^{(2)}_{\xi\eta\zeta}$ for the CH_2 group, which has C_{2V} symmetry. We take the symmetry axis as ζ, and ξ is such that the $\xi\zeta$ plane is a mirror plane. For the symmetric stretch mode, the normal coordinate is $Q = \frac{1}{\sqrt{2}}(r_1 + r_2)$, where r_i is again the C-H bond distance for the i^{th} H atom. A similar calculation gives the following nonvanishing $\alpha^{(2)}$ elements for the CH_2 symmetric stretch

$$\alpha^{(2)}_{\xi\xi\zeta} = \frac{2}{\sqrt{3}}\left(\frac{2+R}{3}\right)\frac{\alpha_o \mu_o}{2\omega_q}\Delta\rho_q$$

$$\alpha^{(2)}_{\zeta\zeta\zeta} = \frac{2}{\sqrt{3}}\left(\frac{1+2R}{3}\right)\frac{\alpha_o \mu_o}{2\omega_q}\Delta\rho_q \qquad (2.22).$$

$$\alpha^{(2)}_{\eta\eta\zeta} = \frac{2}{\sqrt{3}}R\,\frac{\alpha_o \mu_o}{2\omega_q}\Delta\rho_q$$

With this simple bond aditivity model, we can determine not only the nonvanishing elements of $\alpha_{\xi\eta\zeta}$ but also the relative strengths between the CH_3 and CH_2 groups. Finally, we note that for a moiety that is cylindrically symmetric with the infrared transition moment along the symmetry axis ζ, there are only two nonvanishing independent

elements in $\alpha^{(2)}$, $\alpha^{(2)}_{\xi\xi\zeta} = \alpha^{(2)}_{\eta\eta\zeta}$ and $\alpha^{(2)}_{\zeta\zeta\zeta}$. This result also applies to the case of a CH_3 group with C_{3V} symmetry (see Eq. (2.21)). It is also a good model for the cyano group (C≡N) considered in Chapter 5. For these cases, we find from Eq. (2.14) for an azimuthally isotropic surface

$$\chi_{xxz} = \chi_{yyz} = \frac{1}{2} N_s \alpha \left[\langle \cos\theta \rangle (1+r) - \langle \cos^3\theta \rangle (1-r) \right]$$

$$\chi_{xzx} = \chi_{yzy} = \chi_{zxx} = \chi_{zyy} = \frac{1}{2} N_s \alpha \left(\langle \cos\theta \rangle - \langle \cos^3\theta \rangle \right) (1-r) \qquad (2.23)$$

$$\chi_{zzz} = N_s \alpha \left[r \langle \cos\theta \rangle + \langle \cos^3\theta \rangle (1-r) \right]$$

where $\alpha = \alpha_{\zeta\zeta\zeta}$, $r = \alpha_{\xi\xi\zeta} / \alpha_{\zeta\zeta\zeta}$, and θ is the polar angle of the symmetry axis ζ with respect to the lab z-axis. Due to the high symmetry in the hyperpolarizability tensor, the number of nonvanishing independent χ elements is reduced to three. They can be deduced from SFG measurement with three different input and output polarization combinations, for example, SSP, SPS, and PPP. Since an absolute determination of $N_s\alpha$ is usually not of interest, we can determine more conveniently from the measurements the ratios of independent nonvanishing χ elements. Then, from Eqs. (2.23) we can find the orientation θ and the depolarization ratio r of the moiety by assuming a δ-function distribution for θ. It should be noted that the phase of $\chi^{(2)}$ contains information about the absolute orientation of surface molecules. This can easily be seen in Eqs. (2.23), since the sign of cos θ (and therefore of $\chi^{(2)}$) changes if the molecules are pointing up or down at the interface. This will be important in Chapter 6.

In the case of SFG vibrational spectroscopy of alkyl chains (like the ones of surfactant molecules studied in this Thesis), one important feature of the technique is its ability to probe chain conformation. This was first demonstrated by Guyot-Sionnest *et. al.*[25] for a pentadecanoic acid ($CH_3(CH_2)_{13}COOH$) monolayer at the air/water interface. Figure 3 shows three SFG spectra obtained with SSP polarization combination for a pentadecanoic acid monolayer at various surface coverages. In Figure 3(a), the surface density is very high so that the monolayer is fully packed. In this case, the alkyl chains are known to be in a nearly all-trans conformation with the chains approximately along the surface normal. The spectra is then dominated by two peaks at ~ 2875 and 2940 cm^{-1}, which can be assigned to the stretch modes of the terminal CH_3 group (detailed assignments will be discussed in Chapter 3). Even though the sample contains many more CH_2 groups, their stretch modes at ~ 2850 and 2920 cm^{-1} are hardly discernible. This can be explained by considering the geometry of an alkyl chain in the all-trans conformation (see Figure 3(a) of Chapter 1). The CH_2 groups are arranged in a zigzag configuration with adjacent groups pointing in opposite directions. This near inversion symmetry leads to a cancellation of signals generated by the CH_2 groups and therefore their vibrations are inactive in SFG spectroscopy. As the monolayer surface coverage decreases (Figures 3(b) and 3(c)), two changes take place. First, the CH_2 modes become apparent in the spectra and eventually become the prominent peaks. This is accompanied by a reduction in the strength of CH_3 peaks. These features can be explained by recalling that as the monolayer becomes more loosely packed so that the packing constraints and chain-chain interaction are reduced, the population of thermally generated gauche conformations increases. These gauche conformations break the inversion symmetry of an all-trans alkyl chain

(Figure3(b) of Chapter 1) so that CH_2 modes now become allowed in SFG spectroscopy. The gauche conformations also randomize the orientations of terminal CH_3 groups, leading to a reduction in their contribution to the observed spectra ($\langle\cos\theta\rangle$ in Eq. (2.14) decreases). We should note that in the limit of a large number of gauche defects in the alkyl chains the orientations of both CH_2 and CH_3 groups become random, so that one may expect that all peaks should become vanishingly small. This will be discussed in more detail in Chapter 6. From this discussion it is clear that even such qualitative analysis of the SFG spectra of alkyl chains in the CH stretch region can give very important information about the chain conformation at interfaces.

In summary, SFG vibrational spectroscopy has some unique advantages and capabilities as a surface analytical tool. It is shown to be intrinsically surface specific and therefore able to obtain surface spectra even when the bulk is resonantly absorbing, as in the study of a neat liquid surface. It also has submonolayer sensitivity and as an optical technique can probe any interface accessible by light, including buried interfaces. As we will see in the next section, usually ultrashort laser pulses are used, allowing surface dynamics in the picosecond or femtosecond timescales to be studied. In the case of vibrational spectroscopy of alkyl chains, we have seen that SFG provides very direct qualitative information about chain conformation. This kind of information is not easily obtained by other techniques in such a direct way. We will now briefly outline the experimental setup for SFG vibrational spectroscopy.

C. Experimental Implementation

Typical values of resonant $\chi^{(2)}$ for a monolayer of alkyl chains can be estimated using Eq. (2.17) and the appropriate parameters from measured Raman cross sections and infrared absorption spectra.[4,21,26] Such estimates give $\chi^{(2)} \sim 10^{-15}$ esu, in good agreement with experimental values. For detecting such small nonlinearities, usually pulsed lasers are needed. As a comparison, if 1 W CW lasers are used as sources for both ω_1 and ω_2, and focussed to a 1 mm^2 spot size on the surface, the output signal calculated from Eq. (2.6) would be only 0.16 photons/s. Such a small signal can easily be masked by fluorescence or stray light. If a pulsed laser (pulsewidth 10 ps) is used instead, typical intensities at the sample with a 1 mm^2 beam size are about 1 GW/cm^2. In this case the output signal is about 160 photons/pulse, which is easily detectable since a photomultiplier gated detection system can detect less than one photon/pulse.

Therefore a typical SFG setup consists of a pulsed laser system able to generate tunable IR pules and a fixed frequency visible pulse. The pulses are temporally and spatially overlapped at the sample surface and the reflected signal is detected by a photomultiplier/gated integrator detection system after spatial and spectral filtering to eliminate fluorescence and stray light. A schematic diagram of our SFG setup is shown in Figure 4. It is usual to have the visible input beam with larger pulse energy than the IR pulse. The visible beam is lightly focussed with a long focal length lens ($f \sim 1$ m) with the waist beyond the sample. This makes the reflected SFG output to be convergent (see the Appendix for a discussion on the divergence of the SFG output), so that spatial separation of SFG and visible beams is facilitated. The IR beam, on the other hand, should be focussed before the sample by a shorter focal length lens ($f \sim 10$ to 20 cm), so that the sample is close to the imaging point for the IR source. This minimizes changes in the

spatial overlap of the two beams due to variations in the IR beam direction as its frequency is tuned, as in the case where difference-frequency generation in a nonlinear crystal is used to generate the IR pulses. It is also good to have the spot size of one of the beams at the sample a few times larger than the other beam. This minimizes the effect of overlap changes on the output signal.

A major component in an SFG setup is a broadly tunable source of high power infrared pulses. They can be generated by frequency conversion in nonlinear crystals, as done in our laboratory, by stimulated Raman scattering of a tunable visible laser in a high-pressure gas cell[27] or by a free-electron laser.[28,29] For the work reported in this Thesis, two SFG setups have been used. Most data were obtained in an existing setup (hereafter called setup A) but the spectra in the CO stretch range in Chapter 4 and all spectra in Chapter 5 were taken in a newly constructed setup (hereafter called setup B). In setup A the main laser source is a homebuilt high power Nd:YAG laser with wavelength 1.06 μm, 10 mJ pulse energy and ~ 40 ps pulsewidth, operating at a repetition rate of 10 Hz. The infrared generation is done in an optical parametric oscillator and amplifier (OPG/OPA) based on $LiNbO_3$ crystals. It generates pulses of energy ~ 300 μJ and pulsewidth ~ 20 ps, tunable from 1.45 to 4 μm (6900 to 2500 cm^{-1}) and it has been thoroughly describe elsewhere.[30] The IR bandwidth varies throughout the tuning range from ~ 8 cm^{-1} at 2800 cm^{-1} to ~ 45 cm^{-1} at 3700 cm^{-1}. The visible pulses at 532 nm are generated by SHG in a KD^*P crystal and have energies about 700 μJ and pulsewidth ~ 28 ps. The visible and IR pulses are incident on the sample at angles 42° and 51° and have spot sizes of approximately 300 μm and 500 μm, respectively. The reflected SFG output was selected with a set of pinholes defining a narrow detection solid angle, spectrally

filtered with two dielectric short-pass edge filters (OD 6 blocking at 532 nm and ~ 75% transmission at 480 nm) and directed by an aluminum mirror to a photomultiplier tube (PMT). The PMT pulses were amplified by a gated integrator and stored in a computer. Most spectra were taken with an average of 2 or 3 scans, each with accumulation of 100 or 150 laser shots per data point. The data acquisition time for one scan of 50 points was about 20 minutes.

In setup B the main laser source is a commercial high power Nd:YAG laser with wavelength 1.06 μm, 30 mJ pulse energy and ~ 25 ps pulsewidth, operating at a repetition rate of 20 Hz. The infrared generation is done by difference-frequency mixing (DFG) between part of the laser fundamental and a tunable near IR laser in a $AgGaS_2$ crystal. The near IR laser is the output of an OPG/OPA based on BBO crystals and pumped by the third harmonic of the laser (355 nm). This system has also been described in detail elsewhere[31,32] and is shown schematically in Figure 5. The DFG stage generates IR pulses of energy ~ 100 μJ and pulsewidth ~ 15 ps, tunable from 2.5 to 9 μm (4000 to 1100 cm^{-1}) with a 10 cm^{-1} bandwidth. The visible pulses at 532 nm are generated by SHG in a BBO crystal and have energies about 1.5 mJ and pulsewidth ~ 18 ps. The visible and IR pulses are incident on the sample at angles 44° and 57° and have spot sizes of approximately 1.2 mm and 0.6 mm, respectively. The spectra of Chapter 4 in the CO stretch range were taken with spot sizes of 300 μm and 500 μm for the IR and visible beams, respectively. The SFG detection system is very similar to the one of system A. Most spectra were taken with an average of 2 or 3 scans, each with accumulation of 100 or 150 laser shots per data point. The data acquisition time for one scan of 50 points was about 10 minutes.

As a final note, we should mention that the SFG detection can also be implemented with a low-noise, slow-scan CCD camera. This has the advantage that the CCD cameras have higher quantum efficiencies (~ 70%, compared to typically 25% for the best PMT's) and a much broader spectral response (typically from 900 to 400 nm). This allows, for example, the use of near IR pump as the "visible" beam. In some cases two-photon fluorescence caused by the near IR excitation can be considerably reduced, or the surface damage threshold in the near IR is higher than in the visible, leading to an increase in signal-to-noise ratio. One disadvantage of using a CCD camera is that the detection system cannot be gated and therefore becomes very sensitive to stray light, although with careful shielding of the detector and sample area this background noise can be reduced to acceptable levels.

The imaging capabilities of a CCD camera offer two more great advantages. First, the divergences of SFG beam and fluorescence or scattered light from the sample are not the same. If the SFG beam is focussed on the CCD detector, the background light will be spread over a much larger area and could therefore be easily subtracted out. Second, from Eq. (2.5) we see that the output direction of the sum-frequency beam depends on the frequencies of both IR and visible inputs. Therefore as the IR is tuned there is a small change in the output direction. If the IR bandwidth is very broad, as in the case of femtosecond pulses, this effect can be used to obtain spectra with frequency resolution better than the laser bandwidth. Different IR frequency components will generate output in different directions that will be detected in different pixels of the camera. This mode of operation has been recently demonstrated[33,34] and is called self-dispersive SFG. In this geometry, it is advantageous to have the IR and visible beams in a counter-propagating

geometry ($\beta_2 < 0$) to maximize the angular dispersion $\Delta\theta$ of the output (of the order of ~ 1 mrad/cm^{-1}), which can be calculated from Eq. (2.5). The spectral resolution F in this self-dispersive mode is determined by the ratio of beam diameter at the CCD chip to its linear dispersion (μm/cm^{-1}). If the SFG beam is focussed on the CCD chip, it is easy to show that F is given by

$$F \equiv \frac{2w_o}{\Delta x} = \frac{2\lambda}{\pi w_s \Delta\theta} \tag{2.24}$$

where w_o is the beam waist radius at the CCD chip, Δx is the linear dispersion on the chip, $\Delta\theta$ is the output angular dispersion, w_s is the output beam radius at the sample position (measured perpendicular to the propagation direction) and λ is the output wavelength. We see that F depends only on the beam size at the sample and on the SFG angular dispersion and is independent of the lens used to image the beam on the CCD chip, provided that it is free from spherical or chromatic aberrations. In Ref. 33, a resolution of 5 cm^{-1} was obtained with an IR source of ~ 50 cm^{-1} bandwidth.

References

(1) Y. R. Shen, *The Principles of Nonlinear Optics*, Wiley-Interscience, New York (1984).

(2) For a review of the development of SHG and SFG as surface probes from a historic perspective, see Y. R. Shen, *Surf. Sci.* **299/300**, 551 (1994).

(3) Y. R. Shen, *Annu. Rev. Phys. Chem.* **40**, 327 (1989).

(4) Y. R. Shen, in *Nonlinear Spectroscopy for Molecular Structure Determination*, R. W. Field, E. Hirota, J. P. Maier and S. Tsuchiya, eds., IUPAC Chemical Data Series, Blackwell Science, Oxford, UK, Chapter 10, (1998).

(5) Y.R. Shen, in *Fundamental Systems in Quantum Optics* (53rd Ecole d'ete de Physique Theorique, Les Houches, France, 1990), J. Dalibard, J. M. Raimond and J. Zinn-Justin, eds., North-Holland, New York, Course 15, p. 1053, (1992).

(6) P. Guyot-Sionnest, W. Chen and Y. R. Shen, *Phys. Rev. B* **33**, 8254 (1986).

(7) P. Guyot-Sionnest and Y. R. Shen, *Phys. Rev. B* **38**, 7985 (1988).

(8) R. Superfine, Ph.D Thesis, University of California, Berkeley (1991), unpublished.

(9) R. Superfine, J. Y. Huang and Y. R. Shen, *Phys. Rev. Lett.* **66**, 1066 (1991).

(10) Q. Du, R. Superfine, E. Freysz, Y. R. Shen, *Phys. Rev. Lett.* **70**, 2313 (1993).

(11) G. A. Sefler, Q. Du, P. B. Miranda, Y. R. Shen, *Chem. Phys. Lett.* **235**, 347 (1995).

(12) P. B. Miranda, Q. Du, Y. R. Shen, *Chem. Phys. Lett.* **286**, 1 (1998).

(13) B. D. Casson and C. D. Bain, *Langmuir* **13**, 5465 (1997).

(14) G. R. Bell, C. D. Bain and R. N. Ward, *J. Chem. Soc. Faraday Trans.* **92**, 515 (1996).

(15) R. Braun, B. D. Casson, and C. D. Bain, *Chem. Phys. Lett.* **245**, 326 (1995).

(16) T. G. Zhang, C. H. Zhang and G. K. Wong, *J. Opt. Soc. Am. B* **7**, 902 (1990).

(17) In the case of SFG, the *first* two indices of $\chi^{(2)}$ are also interchangeable, if the sum-frequency and visible beams are away from electronic resonances, as will be mentioned later.

(18) P. Ye and Y. R. Shen, *Phys. Rev. B* **28**, 4288 (1983).

(19) Ref. 1, page 17.

(20) Ref. 1, page 171.

(21) Q. Du, Ph.D Thesis, University of California, Berkeley (1994), unpublished.

(22) D. A. Long, *Raman Spectroscopy*, McGraw-Hill, New York (1977).

(23) K. M. Gough, *J. Phys. Chem.* **91**, 2424 (1989).

(24) R. G. Snyder, *J. Molec. Spectrosc.* **36**, 221 (1970).

(25) P. Guyot-Sionnest, J. H. Hunt and Y. R. Shen, *Phys. Rev. Lett.* **59**, 1597 (1987).

(26) X. D. Zhu, Ph.D Thesis, University of California, Berkeley (1989), unpublished.

(27) P. Rabinowitz, B. N. Perry and N. J. Levinos, *IEEE J. Quantum Electron.* **QE-22**, 797 (1986).

(28) A. Peremans, A. Tadjeddine, M. Suhren, R. Prazeres, F. Glotin, D. Jaroszynski and J. M. Ortega, *J. Electron. Spectrosc. Rel. Phen.* **64/65**, 391 (1993).

(29) M. Barmentlo, G. W. 't Hooft, E. R. Eliel, E. W. M. van der Ham, Q. H. F. Vrehen, A. F. G. van der Meer and P. W. van Amersfoort, *Phys. Rev. A* **50**, R14 (1994).

(30) J. H. Hunt, Ph.D Thesis, University of California, Berkeley (1987), unpublished.

(31) D. S. Kim, Ph.D Thesis, University of California, Berkeley (1997), unpublished.

(32) J. Y. Zhang, J. Y Huang, Y. R. Shen and C. Chen, *J. Opt. Soc. Am. B* **10**, 1758 (1993).

(33) E. W. M. van der Ham, Q. H. F. Vrehen and E. R. Eliel, *Opt. Lett.* **21**, 1448 (1996).

(34) E. W. M. van der Ham, Q. H. F. Vrehen and E. R. Eliel, *Surf. Sci.* **368**, 96 (1996).

Figure Captions

Figure 1. Geometry for Sum-Frequency Generation from an interface in the reflected direction. The polarization sheet generated at the interface by the input fields is imbedded in a thin interfacial layer *i* of refractive index n′.

Figure 2. Possible lineshapes of an SFG resonance with χ_{NR} complex and χ_q real (see Eq. (2.13)): (a) χ_{NR} is real and has the same sign as χ_q; (b) χ_{NR} is negligible compared to χ_q/Γ_q; (c) χ_{NR} is real and has the opposite sign as χ_q; (d) χ_{NR} is imaginary and has the opposite sign as χ_q/Γ_q, with $|\chi_{NR}| > |\chi_q/\Gamma_q|$. Adapted from Ref. 4.

Figure 3. SFG spectra for a pentadecanoic Langmuir film at various surface coverages: (a) 22 $Å^2$/molecule, (b) 34 $Å^2$/molecule, (c) 47 $Å^2$/molecule. The polarization combination is SSP. The spectra have been normalized by N_s^2 to account for the different surface densities (see Eq. (2.14)). Adapted from Ref. 25.

Figure 4. Typical setup for sum-frequency vibrational spectroscopy. The generated SFG signal is filtered spatially and spectrally from the scattered visible light and detected by a photomultiplier (PMT).

Figure 5. Schematic diagram of the OPG/OPA and DFG stage used as IR source in the SFG setup B.

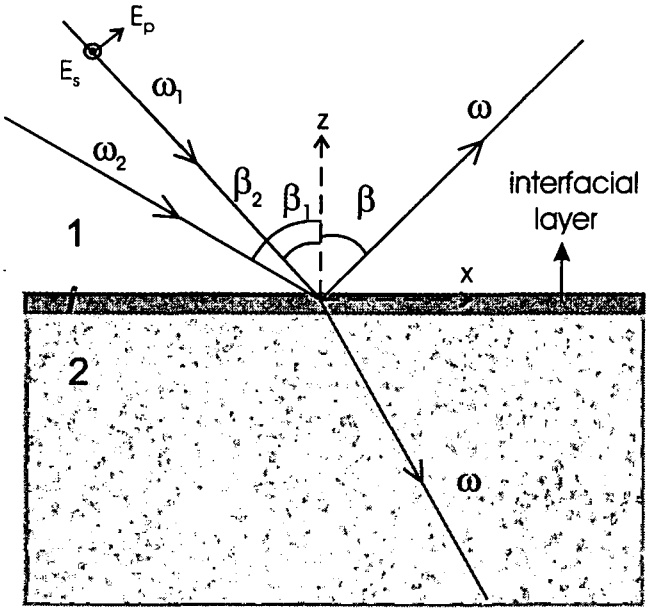

Figure 1

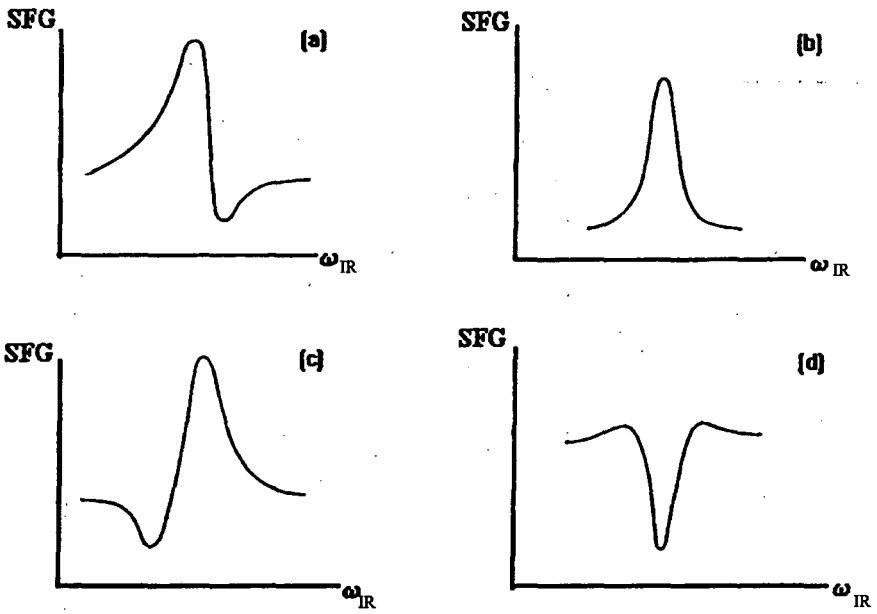

Figure 2

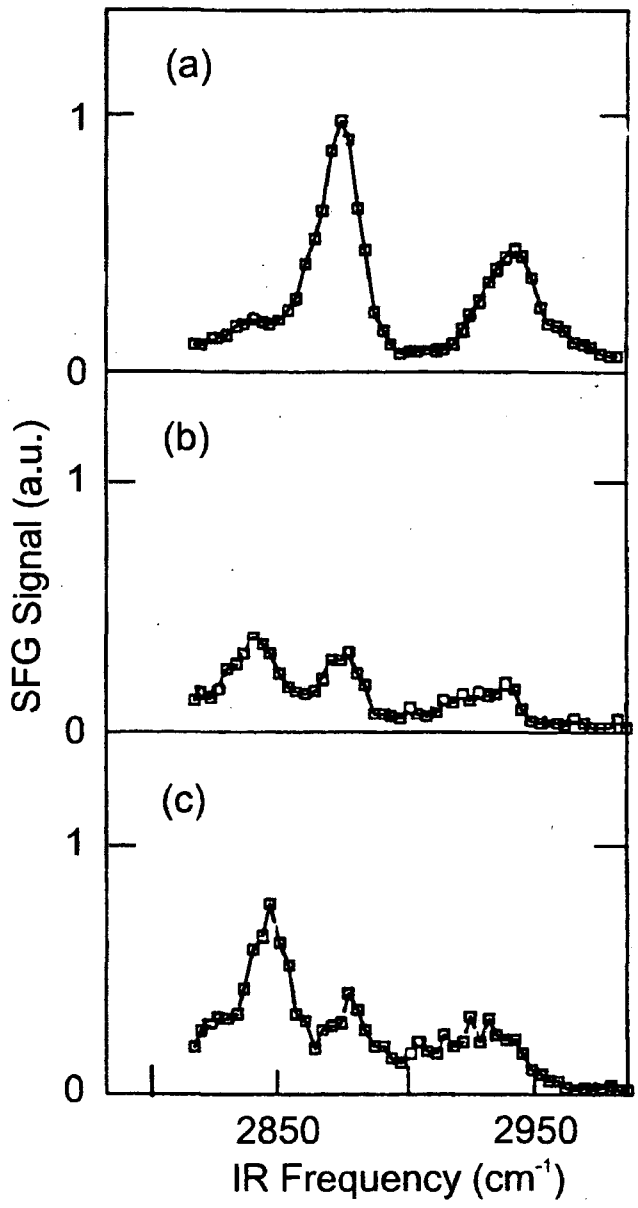

Figure 3

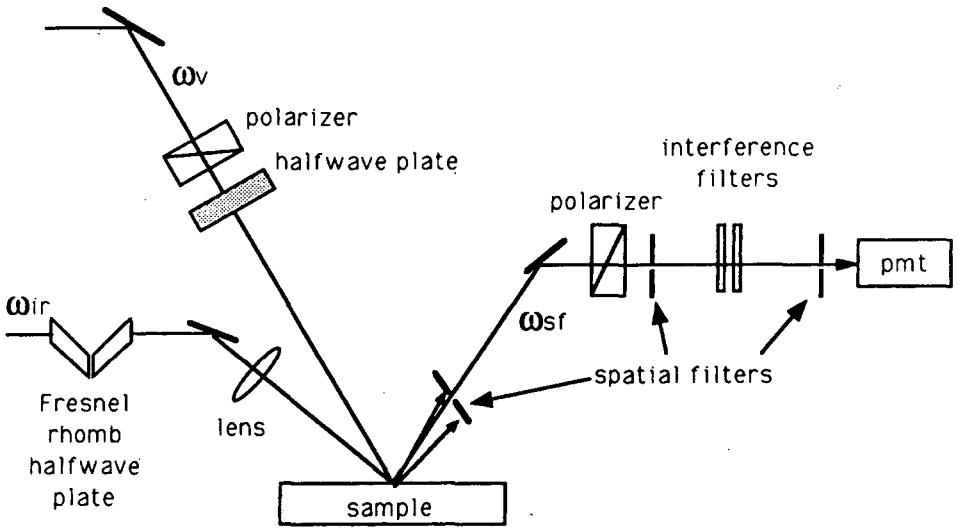
ωv
polarizer
halfwave plate
interference
filters
polarizer
pmt
ωir
ωsf
spatial filters
Fresnel
rhomb
halfwave
plate
lens
sample

Figure 4

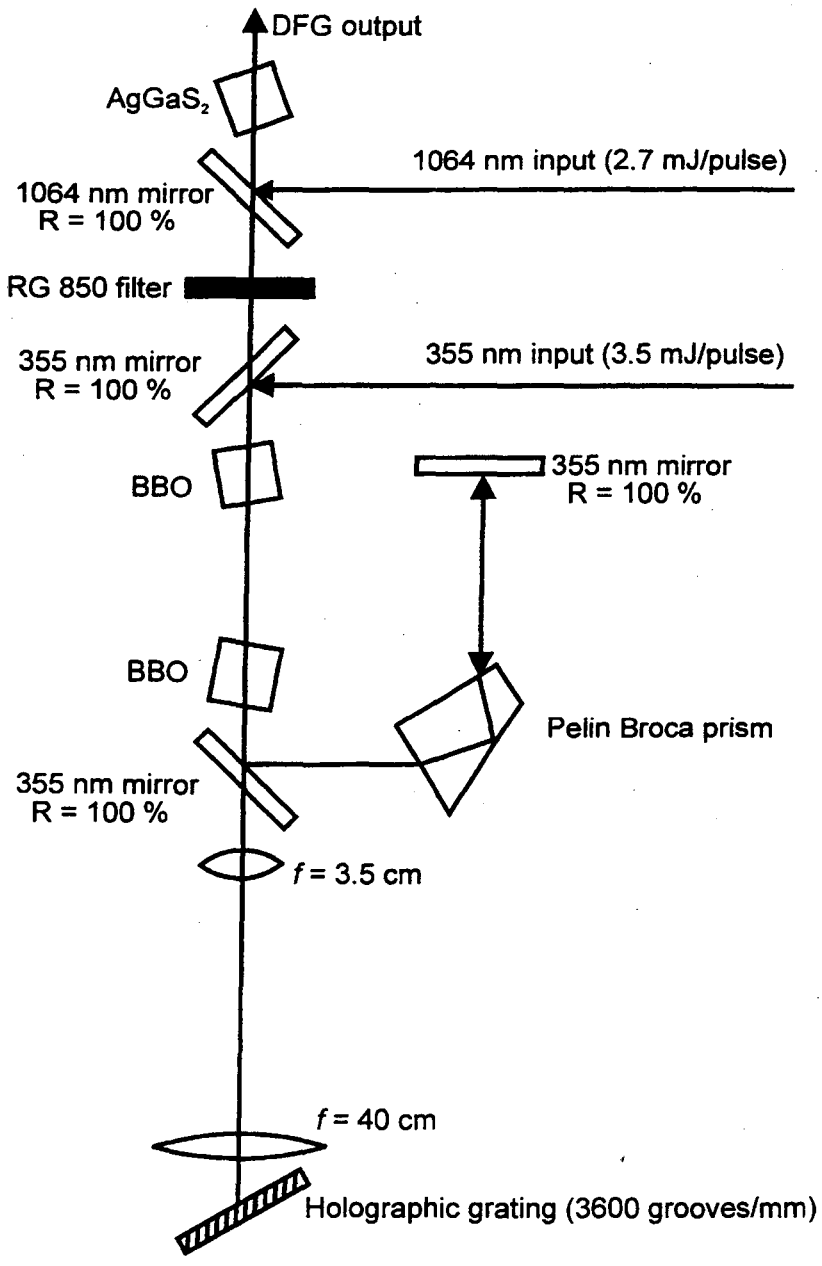
DFG output
$AgGaS_2$
1064 nm input (2.7 mJ/pulse)
1064 nm mirror
R = 100 %
RG 850 filter
355 nm mirror
R = 100 %
355 nm input (3.5 mJ/pulse)
BBO
355 nm mirror
R = 100 %
BBO
Pelin Broca prism
355 nm mirror
R = 100 %
f = 3.5 cm
f = 40 cm
Holographic grating (3600 grooves/mm)

Figure 5

Chapter 3. Surface Crystallization of Alcohol Langmuir Films and Liquid Alkanes

A. Introduction

Linear hydrocarbon chains (alkyl chains) are basic ingredients for many important organic molecules such as lipids, liquid crystals, and lubricants. They play an important role in determining the characteristic properties of such molecules and have been the subject of much continuing research.[1] One simple system involving such chains consists of a monolayer of fatty acid ($CH_3(CH_2)_{n-2}COOH$) or alcohol ($CH_3(CH_2)_{n-1}OH$) molecules spread on a water surface. These films, known as Langmuir films, have received considerable attention as representatives of numerous biological systems.[2] The rich phase behavior of Langmuir films has been well documented.[3] Recently, both the free liquid surface (vapor/liquid interface) of longer chain n-alkanes ($CH_3(CH_2)_{n-2}CH_3$) and Langmuir films of 1-alcohols in equilibrium with an excess alcohol drop have been shown to undergo surface-ordering phase transitions at prescribed temperatures.[4-9] The transitions possess many common features though the systems are fundamentally different. Free exchange of molecules occurs between the surface and bulk in the case of liquid n-alkanes while alcohol molecules are constrained by insolubility to remain at the water surface. The alcohol monolayer also interacts strongly with the water surface via hydrogen bonding. It is clear, however, that the strong van der Waals chain-chain interaction is a major driving force for surface crystallization in both cases.

Surface freezing of liquid n-alkanes has been examined using X-ray reflectivity,[4,5] grazing incidence X-ray diffraction,[4] surface tension measurements,[4-6] and molecular-

dynamics simulations.[7] All these studies have indicated an abrupt formation of a dense, crystalline surface monolayer at a temperature above the bulk freezing point if the alkyl chain length n is $15 \leq n \leq 50$.[10] The structure of the monolayer is reported to be similar to that of a lamella of the high-temperature crystalline rotator phase found in many alkanes. In this phase, nearly all-trans chains are hexagonally packed into lamellar layers with the molecular axes oriented normal to the layers.[1] Resolution-limited diffraction peaks indicate crystalline coherence lengths exceeding 1000 Å within the frozen surface monolayer.[4]

X-ray diffraction,[8] ellipsometry,[9] and surface tension[9] experiments have been performed on Langmuir films of medium-chain fatty alcohols formed by spontaneous spreading from an alcohol drop placed on the water surface. The surface monolayer is then in equilibrium with the remaining drop.[3] Upon temperature changes, the structure of the monolayer is expected to vary until the new equilibrium is established. The experiments have revealed that an alcohol monolayer can experience a first-order phase transition several degrees above the bulk freezing temperature of the excess alcohol drop. The monolayer crystallizes into a two-dimensional hexagonal close-packed structure. The packing density of the molecules continues to increase below the transition point. The long-range positional ordering can exceed 2000 Å.

Here we study these surface crystallization phenomena using SFG vibrational spectroscopy.[11] As we have mentioned in Chapter 2, the technique provides information about the conformation and orientation of alkyl chain at the interface. Our main goal is to compare the nature of the surface phase transitions by studying the surface structure before and after the transition for both a liquid alkane and an alcohol Langmuir film.

B. Experimental Details

For the study of the surface freezing transition of liquid alkanes, n-eicosane ($C_{20}H_{42}$) was used. The material was purchased from Sigma Chemical Company and used without further purification. The bulk freezing temperature of n-eicosane is 35.6 °C, and the surface freezing transition occurs 3 °C higher. The sample was contained in a thin-wall Teflon cell surrounded by copper plates, except for a slit at the top for access of the laser beams. The sample temperature was controlled by changing the temperature of the copper block with a commercial temperature controller. It was monitored directly with a Teflon-coated thermocouple and was stable to less than 0.1 °C. To make sure that our system was the same as that studied by others, surface tension as a function of temperature was measured using a balance with a Wilhelmy plate.[12] A slightly deeper cell was used for the surface tension measurement. The cell construction was similar to the one used for SFG measurements, except that instead of a slit, there was a small hole on the top to allow a thin wire through for hanging the Wilhelmy plate. The temperature control was again better than 0.1 °C. Our results were identical to those published.[4-6]

Near the surface freezing temperature, the laser repetition rate was reduced from 10 Hz to 1 Hz to avoid problems associated with laser heating. The energy absorbed from each IR pulse could be enough to locally heat up and melt the solid monolayer. At a 10 Hz repetition rate, the melted monolayer was unable completely recrystallize between successive laser pulses when the temperature of the system was too close to the surface freezing temperature ($\Delta T < 1$ °C). (The resulting spectra were found to be a mixture of the spectrum of the air/liquid interface and that of the liquid surface covered by a

crystalline monolayer.) At the reduced rate of 1 Hz, the spectra were found to change abruptly (within 0.1 °C) at the surface freezing temperature, indicating complete recrystallization of the surface monolayer between successive laser pulses and the first-order nature of the phase transition.

For the study of a fatty alcohol Langmuir film, 1-dodecanol ($C_{12}H_{25}OH$) purchased from Sigma Chemical Company and Millipore ultrapure water with resistivity higher than 18 MΩ·cm were used. Liquid dodecanol freezes at 22.0 °C while the surface-ordering temperature of the monolayer is 39.0 °C (measured from the temperature dependence of surface tension). The film was formed by placing a piece of solid dodecanol on a heated water surface. The dodecanol piece immediately melted and spread into a monolayer with the excess remaining aggregated in the form of a lens. The same temperature-controlled cell described above was used to control the temperature of the alcohol film.

C. Results and Discussion

As already mentioned in Chapter 2, within the electric dipole approximation, SFG can only be generated at surfaces or interfaces of a liquid that has inversion symmetry. However, multipole contributions due to discontinuity of materials parameters across the interface can in principle be as big as the dipole contribution from the surface. One of the challenges of surface SFG spectroscopy is then to determine the bulk or surface origin of the features observed in the spectra. In the case of Langmuir films of fatty alcohols, the surface specificity of SFG is guaranteed when probing CH stretches since only a monolayer of alcohol molecules is present on the water surface. To establish the surface

specificity of SFG when studying liquid n-alkanes, spectra were taken at the air/liquid and fused quartz/liquid interfaces with n-hexadecane ($C_{16}H_{34}$). The spectra taken with SSP polarization combination at room temperature (20 °C) are shown in Figure 1. As both systems possess the same bulk liquid structure, differences between the spectra can be directly attributable to differences in interfacial properties. The contrast in Figure 1 is then a clear proof that the contribution from the interfacial regions dominates over any bulk contributions.

To assign the peaks in Figure 1 to vibrational modes of alkyl chains, we follow the assignments of IR and Raman spectra of bulk alkanes.[13-16] The CH stretch modes are assigned as follows: ~ 2875 cm^{-1} to the CH_3 symmetric stretch (r^+), ~ 2960 cm^{-1} to the two nearly degenerate CH_3 asymmetric stretches (r^-), ~ 2850 cm^{-1} and ~ 2920 cm^{-1} to CH_2 symmetric (d^+) and asymmetric (d^-) stretch modes, respectively. The CH_3 symmetric stretch (r^+) is actually split by Fermi resonance interaction of the CH_3 symmetric stretch (r^+) with overtones of CH_3 bending modes, leading to another peak at ~ 2935 cm^{-1} which we will refer to as r^+_{FR}. These assignments are based on bulk IR and Raman measurements, and slight shifts may occur in peak positions reflecting changes in the chemical environment when going from the bulk to the surface. Since our laser bandwidth is about 10 cm^{-1}, frequency shifts of a few wavenumbers cannot be easily discernible. This large bandwidth also leads to strong overlap of the d^-, r^+_{FR} and r^- peaks, making a detailed discussion of their changes less straightforward. The r^+ and d^+ modes are however easily resolved and most quantitative analysis is usually done for those peak strengths.

C.1 Quartz / Alkane and Air / Alkane Interfaces

We begin our discussion by comparing the spectrum of air/hexadecane interface with that of fused quartz/hexadecane. As shown in Figure 1(a), the spectrum of the air/hexadecane interface is dominated by contributions from the CH_2 symmetric stretch (d^+) with a reasonably strong contribution from the CH_3 symmetric stretch (r^+). The peaks due to d^-, r^+_{FR} and r^- are unresolved and show up as one broad resonance at ~ 2930 cm^{-1}, with at most a very small contribution due to the CH_3 asymmetric stretch r^-. The spectrum of the quartz/hexadecane interface, on the other hand, is dominated by the signal from the CH_2 and CH_3 asymmetric stretches (d^- and r^-, respectively), with a small peak from d^+ and no contribution from r^+. As mentioned in the previous Chapter, if the hydrocarbon chains adopt an all-trans conformation at the interfaces, the CH_2 groups should not be active in SFG spectroscopy due to inversion symmetry.[17] The presence of strong peaks due to CH_2 stretches then suggests that the hexadecane molecules on the surface have a considerable amount of gauche defects. The difference in the activity of the CH_3 stretch modes is due to the different orientation of the molecules at the interface. With the SSP polarization, the vibrational transitions participating in the SFG spectra must have a finite component of the IR transition moment along the surface normal. For the CH_3 groups, this means that if their symmetry axis is along the surface normal the r^+ mode will be most pronounced, while the r^- peak will be missing; if the symmetry axis is however along the surface plane, the reverse will happen (r^+ missing, r^- strong); if the symmetry axis is on average tilted from the surface normal, both r^+ and r^- should appear in the spectrum. Our spectra in Figure 1 then suggests unambiguously that the hexadecane molecules on average stand upright at the air/hexadecane interface with a significant

amount of gauche defects in the chains, while they lie nearly flat at the quartz/hexadecane interface.

Analogous spectra have been observed for the air/liquid interfaces with n-eicosane (see Figure 3) and n-tridecane (not shown). Having fewer than 15 carbon atoms, tridecane is one of those alkanes that do not exhibit surface freezing.[5,6] With decreasing chain length, the strength of the CH_3 symmetric peak increases relatively to the CH_2 symmetric peak in the SSP spectra of the air/liquid interface. This can be attributed to the increase in the relative concentration of CH_3 groups versus CH_2 groups, as well as to the decrease in the overall percentage of gauche conformations as the chain length is shortened, which would tend to lower the CH_2 contribution. Otherwise, liquid n-alkanes with or without the capability of surface freezing appear to share similar free liquid surface structures. The air/liquid spectra also showed no changes when heated up to 100 °C.

The CH_3 signals present in the SFG spectra of n-alkanes require some explanation. Unlike an alcohol molecule, n-alkanes are symmetric molecules with methyl groups terminating the alkyl chains at both ends. The sum-frequency signals generated from CH_3 vibrations at opposite ends of a molecule are largely out of phase due to opposing orientations of the two end groups, if the chains are in an all-trans conformation. A net CH_3 signal may still be observed from an n-alkane molecule, as in the spectra of Figure 1, due to differences in the end-groups orientations and/or due to differences in the fields of the IR and visible inputs experienced by the two end-groups. We will discuss this in more detail in the following.

The molecular orientation revealed by SFG is consistent with other observations. At the liquid/graphite interface, STM studies[18,19] have shown that the n-alkane molecules organize in lamellae with the extended alkyl chains oriented parallel to the lattice axis within the basal plane of graphite. In our case, since we have used fused quartz, the molecular orientation should be azimuthally isotropic in the surface plane. Furthermore, the quartz/hexadecane spectrum did not change significantly upon heating to temperatures as high as 100 °C, consistent with a azimuthally isotropic arrangement of flat, kinked alkyl chains. Studies by molecular dynamics simulations have also suggested that for a thin film of hexadecane adsorbed on a solid surface, the first monolayer adjacent to the solid surface preferentially lie parallel to the surface, while the outermost layer at the vapor/liquid interface prefers to orient normal to the surface.[7]

C.2 Surface Crystallization of an Alcohol Langmuir Film

SFG spectra of the dodecanol Langmuir film are shown in Figure 2 for temperatures above (T = 43 °C) and below (T = 27 °C) its surface ordering phase transition. For both high and low temperatures, CH_3 r^+ and r^- peaks dominate the SSP and SPS spectra, respectively. Signals due to CH_2 stretches are relatively weak and show up only in the SSP spectra as a shoulder at ~ 2850 cm^{-1}, which almost disappears below the surface ordering transition.

In an alcohol Langmuir film, the molecules are anchored to the water surface by their hydrophilic OH groups while the hydrophobic alkyl tails are directed away from the surface. The weakness of CH_2 signals indicates that the alkyl chains are in a predominately all-trans configuration, and it is more so after the surface crystallization.

This is because when the alkyl chains are in the all-trans conformation, the sum-frequency signal from different CH_2 groups should nearly cancel out through inversion symmetry. Gauche defects along the chains would break the symmetry and yield an observable CH_2 signal.[17] The situation is very similar to the fully packed pentadecanoic acid Langmuir film studied earlier by SFG and discussed in Chapter 2.

Orientational order of the methyl groups (CH_3) at the end of the elongated alkyl chains is responsible for the pronounced CH_3 r^+ and r^- peaks. As outline in Chapter 2 (see Eqs. (2.8) and (2.23)), the ratios of χ_{yyz} to χ_{yzy} for the CH_3 symmetric stretch (obtained from the SFG spectra with SSP and SPS polarizations, respectively) may yield information about the orientation of the terminal CH_3 groups. If we assume a δ-function distribution for the tilt angles of the dodecanol molecules and R = 0.14 (see Eq. (2.21)) as determined from theoretical calculations of polarizability derivatives for the CH bond,[20] we obtain tilt angles of a dodecanol molecule of about 5° at 43 °C and 3° at 27 °C. Because of the simplifying assumption in the orientational distribution function, these tilt angles merely establish that the alkyl chains are oriented primarily vertically both above and below the surface crystallization transition temperature.

The considerable increase in the SFG signal of the CH_3 peaks below the phase transition temperature, shown in Figure 2, can be largely attributed to an increase in surface density. The small variation of the chain orientation results only in a minor change in the SFG susceptibilities (≈ 5%) of the r^+ mode, insufficient to explain the significant change in signal strength observed experimentally. An increase in surface density of ≈ 20% is then required to explain the observed changes in the SSP and SPS spectra. With a reported surface area of 21.0 $Å^2$ per alcohol molecule at 27 °C,[8] this

would give ≈ 25 Å^2 per alcohol molecule before the transition at 43 °C. An area of 25 Å^2 per molecule is known for the liquid condensed phase of many fatty alcohol and fatty acid Langmuir films.[3] The increased steric interactions between molecules after the surface monolayer ordering force them into a configuration where gauche defects in the alkyl chains become less likely, as evidenced by the significantly weaker d^+ shoulder in Figure 2(b).

Our results are at variance with the conclusion drawn from the recent ellipsometry experiment on the dodecanol Langmuir film.[9] The reported increase of 8 Å in monolayer thickness upon surface crystallization is unlikely, given that both before and after the phase transition the alkyl chains are nearly all-trans and erect as revealed by SFG and that 8 Å is more than half the length of an extended dodecanol molecule with 1.27 Å per C-C bond.[1] The cause for misinterpretation of the ellipsometry data can be traced to the use of the liquid refractive index for the monolayer film above the transition temperature. Though lacking crystalline order, there is no reason to believe that the high-temperature monolayer film should take on bulk liquid parameters. Modeling the film by an adjustable refractive index n and a constant thickness of d = 14 Å as suggested by the SFG measurements, an increase in (n-1) of only 7% upon surface crystallization is sufficient to account for the observed jump in the phase difference between reflected S- and P- polarized beams. The estimated increase in surface density of ≈ 20% would be enough to provide for the necessary change in refractive index of the film according to the simple Lorentz oscillator model where (n^2 - 1) is proportional to molecular density. More recently, Bain *et. al.*[21] have used a combination of both SFG spectroscopy and ellipsometry to obtain quantitative measurements of both surface density and average

orientation of alcohol molecules above the surface crystallization temperature. Our estimates given above agree well with their more quantitative results.

C.3 Surface Crystallization at the Air / Alkane Interface

The n-eicosane SFG spectra before and after surface freezing are shown in Figure 3. The SSP spectrum of n-eicosane above the phase transition is quite similar to the one of hexadecane, shown in Figure 1(a), with only a minor change in the relative strength of CH_2 and CH_3 peaks as discussed above. The SPS spectrum at the same temperature exhibits three peaks: the CH_3 asymmetric stretch r^- appears at the usual frequency of ~ 2960 cm^{-1}, while r^+ and d^- appear to be pulled towards each other by interference of the two peaks. We can conclude that like the hexadecane molecules oriented at the air/hexadecane interface, the eicosane chains are vertically oriented at the surface but have a significant amount of gauche defects. Below the surface freezing temperature, the CH_3 peaks in both spectra are significantly more pronounced, as the number of conformational defects in the chains are reduced and the chains are better oriented along the surface normal. However, the CH_2 peaks that appear at the air/liquid spectra at higher temperatures persist into the surface-ordered spectra, although reduced in strength. In the SPS spectrum after surface freezing the CH_2 asymmetric stretch is still visible, and in the SSP spectrum the d^+ peak is obvious while the d^- peaks appears as a shoulder on the r^+_{FR} peak.

The CH_3 r^+ and r^- peaks in the surface-frozen eicosane spectra are found to be 1.8 times weaker than those in the spectra of the crystallized dodecanol monolayer. Also, in the former, the peaks due to CH_2 stretches are obvious, but they are hardly visible in the

spectra of alcohol monolayers below the surface transition temperature. The difference between the two cases is due to the multiple sources of contributions to the CH stretch signal in the eicosane system. For the dodecanol monolayer, the only source contributing to the CH_3 signal is the single methyl group at the end of the alcohol molecules. For the surface-ordered eicosane, there are three different sources contributing to the CH_3 signal: the methyl groups at one end of the eicosane molecules facing the air, the methyl groups at the other end of the eicosane molecules facing the liquid, and the methyl groups of the subphase liquid eicosane molecules. The CH_2 peaks also have contributions from the liquid subphase and from the surface monolayer if defects exist in the alkyl chains.

To evaluate the sum-frequency signal from the liquid eicosane subphase at the monolayer/liquid interface, we assume that the liquid structure is essentially the same at the interfaces with air and with the solid monolayer. Then the SFG signals from the liquid eicosane subphase at the two interfaces differ only by the product of the Fresnel factors for IR, visible and sum-frequency fields. It amounts to a reduction factor of ~ 0.60 when changing from the air/liquid to the monolayer/liquid interface. In calculating the Fresnel factors, the appropriate refractive index of the surface monolayer was determined experimentally by ellipsometry. Treating the monolayer as an isotropic layer of thickness d = 21.9 Å as suggested by X-ray reflectivity,[4] we found that the small shift in the ellipsometric phase angle at the surface freezing transition corresponded to a monolayer refractive index change of only 1%.

The signal produced by the crystallized eicosane surface monolayer can be estimated by comparison with that from the surface-ordered dodecanol film. The dodecanol CH_3 sum-frequency signal comes from a single layer of ordered methyl groups

terminating the vertical alkyl chains. For the eicosane monolayer, there are two methyl layers, one on each side of the alkyl chain. The sum-frequency signals from the two methyl layers are 180° out of phase. The signal from the layer at the air side is expected to be nearly the same as that from the dodecanol monolayer. The signal from the layer at the liquid side should be reduced by the change in the Fresnel factors. We also have for the eicosane monolayer a surface area per molecule of 19.9 $Å^2$,[4] as compared to 21.0 $Å^2$ for the dodecanol film at 27 °C. With all these taken into account, the resultant CH_3 sum-frequency field generated by the eicosane monolayer is estimated to be ~ 40% of the dodecanol monolayer at 27 °C.

Adding the sum-frequency fields from the surface eicosane monolayer and the liquid subphase leads to a total field strength for CH_3 stretches of the surface-ordered eicosane system about ~ 60% of that from the crystallized dodecanol Langmuir film. The measured ratios of the CH_3 r^+ and r^- from the SSP and SPS spectra are ~ 75%, somewhat higher than the estimated value. The result supports the physical picture of a dense monolayer of vertically oriented chains floating on the free liquid surface for the surface-frozen eicosane system.

The observed CH_2 signal from the surface-frozen eicosane system is also somewhat higher than the predicted values assuming the signal coming only from the subphase liquid eicosane at the monolayer/liquid interface. Disorder in the monolayer chains towards the monolayer/liquid interface is a reasonable explanation for the greater-than-predicted CH_3 and CH_2 signals. First, it decreases the out-of-phase signal from the methyl end groups of the molecular monolayer facing the liquid and hence increases the overall CH_3 signal. Second, it leads to a contribution to the CH_2 signal from the

monolayer. Thus a picture of a dense monolayer of vertically oriented molecular chains with increasing conformational disorder towards the monolayer/liquid interface is perhaps more appropriate. It is certainly compatible with the X-ray reflectivity measurements.[4,5] In the latter studies, the reflectivity data were fit by the electron density profile of a solid surface layer with thickness slightly shorter than the length of an all-trans chain.

D. Summary

In this Chapter we have studied the surface crystallization transition of liquid alkanes and of an alcohol Langmuir film. Although the underlying driving force for the surface crystallization is clearly similar in both cases (the strong van der Waals chain-chain interaction between long alkyl chains), the two systems have fundamental differences: the surface monolayer interacts with the water subphase in the case of the alcohol Langmuir film while it interacts with like molecules in the subphase in the case of liquid alkanes. This is reflected in the different natures of these two surface phase transitions.

For liquid eicosane, it was found that the vibrational spectrum of the air/liquid interface undergoes a sudden change at ~ 3 °C above the bulk melting temperature. This supports the reported observation of a first-order, surface monolayer order-disorder transition. The spectra indicate that both above and below the transition, molecules in the surface monolayer are vertically oriented with a significant amount of gauche defects in the alkyl chains, but the number of defects is significantly reduced below the transition temperature as the monolayer becomes more compact.

For a 1-dodecanol monolayer on water in equilibrium with an excess drop, only the strength but not the features of the SFG spectrum changes significantly at the surface ordering transition. It indicates that the alcohol molecules are nearly all-trans and vertically oriented both before and after the surface crystallization, although conformational defects are somewhat reduced below the surface phase transition. The increase in spectral intensity below the transition results from an increase in the surface density of the monolayer. This is at variance with the conclusion from an ellipsometry study suggesting that the observed jump in the ellipsometric phase shift at the surface ordering transition is due to an appreciable change in the monolayer film thickness.

References

(1) D. M. Small, *The Physical Chemistry of Lipids*, Plenum, New York (1986).

(2) M. N. Jones and D. Chapman, *Micelles, Monolayers and Biomembranes*, Wiley-Liss, New York (1995).

(3) G. L. Gaines, *Insoluble Monolayers at Liquid-Gas Interfaces*, Wiley, New York (1966).

(4) X. Z. Wu, E. B. Sirota, S. K. Sinha, B. M. Ocko and M. Deutsch, *Phys. Rev. Lett.* **70**, 958 (1993).

(5) X. Z. Wu, B. M. Ocko, E. B. Sirota, S. K. Sinha and M. Deutsch, *Physica A* **200**, 751 (1993).

(6) X. Z. Wu, B. M. Ocko, E. B. Sirota, S. K. Sinha, M. Deutsch, B. H. Cao and M. W. Kim, *Science* **261**, 1018 (1993).

(7) T. K. Xia and U. Landman, *Phys. Rev. B* **48**, 11313 (1993).

(8) A. Renault, J. F. Legrand, M. Goldman and B. Berge, *J. Phys. II (France)* **3**, 761 (1993).

(9) B. Berge and A. Renault, *Europhys. Lett.* **21**, 773 (1993).

(10) B. M. Ocko, X. Z. Wu, E. B. Sirota, S. K. Sinha, O. Gang and M. Deutsch, *Phys. Rev. E* **55**, 3164 (1997).

(11) G. A. Sefler, Q. Du, P. B. Miranda and Y. R. Shen, *Chem. Phys. Lett.* **235**, 347 (1995).

(12) A. W. Adamson, *The Physical Chemistry of Surfaces*, Wiley, New York (1982).

(13) L. J. Bellamy, *The Infrared Spectra of Complex Molecules*, Wiley, New York (1975).

(14) R. G. Snyder, H. L. Strauss and C. A. Elliger, *J. Phys. Chem.* **86**, 5145 (1982).

(15) R. A. MacPhail, H. L. Strauss, R. G. Snyder, *J. Phys. Chem.* **88**, 334 (1984).

(16) R. C. Spiker and I. W. Levin, *Biochim. Biophys. Acta* **338**, 361 (1995).

(17) P. Guyot-Sionnest, J. H. Hunt and Y. R. Shen, *Phys. Rev. Lett.* **59**, 1597 (1987).

(18) L. Askadskaya and J. P. Rabe, *Phys Rev. Lett.* **69**, 1395 (1992).

(19) J. P. Bucher, H. Roeder and K. Kern, *Surf. Sci.* **289**, 370 (1993).

(20) K. M. Gough, *J. Phys. Chem.* **91**, 2424 (1989).

(21) B. D. Casson, R. Braun and C. D. Bain, *Faraday Discuss.* **104**, 209 (1996).

Figure Captions

Figure 1. SFG spectra of (a) air/ hexadecane interface, and (b) fused quartz/hexadecane interface, with the SSP polarization combination.

Figure 2. SFG spectra of a 1-dodecanol monolayer on the water surface at (a) 43 °C and (b) 27 °C; solid circles are for SSP polarization combination and open circles are for SPS polarization combination.

Figure 3. SFG spectra of n-eicosane ($C_{20}H_{42}$) at (a) 40 °C and (b) 37 °C; solid circles are for SSP polarization combination and open circles are for SPS polarization combination.

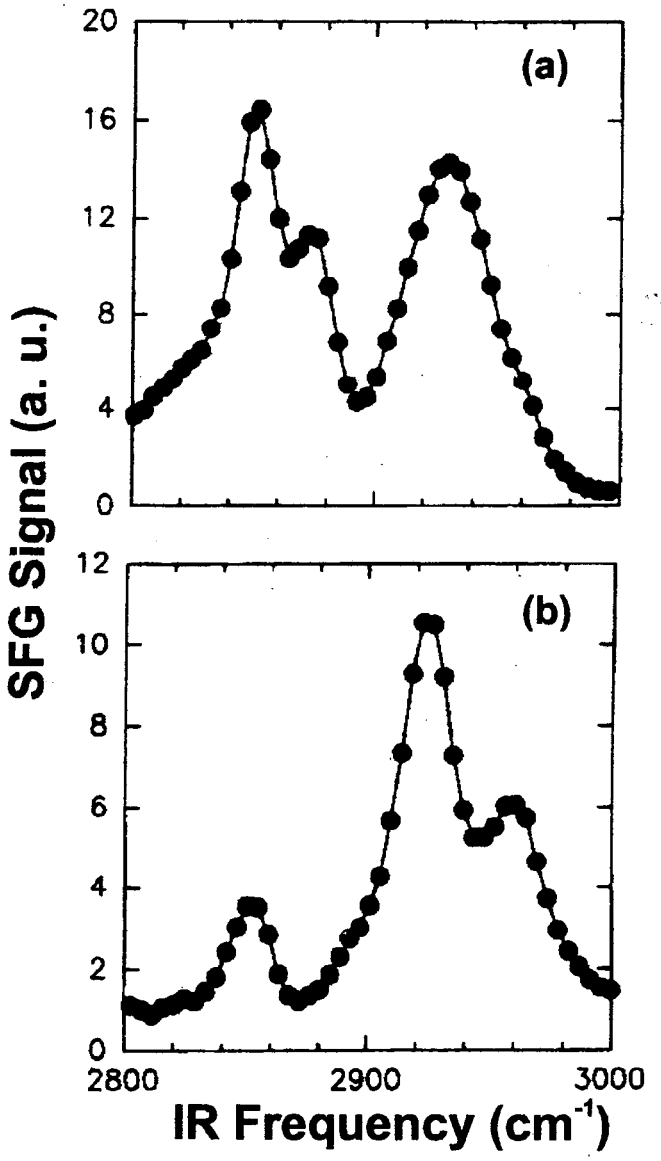
(a)
(b)
SFG Signal (a. u.)
IR Frequency (cm^{-1})
20
16
12
8
4
0
12
10
8
6
4
2
0
2800
2900
3000

Figure 1

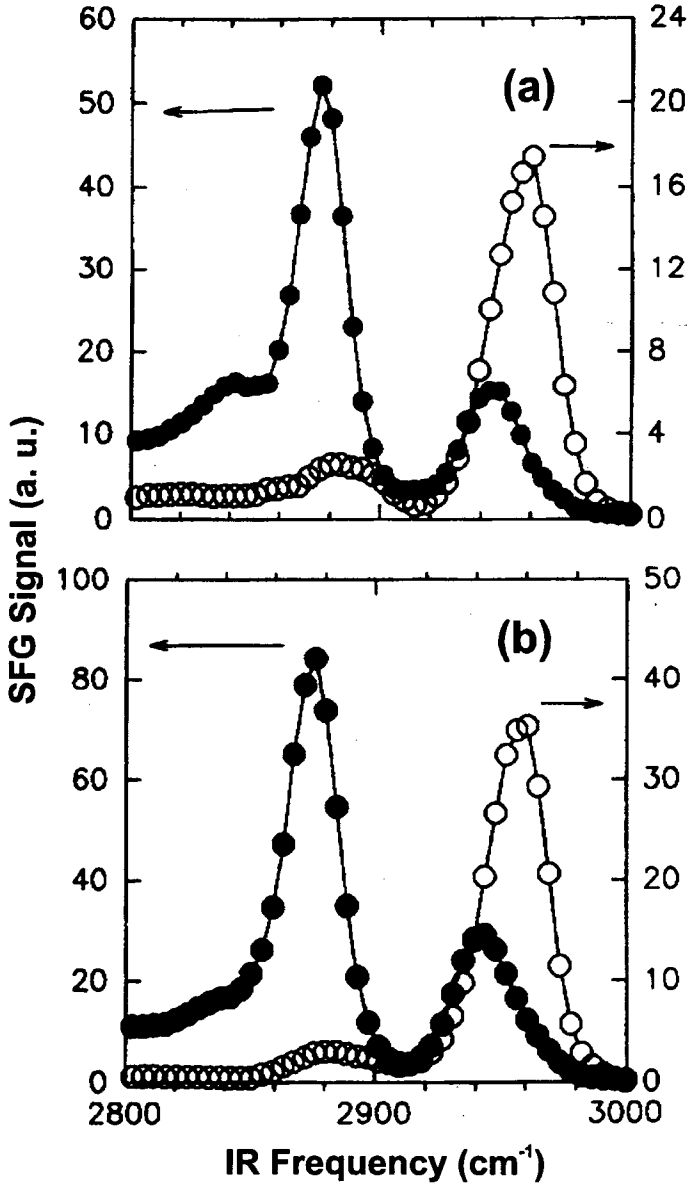
(a)
(b)
SFG Signal (a. u.)
IR Frequency (cm-1)
2800
2900
3000
60
50
40
30
20
10
0
24
20
16
12
8
4
100
80
60
40
20
50
40
30
20
10

Figure.2

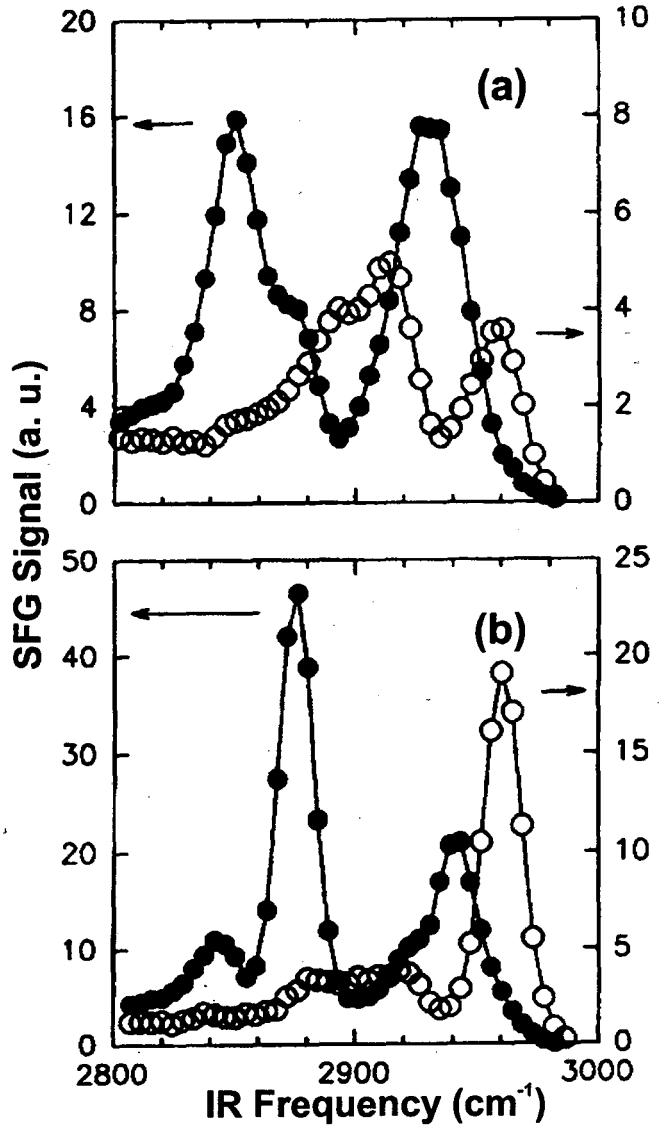
(a)
(b)
SFG Signal (a. u.)
IR Frequency (cm^{-1})
20
16
12
8
4
0
10
8
6
4
2
0
50
40
30
20
10
0
25
20
15
10
5
0
2800
2900
3000

Figure 3

Chapter 4. Interaction of Water with a Langmuir Film

A. Introduction

As we have mentioned in Chapter 3, Langmuir films have attracted enormous interest in recent years, especially because these two-dimensional systems exhibit a very rich phase-transition behavior[1,2] and are often taken as potential models for biological membranes[3] or crystalline templates for epitaxial growth of three-dimensional crystals at the air/water interface.[4,5] When transferred to a solid substrate (Langmuir-Blodgett films) high-quality multilayer films can be formed, with applications ranging from optoelectronics[6] to biology.[7] For most applications, it is essential to know the detailed structure of the monolayer films. However, it was only in the last decade that direct structural information has been obtained with X-ray[1,2,8,9] and neutron diffraction techniques.[10]

These films interact strongly with the water surface via their polar head-groups so that one may expect the interfacial water structure to be perturbed by the presence of such monolayer. Since in some cases these monolayers can have two-dimensional crystalline order (as discussed in Chapter 3), it is possible that they may act as templates for ordering of surface water molecules via epitaxial interaction, if there is good lattice matching between the monolayer and ice structures. Although some detailed information is now available about the structure of a few Langmuir films,[2,9,11] the structure of the water layer underneath the monolayer has only been studied very recently by SFG vibrational spectroscopy.[12-14] Some information about the interaction of water with monolayers can be obtained from thermodynamic measurements. For example, ice nucleation

experiments[4,5] have shown that a long-chain alcohol monolayer is able to reduce supercooling of water by several degrees, while fatty acid monolayers are poor ice nucleators. This difference was thought to arise mainly from the different crystalline structures of the monolayers. The alcohol monolayer has a hexagonal packing that closely matches the hexagonal ice structure in the basal plane. The alcohol OH groups interact via hydrogen bonding with water molecules underneath, forming epitaxially an ordered water layer that easily nucleates ice. On the other hand, the structure of the fatty acid monolayer does not closely match that of ice, resulting in its inability to nucleate ice.

In this Chapter, we use SFG vibrational spectroscopy to study the microscopic structure of water underneath a monolayer of hexacosanoic acid ($CH_3(CH_2)_{24}COOH$) and we compare our results to the previously studied water surface covered by an octadecanol ($CH_3(CH_2)_{17}OH$) monolayer.[12] By changing the pH of the water subphase, the fatty acid monolayer can be neutral or negatively charged, due to ionization of the acid OH groups. At low pH values the monolayer is neutral and the vibrational spectra of water molecules at the interface reveal remarkable differences from the case of the alcohol monolayers studied previously[12]. When the pH value is high, the ionized monolayer generates a strong electric field that can effectively reorient the interfacial water molecules into a hydrogen-bonding network. We also observe reorientation of the head-group of the acid monolayer as a function of pH. These results corroborate the proposed mechanism[4,5] for explaining the different behavior in ice nucleation of the two monolayers and directly show that the water surface structure can be considerably altered by interaction with Langmuir monolayers.

B. Experimental Details

Each spectrum was taken with a freshly prepared monolayer on the surface of water of appropriate pH. The pH value was attained by mixing an appropriate amount of 1 M HCl or 1 M NaOH solutions (Fisher Scientific) with ultra-pure water with a resistivity higher than 18.0 MΩ·cm (Barnstead Nanopure II). The pH was then allowed to equilibrate for at least 30 min to take care of the buffering effect of atmospheric CO_2, which was especially important in the pH range 4 to 8. To avoid contamination from heavy metal or rare earth ions (which have strong specific interactions with the acid head-group, modifying the monolayer structure), no salt was added to keep the ionic strength constant and no buffers were used to stabilize the bulk pH. Therefore the pH values quoted are only approximate to within ± 0.2. Hexacosanoic acid was purchased from Sigma (purity > 99%) and used as received. The monolayers were spread from a chloroform solution (J. T. Baker, reagent grade, concentration 0.86 mM) onto ultra-pure water and the solvent was allowed to evaporate for 10 minutes. The monolayer on water was then slowly compressed to a surface pressure of 3 mN/m measured with a Wilhelmy plate in a thoroughly cleaned Teflon trough. For fatty acid with chain length as long as C_{26}, even uncompressed monolayers appear in a crystalline phase.[9] Even for the highest pH value (~ 12) our fatty acid monolayer was stable for many hours with no appreciable dissolution observed.

C. Results and Discussion

C.1 Low pH Values

Figure 1 shows the SFG spectra with the SSP polarization combination in the OH stretch range for a fully packed hexacosanoic acid Langmuir film on water with different pH values. At very low pH (pH = 2), the monolayer is expected to be neutral[15] and both water molecules and the acid OH groups contribute to the spectrum. Two broad peaks appear in the spectrum: one around 3050 cm^{-1} and another weaker one around 3560 cm^{-1}. We notice that the peak at 3050 cm^{-1} has a too low frequency to be assigned to any stretch vibration of water molecules. Even in ice, where the hydrogen bonded network is strong and well ordered, the lowest peak in the IR spectrum is at 3200 cm^{-1}, with a shoulder around 3150 cm^{-1}.[16] On the other hand, this 3050 cm^{-1} peak is similar in frequency and width to that observed in the IR spectrum[17,18] of carboxylic acids in the liquid phase or in solution. In the IR spectrum, it was associated with the cyclic dimers of carboxylic acids. However, in the case of the fatty acid monolayer the formation of cyclic dimers is very unlikely.[9] We therefore assign this peak to the OH stretch of fatty acid head-groups with both CO and OH hydrogen-bonded. The assignment of the peak at 3560 cm^{-1} is also not easy. The high frequency suggests that it is related to an OH stretch of groups weakly interacting with neighbors. In dilute CCl_4 solution, the OH stretch of carboxylic acid monomers[17,19] appears at about 3530 cm^{-1}. The dangling OH bond of water at an interface[12] has a stretch frequency of 3690 cm^{-1}. It is likely that the peak arises from weakly interaction OH groups of both fatty acid and water and appears as a signature of a disordered hydrogen-bonding network of the fatty acid monolayer / water interface. Note that the characteristic peaks at 3200 and 3450 cm^{-1}, previously observed for a more or less ordered water interface[12] are absent in this case. We therefore conclude that the hydrogen-bonding network of water underneath a *neutral* fatty acid monolayer is

very much disrupted, presumably because of the large lattice mismatch between the fatty acid monolayer and ice, as suggested before.[5] We also note that a molecular dynamics simulation of a neutral fatty acid monolayer has shown that the water structure is disordered at the interface.[20] This explains why fatty acids are poor ice nucleation agents. In contrast, the SFG spectrum of water underneath a long-chain alcohol monolayer,[12] shown (empty circles) in Figure 1 in the panel for the spectrum of a fatty acid monolayer at pH = 3.9, is dominated by a peak at 3200 cm^{-1}, which is characteristic of a well ordered hydrogen-bonding network that resembles the ice structure. This clearly supports the notion that the alcohol monolayer induces an epitaxial layer of ordered structure in the water subphase via hydrogen bonding and explains why alcohol monolayers are good ice nucleation agents.

C.2 High pH Values

At high pH values (pH ≥ 7.0), the fatty acid OH groups should be significantly deprotonated, leaving the monolayer negatively charged.[15] The spectra in Figure 1 show a gradual increase in signal strength by about one order of magnitude from pH = 7.0 to 10.5. The peaks for water at 3200 and 3450 cm^{-1} now appear and dominate the spectra. For higher pH, the 3200 cm^{-1} peak becomes relatively stronger than the one at 3450 cm^{-1}. For pH = 12 the peak at 3200 cm^{-1} dominates the surface water spectrum completely and it now resembles the IR spectrum of bulk ice, also shown (solid line) in the same panel in Figure 1 for comparison.[16] The situation is reminiscent of previous SFG and SHG measurements of water at charged interfaces.[13,21,22] Deprotonation of the acid monolayer creates a surface electric field that can orient the surface water molecules and induce an

ordered ("ice-like") hydrogen-bonding network.[21] This is consistent with the notion that an applied electric field can nucleate ice structure in the water subphase[23,24] and with a molecular dynamics simulation of a fully ionized fatty acid monolayer on water that showed that at least three water monolayers at the interface are strongly ordered.[25]

In Figure 1, the spectra at pH values 10.5 and 12 also show two strong sharp peaks at 2875 and 2935 cm^{-1}. They are from the r^+ and r^+_{FR} modes of the terminal CH_3 group of the alkyl chains, respectively. There is no signal from the CH_2 groups of the chain, indicating that the chains are fully extended with little gauche defects, as expected for such monolayers with chain densities around 21 $Å^2$/molecule.[9] The CH_3 asymmetric stretch (~ 2960 cm^{-1}) is hardly detectable in the spectra indicating that the CH_3 group is oriented nearly normal to the surface. Both conclusions are in agreement with the result from X-Ray diffraction experiments.[9] Although not shown in most panels of Figure 1, the two peaks of the alkyl chains remain the same for all pH values. This means that there are no significant changes in the conformation of the alkyl chains as the pH varies.

C.3 Intermediate pH Values

The spectra of Figure 1 for intermediate pH values ($3.0 \leq pH \leq 5.6$) show another interesting feature. The fatty acid OH peak at 3050 cm^{-1} reduces slightly in strength from pH 2.0 to 3.0, but almost disappears at pH ~ 3.9. One might think that this is the result of deprotonation of the monolayer. If more than half of the acid head-groups were deprotonated at pH ~ 3.9, the remaining surface density of acid OH groups would yield a very weak spectral peak, since the SFG signal is proportional to the square of the surface density. However, this is very unlikely because for fatty acids in bulk water the pH for

half ionization (pH = pK_a) is 4.9. At the interface the local pH should be much lower than in the bulk, resulting from the higher surface proton concentration induced by the surface electric field. This means that half-ionization of the monolayer should occur at a bulk pH much higher than 5. Also, Figure 1 shows that the effect of the surface field on the water spectrum becomes appreciable only for pH above 7.0.

Taking the value of 5.6 for the pK_a of a fatty acid monolayer[26] one can use the simple Gouy-Chapman theory[27] to calculate the degree of ionization of the monolayer as a function of bulk pH under our experimental conditions. The ionized fraction of the monolayer x is defined as $x = N_i/N_T$, where N_i is the number of ionized molecules and N_T is the total number of molecules. The monolayer ionization is determined by the surface pH value (pH_s) and the equilibrium constant pK_a for the acid group dissociation:

$$H^+ + RCOO^- \leftrightarrow RCOOH$$

$$pK_a = pH_s - \log\left(\frac{x}{1-x}\right) \qquad (4.1).$$

The surface pH_s is related to the bulk pH_b and the surface electric potential ψ_o by the Boltzmann relation:

$$pH_s = pH_b + \frac{e\psi_o}{2.3k_BT} \qquad (4.2)$$

where e is the proton charge and k_B is the Boltzmann constant. The Gouy-Chapman model[26,27] is then used to relate ψ_o to the charge density at the interface. For the case of a fatty acid monolayer on a water subphase with a 1:1 electrolyte, ψ_o is given by

$$\psi_o = -\frac{2k_BT}{e}\sinh^{-1}\left(\frac{134\,x}{A\sqrt{C}}\right) \qquad (4.3)$$

where A is the area per molecule in the monolayer (in $Å^2$) and C is the positive ion concentration (ionic strength, in M). Combining Eqs. (4.1), (4.2) and (4.3) we obtain a relation between pH_b and x:

$$pH_b - pK_a = 0.87 \sinh^{-1}\left(\frac{134x}{A\sqrt{C}}\right) + \log\left(\frac{x}{1-x}\right) \qquad (4.4).$$

There is however one complication. Since the ionic strength C was not kept constant in our experiments, we must take into account the variation of C with pH. For pH ≤ 5.6 only HCl is added to water and C is the total concentration of H^+

$$C = 10^{-pH_b} \quad , \qquad \text{for } pH_b \leq 5.6 \qquad (4.5).$$

For pH ≥ 5.6 no HCl is added. C is then the total concentration of H^+ and Na^+ from the known amount of NaOH added to obtain a given pH_b. The ionization fraction x is then calculated by solving Eq. (4.4) for a given pH_b using the appropriate value of C. The results of such a calculation are plotted in Figure 2. In the calculation, the area per molecule A was taken as 20 $Å^2$ as prescribed in the experiment and the monolayer pK_a was assumed to be 5.6.[26] The dotted line in Figure 2 indicates the part that may not be reliable due to questionable validity of the Gouy-Chapman model, since the surface ion concentration is too high.[27] The inflection point at pH ~ 5 is due to the buffering effect of atmospheric CO_2 dissolved in water.[28] It should be emphasized that the results in Figure 2 are calculated with the varying ionic strength in the subphase already taken into account.

Referring to Figure 2, note that although x slowly rises with pH varying from 2 to 4, it is always much less than 1%, so that the surface density of acid OH groups is practically unchanged. Note also that at pH = 7, x is only about 2%. That our SFG spectrum changes noticeably in this range indicates that it is quite sensitive to the

ionization of the monolayer. The calculation suggests that the monolayer should be about half-ionized at pH = 10.5.

In order to further confirm that the monolayer ionization is not significant at pH = 3.9, we have performed SFG measurements in the CO stretch range. The spectra are presented in Figure 3. When the head-group is neutral, the C=O stretch vibration appears as a broad band around 1720 cm^{-1}. With ionized head-groups, we observe a strong peak at 1420 cm^{-1} due to the symmetric COO^- stretch.[29] From pH = 2.0 to 7.5 the spectra show only the band due to the C=O stretch. At pH = 10.5, the COO^- stretch starts to appear. At pH = 12, the monolayer is nearly fully ionized. Accordingly, the C=O band disappears and the COO^- peak appears to dominate. From the variation of the spectrum with pH we can conclude that the ionization of the monolayer is negligible at pH = 3.9 and the monolayer is half-ionized at pH ~ 10.5, in good agreement with the calculation shown in Figure 2.

If the acid OH groups remain largely unionized at pH = 3.9, there is only one possibility to explain the disappearance of their 3050 cm^{-1} peak. The groups must have reoriented into a position such that they do not contribute appreciably to the SFG spectrum with the SSP polarization combination. However, we have also taken spectra with PPP and SPS polarization combinations and in both cases the peak at 3050 cm^{-1} was found to become hardly detectable as the pH value increased from 3.0 to 3.9. Therefore, the only possibility is that at pH ~ 3.9 the acid OH groups have reoriented into an almost in-plane position (see Figure 4), so that the corresponding OH stretch mode can no longer contribute to the SFG spectrum due to the azimuthally isotropic symmetry of the monolayer. The reorientation does not involve the rest of the acid molecule because, as

mentioned earlier, the peaks assigned to the C=O and CH_3 stretch modes hardly change in the range of pH = 2 to 7.5, for any polarization combination.

We now speculate on possible reasons for this acid OH reorientation at pH ~ 3.9. Since it depends on the water pH, it must be related to the ionization of the monolayer. However, it must be very sensitive to the presence of surface charges, since at pH = 3.9 the ionization of the monolayer is expected to be around 0.2% (see Figure 2). One might think that the electric field normal to the surface produced by the ionized head-groups would induce a reorientation of the OH dipole initially oriented towards the water as schematically shown in Figure 4. However, an estimate of the dipole energy in the field of a 0.2% ionized monolayer shows that this effect is too small to be the major mechanism for the OH reorientation. Another possibility is the OH reorientation by an in-plane field. One would say that a uniformly charged plane cannot produce an in-plane electric field, but this is only true on average. There always exists the local field near a charged site that may reorient the neighboring OH groups. Depending on the strength and range of influence of the local field, one ionized head-group may be able to reorient several neighboring OH groups into an in-plane position. To estimate how many OH groups can be reoriented by the ionization of one acid head-group, we neglected screening by the dipoles in the monolayer. In this case, an ionization fraction of only 0.1% is able to reorient the OH groups of about half monolayer. This crude estimate seems to indicate that the in-plane local field is responsible for the reorientation of the acid OH groups.

D. Summary

In summary, we have studied the mutual interaction of water with a fatty acid Langmuir film. The water pH affects the degree of ionization of the monolayer, which modifies the water-monolayer interaction. At pH ~ 2 the monolayer is neutral and hydrogen bonding is the dominant interaction between monolayer head-groups and water molecules. The vibrational spectrum of surface water molecules reveals that they form a disordered hydrogen bonded network weakly interacting with the monolayer. A proposed explanation for this finding invokes poor lattice matching between the crystalline structures of the fatty acid monolayer and hexagonal ice. This is in contrast to the water structure underneath an alcohol monolayer,[12] which becomes "ice-like" because of good lattice matching. Our experiment explains at a molecular level the different behaviors of the two monolayers as ice nucleation agents.[5] As the pH is increased from 3.0 to 3.9, there is a reorientation of the acid OH groups from pointing into water to an in-plane position. This is presumably driven by the in-plane local electric field generated by a small fraction of ionized fatty acid molecules. At pH ~ 7.0, the surface field resulting from the ionization of the monolayer is strong enough to start reorienting water molecules and establishing a more ordered water structure at the interface. As the pH increases, the monolayer gets more ionized and the increasing surface field further enhances both polar and ice-like ordering in the subphase. The monolayer is about half ionized at pH ~ 10.5 and fully ionized at pH ~ 12. It is interesting to note from results of this study that even systems as simple as a fatty acid Langmuir film may exhibit diverse and complex behavior resulting from interactions with the water subphase.

References

(1) B. Lin, M. C. Shih, T. M. Bohanon, G. E. Ice and P. Dutta, *Phys. Rev. Lett.* **65**, 191 (1990).

(2) R. M. Kenn, C. Böhm, A. M. Bibo, I. R. Peterson, H. Möhwald, J. Als-Nielsen and K. Kjaer, *J. Phys. Chem.* **95**, 2092 (1991).

(3) J. H. Fendler, *Membrane Mimetic Chemistry*, Wiley-Interscience, New York (1982).

(4) M. Gavish, R. Popovitz-Biro, M. Lahav and L. Leiserowitz, *Science* **250**, 973 (1990).

(5) R. Popovitz-Biro, J. L. Wang, J. Majewski, E. Shavit, L. Leiserowitz and M. Lahav, *J. Am. Chem. Soc.* **116**, 1179 (1994).

(6) G. Roberts, *Langmuir-Blodgett Films*, Plenum, New York, ch. 7 (1990).

(7) D. H. Charych, J. O. Nagy, W. Spevak and M. D. Bednarski, *Science* **261**, 585 (1993).

(8) K. Kjaer, J. Als-Nielsen, C. A. Helm, L. A. Laxhuber and H. Möhwald, *Phys. Rev. Lett.* **58**, 2224 (1987).

(9) F. Leveiller, D. Jacquemain, L. Leiserowitz, K. Kjaer and J. Als-Nielsen, *J. Phys. Chem.* **96**, 10380 (1992).

(10) J. R. Lu, Z. X. Li, J. Smallwood, R. K. Thomas and J. Penfold, *J. Phys. Chem.* **99**, 8233 (1995).

(11) S. W. Barton, B. N. Thomas, E. B. Flom, S. A. Rice, B. Lin, J. B. Peng,, J. B. Ketterson and P. Dutta, *J. Chem. Phys.* **89**, 2257 (1988).

(12) Q. Du, R. Superfine, E. Freysz and Y. R. Shen, *Phys. Rev. Lett.* **70**, 2313 (1993).

(13) D. E. Gragson, B. M. McCarty and G. L. Richmond, *J. Am. Chem. Soc.* **119**, 6144 (1997).

(14) P. B. Miranda, Q. Du and Y. R. Shen, *Chem. Phys. Lett.* **286**, 1 (1998).

(15) J. A. Spink, *J. Colloid Interface Sci.* **18**, 512 (1963).

(16) H. J. Labbé and E. Whalley, *J. Chem. Phys.* **50**, 4501 (1969).

(17) S. Bratoz, D. Hadzi and N. Sheppard, *Spechtrochim. Acta* **8**, 249 (1956).

(18) M. Picquart, T. Lefevre and G. Lacrampe, *Appl. Spectrosc.* **49**, 1268 (1995).

(19) J. D. S. Goulden, *Spectrochim. Acta* **6**, 129 (1954).

(20) J. P. Bareman and M. L. Klein, *Mat. Res. Soc. Symp. Proc.* **237**, 271 (1992).

(21) Q. Du, E. Freysz and Y. R. Shen, *Phys. Rev. Lett.* **72**, 238 (1994).

(22) S. Ong, X. Zhao and K. B. Eisenthal, *Chem. Phys. Lett.* **191**, 327 (1992).

(23) X. Xia and M. L. Berkowitz, *Phys. Rev. Lett.* **74**, 3193 (1995).

(24) I. M. Svishchev and P. G. Kusalik, *Phys. Rev. Lett.* **73**, 975 (1994).

(25) M. Schlenkrich, K. Nicklas, J. Brickmann and P. Bopp, *Ber. Bunsenges. Phys. Chem.* **94**, 133 (1990).

(26) J. J. Betts and B. A. Pethica, *Trans. Faraday Soc.* **52**, 1581 (1956).

(27) A. W. Adamson, *The Physical Chemistry of Surfaces*, Wiley-Interscience, New York, ch. 5 (1990).

(28) J. N. Butler, *Carbon Dioxide Equilibria and their Applications*, Addison-Wesley, Reading, MA (1982).

(29) A. Gericke and H. Hühnerfuss, *J. Phys. Chem.* **97**, 12899 (1993).

Figure Captions

Figure 1. SFG spectra for a hexacosanoic acid monolayer at the air/water interface in the OH stretch range. The water pH values are indicated in each graph. The beam polarization combination is SSP. The IR absorption spectrum of ice (Ref. 16) is shown as a solid line together with the spectrum for pH = 12. The SFG spectrum for water underneath a monolayer of octadecanol (from Ref. 12) is shown for comparison as open circles together with the spectrum for hexacosanoic acid on pH = 3.9 water.

Figure 2. Calculated degree of ionization of the monolayer (x) as a function of water pH for our experimental conditions. The dashed line is beyond the validity of the Gouy-Chapman theory and may not be reliable.

Figure 3. SFG spectra for a hexacosanoic monolayer at the air/water interface in the CO stretch range. The water pH values are indicated in each graph. The beam polarization combination is SSP.

Figure 4. Scheme showing the reorientation of the fatty acid OH groups from pH = 3 to 3.9. The acid head-group orientation is deduced from Refs. 9 and 20.

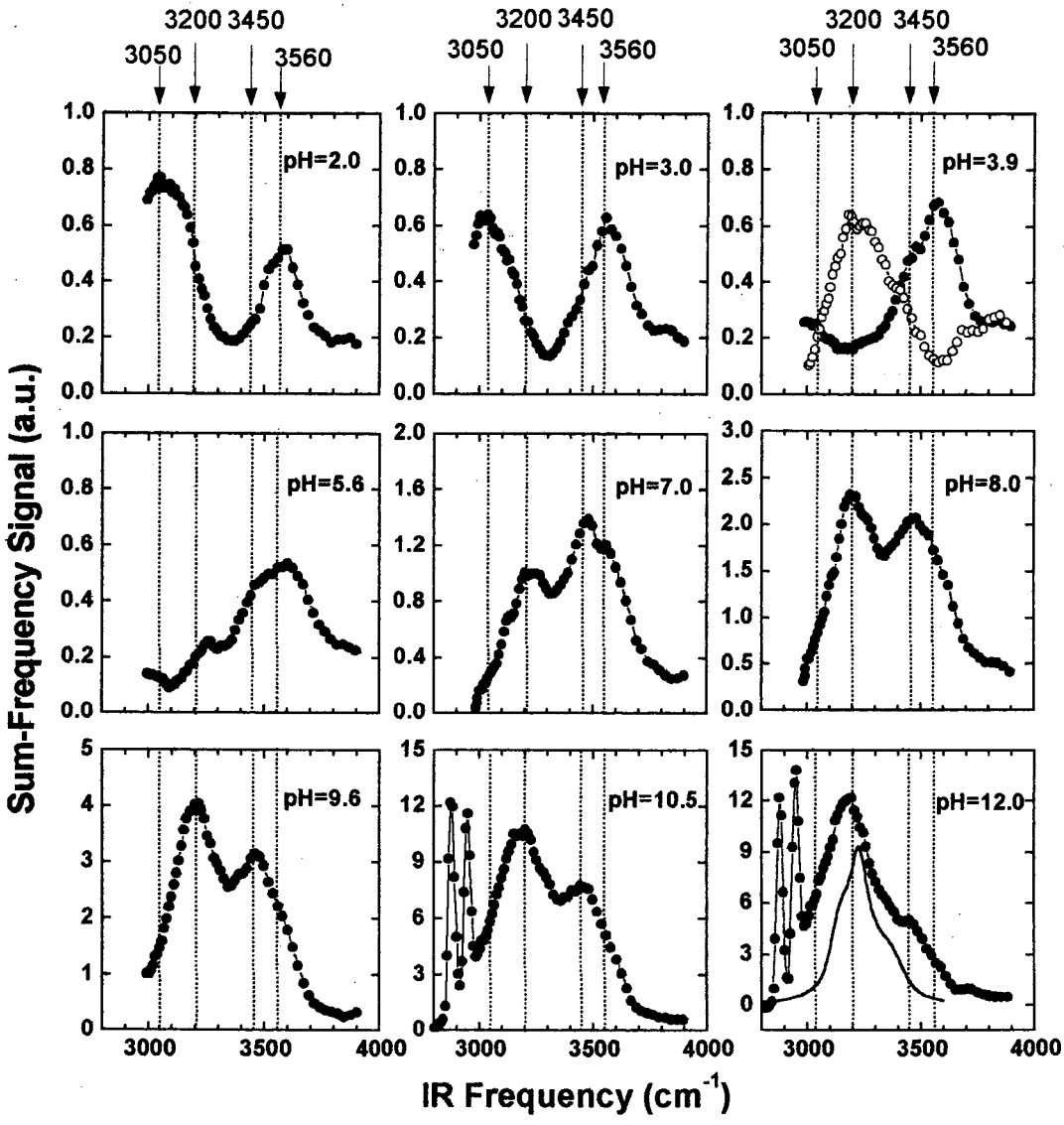
3050
3200
3450
3560
pH=2.0
pH=3.0
pH=3.9
pH=5.6
pH=7.0
pH=8.0
pH=9.6
pH=10.5
pH=12.0
Sum-Frequency Signal (a.u.)
IR Frequency (cm-1)

Figure 1

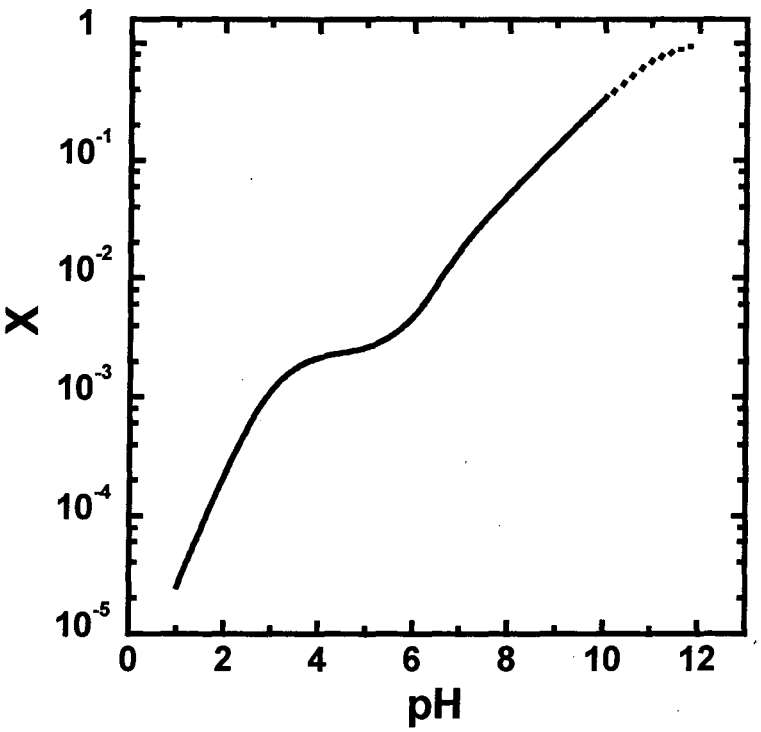

Figure 2

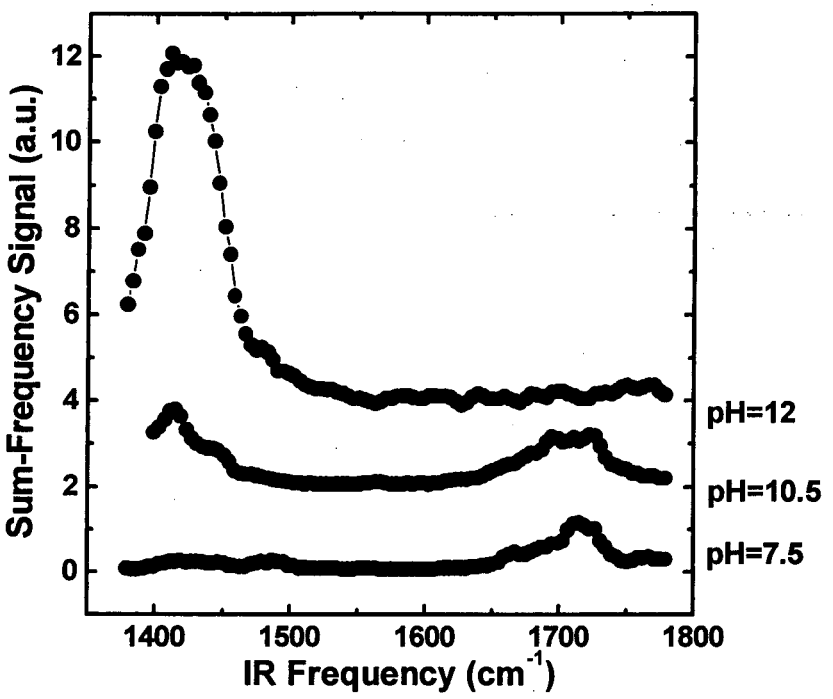
Sum-Frequency Signal (a.u.)
12
10
8
6
4
2
0
1400
1500
1600
1700
1800
IR Frequency (cm-1)
pH=12
pH=10.5
pH=7.5

Figure 3

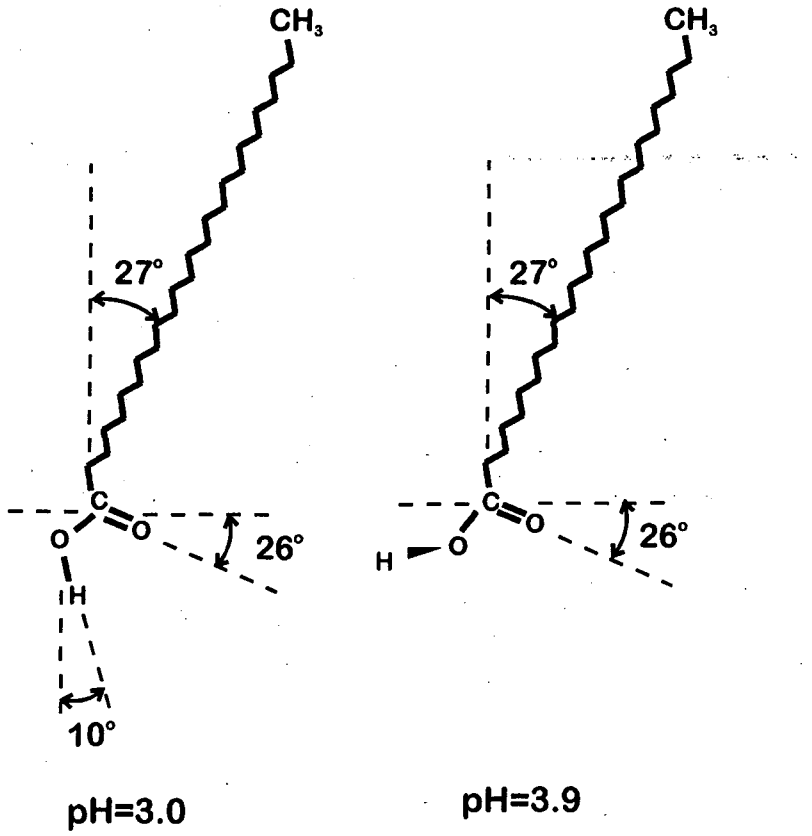

Figure 4

Chapter 5. Mapping Molecular Orientation at Interfaces with SFG and SHG

A. Introduction

Our ability of surface characterization directly affects the progress of surface science, a field of great importance to many disciplines ranging from physics and chemistry to life science and modern electronic technology. Among the various surface properties, molecular orientation is of special interest for its relevance to a wide variety of interesting phenomena such as adhesion, lubrication, catalysis and bio-membrane functions.[1] Many experimental techniques exist for surface studies,[2,3] but only a few can give quantitative information about molecular orientation at an interface. Each has its own shortcomings. Electron scattering[4] and electron energy loss spectroscopy,[5] or any other techniques involving particle scattering can only be operated with samples in high vacuum. Neutron scattering[6,7] and X-ray diffraction[7] require large experimental facilities or the studied surface must be to certain extent crystalline. The latter is also true for optical techniques like Brewster angle microscopy[8,9] (BAM) and Brewster angle autocorrelation spectroscopy[10] (BAAS). Other optical techniques, such as infrared[11,12] (IR), Raman[13,14] or ultraviolet[15] (UV-Vis) spectroscopy and ellipsometry,[16] can be applied to any interfaces accessible by light, but they usually lack sufficient surface specificity to discriminate against bulk contributions.

As we have outlined in Chapter 2, surface SHG and SFG are second-order nonlinear optical processes that have been developed into powerful surface probes.[17-22] They possess all the common advantages of optical techniques, namely, non-destructive,

highly sensitive with good spatial, temporal and spectral resolution, and applicable to any interfaces accessible by light. They are, however, intrinsically surface-specific for interfaces between centrosymmetric media and can also serve as surface spectroscopic tools, since the generated signal is resonantly enhanced if the input or output frequency is tuned over resonances. While SHG has been used to probe electronic transitions,[17,18,21] IR-visible SFG allows studies of surface vibrational resonances.[20-24] We have describe in some detail in Chapter 2 how SHG or SFG can provide information on the average orientation of the molecules or selected sections of the molecules at an interface. They have been extensively used for this purposed by many groups.[25-33] SHG probes electronic response of the surface molecules and is often less selective. Near a resonance, however, it could still be dominated by contribution from a selected part of the molecules. IR-visible SFG probes vibrational resonances that are generally associated with specific moieties or atomic groups on the molecules. Thus, in principle, these two techniques allow us to selectively study different parts of the molecules, particularly their orientations, and completely map out the orientation and conformation of the molecules at the surface or interface. In this Chapter we would like to show that this is indeed the case, even for a fairly complicated molecule forming a Langmuir film at the air/water interface. This would then open up the possibility of studying in detail the orientation and conformation of molecules at various interfaces that have not been studied up to now because of lack of a suitable technique, such as non-crystalline liquid interfaces.

We choose 4″-n-pentyl-4-cyano-p-terphenyl (5CT, $CH_3(CH_2)_4(C_6H_4)_3CN$) molecules at the air-water interface as a demonstrating system in our experiment. The 5CT molecules are amphiphilic and can form a Langmuir monolayer on water surface.

For our purpose, a 5CT molecule can be divided into three sections: a cyano head-group, a terphenyl ring and an alkyl chain (see Figure 1). We can separately measure the orientations of the cyano group and alkyl chain by IR-visible SFG and that of the terphenyl ring by SHG. From the results, we can deduce the conformation and overall orientation of the molecules. As a check, we can compare the deduced 5CT conformation with the accepted one. However, as mentioned in Chapter 2, the analysis to deduce the orientation of a moiety from SHG or SFG relies on the knowledge of the effective refractive index n′ for the interfacial layer (see Eqs. (2.8) and (2.11)). In previous studies, n′ was usually chosen to be equal to the refractive index of one of the two neighboring media,[25,34-36] and the deduced orientation would depend on the n′ chosen. In some studies, n′ was taken as the bulk refractive index of the monolayer material,[35,37] and in others, it was estimated from certain measurements[27,29,38-40] (ellipsometry, Kramers-Kronig analysis, etc). In this Chapter, we show that in order for our results to be physically reasonable and the deduced 5CT molecular conformation to be consistent with the commonly accepted one, we must have a value of n′ different from the bulk refractive index of 5CT and intermediate between those of the neighboring media, namely, air and water. With $n' = 1.18 \pm 0.04$, we find that the 5CT molecules adsorbed at the air/water interface with a tilt angle of $51.5° \pm 1.5°$ from the surface normal.

The Chapter is organized as follows. Section B sketches the experimental system and the sample preparation method. The experimental results are presented in Section C, describing how results are obtained and analyzed for the three sections of the 5CT molecule separately: alkyl chain, cyano group and terphenyl ring. Section D includes a discussion of our results and data analysis. The experimentally determined value for n′ is

justified with a simple model calculation. Section E contains some practical remarks about the curve fitting procedure used to extract peak strengths from the measured SFG spectra.

B. Experimental Details

The IR-visible SFG experiment was performed in setup B described in Chapter 2. In the SHG experiment, a frequency-doubled Q-switched mode-locked Nd:YAG laser at 532 nm and 500 Hz repetition rate was used as the fundamental beam. The second-harmonic output was measured by a photomultiplier with gated electronics after a set of spectral filters. In both cases the signal was attenuated when necessary to obtain signal levels suitable for detection in the photon counting mode. This was done to avoid saturation of the detection system, which was severe even with relatively weak signals (~ 10 photons/pulse).

The 5CT Langmuir monolayer was prepared by dissolving 5CT crystals (EM Industries) in chloroform (J. T. Baker, spectranalyzed grade) and spread on ultrapure water (resistivity of 18.3 MΩ·cm, Barnstead Easy-Pure) in a Teflon Langmuir trough. The film was then compressed slowly and the surface pressure was monitored by a Wilhelmy plate and a microbalance. The resulting pressure-area isotherm is shown in Figure 2. All the SHG and SFG measurements were done on films with area per 5CT molecule around 28 $Å^2$. We also used in the experiment a full hexadecanol monolayer on water as a reference sample. It was prepared by placing a small crystal of hexadecanol ($CH_3(CH_2)_{15}OH$) on the surface of ultra pure water. The hexadecanol molecules spontaneously spread to form a stable full monolayer.[33]

C. Results

The 5CT molecule is composed of a CN head-group, a terphenyl-ring chromophore and a C_5 alkyl chain (5 carbons long). We discuss here the results of SFG and SHG measurements on the average orientation of each segment separately.

C.1 Alkyl Chain

We used SFG spectra of CH stretch modes to determine orientation and conformation of the alkyl chain of 5CT. Figure 3 shows the spectra of the 5CT Langmuir monolayer in this range, at three different input and output polarization combinations, SSP, SPS, and PPP. The solid curves in the figure were obtained by fitting using Eq. (2.16); the fitting parameters are listed in Table 1. The peak assignments in the spectra of Figure 3 are the same as discussed in Chapter 3. The vibrational modes at approximately 2875 cm^{-1}, 2960 cm^{-1} and 2940 cm^{-1} can be assigned, respectively, to the symmetric (r^+) and asymmetric (r^-) stretches of the terminal CH_3 group of the alkyl chain and the Fermi resonance (r^+_{FR}) between the symmetric CH_3 stretch and its bending mode. The weak modes at ~ 2850 cm^{-1} and ~ 2920 cm^{-1} can be assigned to the symmetric (d^+) and asymmetric (d^-) stretches of the CH_2 groups on the chain, respectively. The fact that the strengths of these modes are essentially negligible compared to those of CH_3 groups suggests that the alkyl chains are nearly all-trans and contain few gauche defects,[41] as discussed in the previous Chapters.

The orientation of the terminal CH_3 group can be determined by analyzing its symmetric stretch mode.[42] From Eqs. (2.8) to (2.11) and (2.23) we obtain the following

ratios between the effective susceptibilities for different polarization combinations, assuming a δ-function distribution for the tilt angles:

$$\frac{\chi^{(2)}_{eff,SPS}}{\chi^{(2)}_{eff,SSP}} = 0.765\,\frac{\sin^2\theta(1-r)}{\sin^2\theta + r(1+\cos^2\theta)} \tag{5.1}$$

$$\frac{\chi^{(2)}_{eff,PPP}}{\chi^{(2)}_{eff,SSP}} = 0.023\,\frac{\sin^2\theta(1-r)}{\sin^2\theta + r(1+\cos^2\theta)} + \frac{1.876}{(n')^4}\,\frac{r\sin^2\theta + \cos^2\theta}{\sin^2\theta + r(1+\cos^2\theta)} - 0.763 \tag{5.2}$$

where we have used the appropriate beam incidence angles for our setup (44° and 57° for the visible and IR inputs, respectively) and the following values for the refractive indices of water:[43] n_2(VIS) = 1.337, n_2(IR) = 1.393 + 0.013 i, n_2(SF) = 1.343. The polar angle θ and the ratio r between polarizability components transverse and parallel to the CH_3 symmetry axis can then be deduced from the χ_q's listed in Table 1 by solving Eqs. (5.1) and (5.2) simultaneously. Assuming $n' = n_1 = 1$ for all frequencies, we obtain θ = 39° (+ 2°, - 5°) and $r \geq 5.5$. This large value for r is physically unreasonable. Although the value for r is not agreed upon in the literature, it usually ranges from 1.66 to 3.5.[27,33] From Eq. (2.21) one finds that r cannot be larger than 4. The value deduced from Raman measurements and used in a previous SFG work is 2.3 ± 0.3.[32]

We find that the same difficulty appears in the SFG results of hexadecanol monolayers on water as well. The SFG spectra of a hexadecanol monolayer are shown in Figure 4 with the fitting parameters given in Table 2. Following the same procedure, we can again determine θ and r for the terminal CH_3 groups of the hexadecanol monolayer. However, the r^+ mode in the SPS spectrum is nearly absent, so that we can only assess an upper value for $(\chi_{r+})_{SPS}$, leading to a range of possible solutions: $0° < \theta < 28°$ and $r > 3.3$. A fully packed hexadecanol monolayer on water forms a two-dimensional crystalline

structure and has been well studied by X-ray diffraction.[44] The hexadecanol chain has been found to be tilted 15.8° and 2.8° from the surface normal along the crystalline b and a axes of the monolayer, respectively. Furthermore, the two molecules in a unit cell have the planes of their hydrocarbon chains forming a dihedral angle of 120°. From this known herringbone arrangement of the molecules, we find that half of the CH_3 groups have a polar angle of 24.8° and the other half 20.6°. With this orientation for hexadecanol molecules, the values of r that are consistent with the spectra in Figure 4 are $6.6 < r < 14.9$, which again are physically unreasonable. We also notice in Figures 3 and 4 that the CH_3 symmetric stretch peak is one order of magnitude stronger for hexadecanol than for 5CT. This would be difficult to understand if the above values of θ for hexadecanol and 5CT were correct, knowing that the areas per molecule for hexadecanol[44] and 5CT (20 $Å^2$ versus 28 $Å^2$) are comparable. All these difficulties seem to have originated from our assumption $n' = 1$ in the analysis. In fact, Bain and co-workers also found a similar inconsistency in analyzing the SFG spectra for a dodecanol monolayer.[27] They concluded that in order to obtain the known upright orientation for dodecanol molecules, they must assume $n' \cong 1.2$ if r is taken to be 3.5. In the following, we resolve this problem by simultaneously determining n', θ_{5CT} and r using the hexadecanol monolayer as a reference.

With the known orientation for hexadecanol molecules from the X-ray diffraction measurements, the number of parameters to be determined for both monolayers is reduced to three: θ_{5CT}, r and n'. The SFG spectra in Figures 3 and 4 give us five independent ratios of $\chi^{(2)}$ components for the r^+ mode, $\frac{\chi_{SPS}}{\chi_{SSP}}(5CT)$, $\frac{\chi_{PPP}}{\chi_{SSP}}(5CT)$,

$\frac{\chi_{SPS}}{\chi_{SSP}}(C_{16}OH)$, $\frac{\chi_{PPP}}{\chi_{SSP}}(C_{16}OH)$ and $\frac{\chi_{SSP}(5CT)}{\chi_{SSP}(C_{16}OH)}$, from which the three parameters can be derived. However, the ratio $\frac{\chi_{SPS}}{\chi_{SSP}}(C_{16}OH)$ is very small and subject to a very large uncertainty, since the r^+ peak in the SPS spectrum of hexadecanol is practically absent. Also, the ratio $\frac{\chi_{SSP}(5CT)}{\chi_{SSP}(C_{16}OH)}$ depends on the ratio of surface densities of the two monolayers, which is an extra source of uncertainty. Therefore, we chose to use only the ratios $\frac{\chi_{SPS}}{\chi_{SSP}}(5CT)$, $\frac{\chi_{PPP}}{\chi_{SSP}}(5CT)$ and $\frac{\chi_{PPP}}{\chi_{SSP}}(C_{16}OH)$ in order to determine θ_{5CT}, r and n′, with the other two used only for consistency check. We can determine the parameters θ_{5CT}, r and n′ by simultaneously solving three equations: Eqs. (5.1) and (5.2) for the 5CT monolayer, and Eq. (5.2) for the hexadecanol monolayer (assuming the known value of $\theta \cong 23°$ for hexadecanol deduced from the X-ray diffraction results[44]). The results obtained are $\theta_{5CT} = 54°$ (+14°, -8°), r = 2.5 (+1.7, -1.0) and $n' = 1.18 \pm 0.04$. The assumptions used in the above calculation are that r and n′ for 5CT and hexadecanol are the same and the dispersion of n′ is negligible. That r is the same in both cases is to be expected, considering that in both cases we are dealing with the terminal CH_3 group of an all-trans alkyl chain. Neglecting variations in n′ due to dispersion or the slightly different densities of the two monolayers is a simplifying assumption. However, the errors introduced by such an approximation are within the experimental uncertainty in determining n′. Note that the deduced value of r agrees well with the Raman results.[32] Using the values of r and n′ determined above and the tilt angles of the CH_3 groups of hexadecanol determined from the X-Ray diffraction measurements, we can calculate from Eqs. (5.1) and (5.2) the

ratios $\frac{\chi_{SPS}}{\chi_{SSP}}$ = - 0.037 and $\frac{\chi_{PPP}}{\chi_{SSP}}$ = - 0.52 for the hexadecanol monolayer. They compare well with the measured ratios - 0.090 < $\frac{\chi_{SPS}}{\chi_{SSP}}$ < 0 and $\frac{\chi_{PPP}}{\chi_{SSP}}$ = - 0.52 ± .09 obtained from the values of SFG susceptibilities listed in Table 2. This shows that our procedure is self-consistent and supports the choice of n′ = 1.18 for both monolayers. This value of n′ is lower than bulk refractive indices of hexadecane[45] (n = 1.43), hexadecanol[45] (n = 1.44) and 5CT[46] (n_e = 1.89, n_o = 1.54) but is not unreasonable since the CH_3 group is in contact with air and therefore has only a partial screening by nearby neighboring molecules. In Section D we support this choice of n′ with a simple calculation based on a modified Lorentz model for the local-field correction at the interface. In principle, the values for n′ for other moieties in the monolayer could be different, but in the following we will use the same n′ for all moieties and show that our results give a self consistent picture of the molecular geometry at the interface.

It should also be noted from Eq. (5.1) that if r > 1 then $\frac{\chi_{SPS}}{\chi_{SSP}}$ < 0. However, the sign of $\frac{\chi_{PPP}}{\chi_{SSP}}$ in Eq. (5.2) is very important for determining the molecular orientation since this equation has terms of different signs. We have experimentally determined the sign of $\frac{\chi_{PPP}}{\chi_{SSP}}$ for the r^+ mode (and also for the CN stretch) in the following way. If the IR input is tuned on resonance and P-polarized, and the visible input is set midway between S and P polarizations, the sum-frequency output polarization will have S and P components contributed by χ_{SSP} and χ_{PPP}, respectively. If these contributions are in

phase, the sum-frequency polarization will be in the same quadrant as the visible polarization; if they are out of phase, the output polarization will be in another quadrant. Therefore, the polarization direction of the sum-frequency output can reveal the sign of $\frac{\chi_{PPP}}{\chi_{SSP}}$.

C.2 Cyano Group

We have used the CN stretch peak in the SFG spectra to determine the orientation of the CN bond in 5CT. The spectra are shown in Figure 5, where the single peak can be attributed to the stretching of the cyano triple bond. Fitting the spectra with Eq. (2.16) gives the resonant frequency, damping constant and strengths of this mode listed in the last row of Table 1. The hyperpolarizability tensor of this mode again has only two nonvanishing independent components $\alpha_{\zeta\zeta\zeta}$ and $\alpha_{\xi\xi\zeta} = \alpha_{\eta\eta\zeta} = r\,\alpha_{\zeta\zeta\zeta}$ with ζ along the triple bond direction, as discussed in Chapter 2 (the value of r is, however, different than that for the CH_3 group). Using Eqs. similar to (5.1) and (5.2) but with Fresnel factors calculated using[43] $n_2(VIS) = 1.337$, $n_2(IR) = 1.315 + 0.011\,i$, $n_2(SF) = 1.342$, and $n' = 1.18 \pm 0.04$ as determined above from the CH spectra, we can deduce θ and r for the CN bond from the measured ratios $\frac{\chi_{SPS}}{\chi_{SSP}}$ and $\frac{\chi_{PPP}}{\chi_{SSP}}$. We find $\theta = 53° \pm 3°$ and $r = 0.25 \pm 0.03$. In this case we have no *a priori* reason to choose $n' = 1.18$. Considering that the CN groups are buried under the monolayer, in contact with water, we would expect n' to be somewhat larger than 1.18, possibly close to the value of bulk water ($n = 1.34$). This would lead to smaller θ and r. We shall come back to this point in Section D.

C.3 Terphenyl Chromophore

We determined the orientation of the terphenyl chromophore by SHG. This has been studied before with a less complete measurement and analysis.[34] As is well understood, the SHG from 5CT comes mainly from the terphenyl part where the electron cloud is highly delocalized, yielding a large optical nonlinearity. Therefore SHG can be used to selectively measure the orientation of the chromophore. As discussed in Chapter 2, to extract information on the chromophore orientation from the measured χ elements, once again we need to have some knowledge about the hyperpolarizability tensor. In this case, the second harmonic frequency is in resonance with an electronic transition of 5CT involving an excited state that has an electron redistribution along the long axis of the terphenyl ring ζ.[34] Therefore the $\alpha^{(2)}$ components whose first index is ζ should be dominant. We will also assume that the terphenyl ring is cylindrically symmetric about the ζ axis. This assumption is motivated by the fact that the phenyl rings in the chromophore do not lie all in the same plane: paraterphenyl molecules have twist angles between adjacent phenyl rings ranging from 15° to 27° in a low temperature phase.[47] 5CB molecules (similar to 5CT, but with only two phenyl rings) have a twist angle of 26° in the crystalline phase[48] and 38° in the nematic phase.[49] With these assumptions, the hyperpolarizability tensor contains two significant nonvanishing independent elements, $\alpha_{\zeta\zeta\zeta}$ and $\alpha_{\zeta\xi\xi} = \alpha_{\zeta\eta\eta} = r\,\alpha_{\zeta\zeta\zeta}$. (Again we use the same symbol r for the polarizability ratio, although it should take a different value than for the CH_3 or CN groups.) The procedure for obtaining the chromophore orientation is then very similar to the one used in Sections C.1 and C.2. From the experimentally determined ratios $\frac{\chi_{SM}}{\chi_{PS}} = 1.16 \pm 0.04$ and $\frac{\chi_{PP}}{\chi_{PS}} =$

0.55 ± 0.05, we deduce θ = 50.0° ± 2.5° and r = -0.050 ± 0.006 for the terphenyl chromophore using Eqs. (2.9) to (2.12) and (2.23) (with the first and last sub-indices of χ_{ijk} exchanged in Eq. (2.23)) and[43] n_2(VIS) = 1.337, n_2(SH) = 1.381 and n′ = 1.18 ± 0.04. Again, we have no *a priori* reason to choose n′ = 1.18 here. A larger n′ could yield a smaller θ. We also note that the above determined value of r = -0.050 is quite small, implying that our assumption about the axial symmetry of the terphenyl core does not have a significant effect on the value of θ.

D. Discussion

The chemical structure of 5CT molecule is shown in Figure 1. According to this picture, the polar angles of the cyano group and terphenyl chromophore should be equal to each other. If the alkyl chain takes an all-trans conformation, as suggested by the weakness of the d^+ mode in the SFG spectrum of Figure 3, the polar angle of the terminal CH_3 group should also take the same value. The polar orientation deduced from our SHG and SFG measurement agrees well with this picture. The measured polar angles of the cyano group (53° ± 3°), terphenyl ring (50.0° ± 2.5°) and terminal CH_3 group (54° (+ 14°, - 8°)) all agree within the experimental uncertainty. Combining the above measurements we can conclude that the 5CT polar angle is 51.5° ± 1.5°. However, this orientation is quite different from the value obtained previously[34] for the chromophore (60°) from SHG measurements by assuming n′ = 1, indicating again the importance of its proper determination. In this earlier measurement, the assumption of n′ = 1 was supported by the linear relationship between the square root of SHG signal and monolayer density. This can only be true if n′ does not depend on density, which is only true for n′ = 1. However,

from the scatter in the data and limited monolayer density range studied, a small change in linearity caused by $n' \approx 1.2$ at full coverage could not be easily detected.

We should now comment on the values of n′ used in the data analysis. We hope to justify the value of $n' = 1.18$ determined for the hexadecanol and 5CT monolayers with a simple estimate of the local-field correction at the interface using a modified Lorentz model.[50] In calculating the orientation of a moiety, we need to know the ratio of $\chi^{(2)}$ elements, for example, $\frac{\chi^{(2)}_{eff,SPS}}{\chi^{(2)}_{eff,SSP}}$. We consider the moiety at the interface between media 1 and 2 with refractive indices n_1 and n_2, respectively (two-layer model). From Eqs. (2.8) and (2.13), we can write

$$\frac{\chi^{(2)}_{eff,SPS}}{\chi^{(2)}_{eff,SSP}} = \frac{\sin\beta_1}{\sin\beta_2}\left(\frac{L_{zz}l_{zz}}{L_{yy}l_{yy}}\right)_{\omega_1}\left(\frac{L_{yy}l_{yy}}{L_{zz}l_{zz}}\right)_{\omega_2}\frac{\langle\alpha^{(2)}_{yzy}\rangle}{\langle\alpha^{(2)}_{yyz}\rangle} \tag{5.3}$$

where $\langle\alpha^{(2)}_{ijk}\rangle = \sum_{\xi,\eta,\zeta}\langle(\hat{\mathbf{i}}\cdot\hat{\xi})(\hat{\mathbf{j}}\cdot\hat{\eta})(\hat{\mathbf{k}}\cdot\hat{\zeta})\rangle\,\alpha^{(2)}_{\xi\eta\zeta}$ and $L_{ii}(\Omega)$ is given in Eqs. (2.9) to (2.11) except that in $L_{zz}(\Omega)$, n′ is taken as n_1. From the usual three-layer model (Figure 1 of Chapter 2), however, we have

$$\frac{\chi^{(2)}_{eff,SPS}}{\chi^{(2)}_{eff,SSP}} = \frac{\sin\beta_1}{\sin\beta_2}\left(\frac{L_{zz}(n')}{L_{yy}}\right)_{\omega_1}\left(\frac{L_{yy}}{L_{zz}(n')}\right)_{\omega_2}\frac{\langle\alpha^{(2)}_{yzy}\rangle}{\langle\alpha^{(2)}_{yyz}\rangle} \tag{5.4}$$

with $L_{ii}(\Omega)$ given in Eqs. (2.9) to (2.11). Comparison of Eqs. (5.3) and (5.4) then yields, at each ω,

$$\frac{l_{zz}}{l_{yy}} = \left(\frac{n_1}{n'}\right)^2 \tag{5.5}.$$

This result can be proved to be true in general. To find n′, we must evaluate l_{zz} and l_{yy}. Consider the geometry shown in Figure 6, where we have assumed $n_1 = 1$ for simplicity. The extension to the case of $n_1 \neq 1$ is straightforward. We want to calculate the local field at the point P at the surface for the input field parallel (Figure 6(a)) or perpendicular (Figure 6(b)) to the surface. The local field at P is the sum of the input field and the dipole fields generated by polarizations inside the hemisphere around P and in the rest of the semi-infinite medium. Because of the assumed isotropic symmetry of the medium, dipole field from the polarization in the hemisphere vanishes and E_P is given by

$$E_P = E_0 + E_{surf} \tag{5.6}$$

where E_{surf} is the contribution from the bound charges at the slab surface, as shown in Figure 6. We can calculate E_{surf} in the electrostatic limit. The results for E_0 parallel and perpendicular to the surface are

$$E_P^{//} = E_0^{//} - \frac{n_2^2 - 1}{3n_2^2} E_0^{//} = E_0^{//}\left(\frac{2n_2^2 + 1}{3n_2^2}\right), \qquad \text{with } E_0^{//} \,//\, z \tag{5.7}$$

$$E_P^{\perp} = E_0^{\perp} + \frac{n_2^2 - 1}{6} E_0^{\perp} = E_0^{\perp}\left(\frac{n_2^2 + 5}{6}\right), \qquad \text{with } E_0^{\perp} \perp z. \tag{5.8}.$$

Knowing $l_{xx} = l_{yy} = E_P^{\perp} / E_0^{\perp}$ and $l_{zz} = E_P^{//} / E_0^{//}$, we then get from Eq. (5.5)

$$\left(\frac{1}{n'}\right)^2 = \frac{(2n_2^2 + 1)/(3n_2^2)}{(n_2^2 + 5)/6} = \frac{4n_2^2 + 2}{n_2^2(n_2^2 + 5)} \tag{5.9}.$$

The above equation gives $n' = 1.22$ for $n_2 = 1.5$ (close to the value for hydrocarbons) and $n' = 1.15$ for $n_2 = 1.34$ (close to the value for water). The value of $n' = 1.18$ we used in the data analysis is between these two values. This means that for any reasonable choice for n_2 the value of n′ calculated from this simple model is close to 1.18,

which, as we have shown in this paper, does give a consistent picture of the 5CT orientation and conformation within our experimental uncertainty.

As shown by this simple calculation, the value $n' = 1.18$ determined from SFG measurements for the terminal CH_3 group is not unreasonable, considering that this group is right at the interface between air and the rest of the monolayer and therefore has only a partial screening by neighboring molecules. However, the use of $n' = 1.18$ for the analysis of terphenyl chromophore and CN orientations is less justifiable. Intuitively, one would expect that n' for the terphenyl chromophore and CN would assume values very close to the bulk refractive indices of the monolayer material and the water subphase, respectively. The polar angles obtained would be 30° for the terphenyl chromophore (taking $n' = 1.60$) and 41° for the CN group (taking $n' = 1.34$). These values are in clear disagreement with the CH_3 orientation, even with its large error bar. Therefore, the value of n' for the core part cannot be considerably larger than the value 1.18 determined for the CH_3 group. This suggests that the proper value for n' for the analysis of SFG or SHG measurements has to be determined with care. It may not necessarily be the same as the bulk refractive index of the material at the interface or the one determined by ellipsometry ($n_e' = 1.49$, $n_o' = 1.46$ for a dodecanol monolayer at the air/water interface[13]), since the effective n' depends on the local-field correction and on which moiety being probed.

To conclude, we have shown that the second-order nonlinear optical processes, SFG and SHG, can be used to quantitatively determine the average orientation of selective atomic groups or moieties of surface molecules. The combined results allow us to completely map out the orientation and conformation of a fairly complicated molecule

at an interface. The 5CT Langmuir monolayer is chosen as a demonstrating system. The orientations of all three parts of the molecule, cyano group, terphenyl ring and pentyl chain, have been measured separately by optical SHG and SFG. The results give a quantitatively consistent picture of the molecular configuration if the appropriate refractive indices for the monolayer are used. The latter can be obtained from measurements on a similar monolayer of known orientation.

E. Remarks about Curve Fitting

As was mentioned in Chapter 2, the resonant features in an SFG spectrum interfere with the nonresonant background and other overlapping resonances, so that the lineshape can be severely distorted. In most of the spectra presented in this Thesis this interference may not appear very obvious, except for a few cases in Chapter 6. However, even when not obvious this effect has to be considered when a quantitative determination of peak positions, linewidths and strengths is desired. This is especially important for the determination of molecular orientation, as discussed in this Chapter. Also, from the fitting parameters one may extract more information from the spectra, such as the relative phase among various peaks and also between peaks and the nonresonant background. This will be exemplified in Chapter 6.

Here we want to make some general comments about curve fitting of SFG spectra from a practical point of view. The curve fitting was done with a commercial data analysis and graphing software (Microcal Origin, version 4.1) that uses the iterative Levenberg-Marquardt algorithm. The spectra were fitted with the signal proportional to $|\chi^{(2)}(\omega)|^2$, and $\chi^{(2)}(\omega)$ of the form of Eq. (2.16) (simple Lorentzian resonances). If

inhomogeneous broadening is severe and the IR bandwidth is small enough a Voigt profile may be more appropriate,[51] but in our case we found that this additional complication is not justified, since a Lorentzian function gives a good fit to most spectra.

In simple cases like the spectra in Figure 5 where only one peak and the nonresonant the background are present, the fitting procedure is straightforward and it converges rapidly for any reasonable input for the initial parameters. However, when many overlapping peaks are present it becomes considerably more difficult to obtain a good fit. This is the case for SFG spectra of alkyl chains in the CH stretch range (see for instance Figures 3 and 4) where at least 5 resonances (r^+, r^+_{FR}, r^-, d^+ and d^-) should be expected in a 200 cm^{-1} frequency range. In such cases, one should use physical arguments as much as possible in order to reduce the number of parameters in the fitting procedure. For instance, if the visible input and output beams are away from electronic resonances in any media (transparent interfaces like the ones considered here), both the resonant strengths χ_q and χ_{NR} should take on real values. In some cases, *a priori* knowledge of the relative signs for various resonances may be available from simple polarizability models, as the one described in Chapter 2, so that they can be fixed in the fitting procedure. Even with these simplifications, a typical spectrum for alkyl chains consisting of at most 100 points would be fitted with 16 parameters. Therefore, we should strive for the best possible fit. It is very helpful to use linear constraints to the fitting parameters to restrict them within physically acceptable ranges, especially for linewidths and positions of relatively weak peaks. Sometimes the fit seems to converge to an obviously worse fit, even if we start from initial parameters that give a better fit. In such cases, the better input parameters for peak positions and linewidths should be kept constant in the fitting and

only the strengths should be allowed to vary. Finally, one is usually interested in fitting a set of spectra with the same resonances, such that only their amplitudes are expected to be different for each spectrum. In these cases, a simultaneous fit of all spectra with the linewidths and peak positions shared among all of them can greatly improve the convergence and quality of the final fit. This procedure was used to fit the spectra with different polarization combinations and obtain the fitting parameters listed in Tables 1 and 2.

References

(1) A.W. Adamson and A. P. Gast, *Physical Chemistry of Surfaces*, 6th edition, Wiley-Interscience, New York, NY (1997).

(2) A. Zangwill, *Physics at Surfaces*, Cambridge University Press, Cambridge, UK (1988).

(3) See for example the special issue of *Surface Science* **299/300** (1994).

(4) R. E. Palmer and P.J. Rous, *Rev. Mod. Phys.* **64**, 383 (1992).

(5) P. Avouris and J. Demuth, *Annu. Rev. Phys. Chem.* **35**, 49 (1984).

(6) J. R. Lu, Z. X. Li, J. Smallwood, R. K. Thomas and J. Penfold, *J. Phys. Chem.* **99**, 8233 (1995).

(7) J. Als-Nielsen, D. Jacquemain, K. Kjaer, F. Leveiller, M. Lahav and L. Leiserowitz, *Phys. Rep.* **246**, 251 (1994).

(8) K. Hosoi, T. Ishikawa, A. Tomioka and K. Miyano, *Jpn. J. Appl. Phys. Part 2* **32**, L135 (1993).

(9) M. W. Tsao, T. M. Fischer and C. M. Knobler, *Langmuir* **11**, 3184 (1995).

(10) C. Lautz, Th. M. Fischer, M. Weygland, M. Lösche, P. B. Howes and K. Kjaer, *J. Chem. Phys.* **108**, 4640 (1998).

(11) R. Mendelsohn, J. W. Brauner and A. Gericke, *Annu. Rev. Phys. Chem.* **46**, 305 (1995).

(12) D. J. Neivandt, M. L. Gee, M. L. Hair and C. P. Tripp, *J. Phys. Chem. B* **102**, 5107 (1998).

(13) M. A. Hines, T. D. Harris, A. L. Harris and Y. J. Chabal, *J. Electron Spectrosc. Rel. Phen.* **64/65**, 183 (1993).

(14) T. Sueoka, J. Inukai and M. Ito, *J. Electron Spectrosc. Rel. Phen.* **64/65**, 363 (1993).

(15) M. D. Elking, G. He and Z. Xu, *J. Chem. Phys.* **105**, 6565 (1996).

(16) I. Hirosawa, *Jpn. J. Appl. Phys., Part 1*, **36**, 5192 (1997).

(17) Y. R Shen, *Annu. Rev. Phys. Chem.* **40**, 327 (1989).

(18) G. L. Richmond, J. M. Robinson and V. L. Shannon, *Prog. Surf. Sci.* **28**, 1 (1988).

(19) T. F. Heinz, in *Nonlinear Surface Electromagnetic Phenomena*, H. E. Ponath and G. I. Stegeman, eds, p. 353, North Holland, Amsterdam (1991).

(20) Y. R. Shen, *Surf. Sci.* **299/300**, 551 (1994).

(21) K. B. Eisenthal, *Chem. Rev.* **96**, 1343 (1996).

(22) C. D. Bain, *J. Chem. Soc. Faraday Trans.* **91**, 1281 (1995).

(23) Tadjeddine, A. and Peremans, A., *Surf. Sci.* **368**, 377 (1996).

(24) D. E. Gragson, B. M. McCarty, G. L. Richmond and D. S. Alavi, *J. Opt. Soc. Am.* B. **13**, 2075 (1996).

(25) X. Zhuang, D. Wilk, L. Marrucci and Y. R. Shen, *Phys. Rev. Lett.* **75**, 2144 (1995).

(26) C. D. Stanners, Q. Du, R. P. Chin, P. Cremer, G. A. Somorjai and Y. R. Shen, *Chem. Phys. Lett.* **232**, 407 (1995).

(27) G. R. Bell, C. D. Bain and R. N. Ward, *J. Chem. Soc. Faraday Trans.* **92**, 515 (1996).

(28) R. N. Ward, D. C. Duffy, G. R. Bell and C. D. Bain, *Molec. Phys.* **88**, 269 (1996).

(29) R. Braun, B. D. Casson, and C. D. Bain, *Chem. Phys. Lett.* **245**, 326 (1995).

(30) S. R. Hatch, R. S. Polizzotti, S. Dougal and P. Rabinowitz, *J. Vac. Sci. Tech.* A **11**, 2232 (1993).

(31) H. Yamamoto, N. Akamatsu, A. Wada, K. Domen and C. Hirose, *J. Electron Spectrosc. Rel. Phen.* **64/65**, 507 (1993).

(32) D. Zhang, J. H. Gutow, T. F. Heinz and K. B. Eisenthal, *J. Phys. Chem.*, **98**, 13729 (1994).

(33) K. Wolfrum and A. Laubereau, *Chem. Phys. Lett.* **228**, 83 (1994).

(34) G. Berkovic, Th. Rasing and Y. R. Shen, *J. Opt. Soc. Am. B* **4**, 945 (1987).

(35) T. G. Zhang, C. H. Zhang and G. K. Wong, *J. Opt. Soc. Am. B* **7**, 902 (1990).

(36) T. F. Heinz, H. W. K. Tom and Y. R. Shen, *Phys. Rev. A* **28**, 1883 (1983).

(37) M. S. Johal, E. W. Usadi and P. B. Davies, *J. Chem. Soc. Faraday Trans.* **92**, 573 (1996).

(38) H. Hsiung, G. R. Meredith, H. Vanherzeele, R. Popovitz-Biro, E. Shavit and M. Lahav, *Chem. Phys. Lett.* **164**, 539 (1989).

(39) G. Cnossen, K. E. Drabe and D. A. Wiersma, *J. Chem. Phys.* **97**, 4512 (1992).

(40) R. M. Corn and D. A. Higgins, in *Characterization of Organic Thin Films*, A. Ulman, ed., p.227, Butterworth-Heinemann, Boston, MA (1995).

(41) P. Guyot-Sionnest, J. H. Hunt and Y. R. Shen, *Phys. Rev. Lett.* **59**, 1597 (1987).

(42) Several schemes for obtaining the orientation of CH_3 groups of an alkyl chain by SFG have been discussed in the literature. Bain and co-workers have critically reviewed them recently.[27]

(43) M. R. Querry, D. M. Wieliczka and D. J. Segelstein, in *Handbook of Optical Constants of Solids II*, E. D. Palik, ed., p. 1059, Academic Press, Boston, MA (1991).

(44) J. Majewski, R. Popovitz-Biro, W. G. Bouwman, K. Kjaer, J. Als-Nielsen, M. Lahav and L. Leiserowitz, *Chem Eur. J.* **1**, 304 (1995).

(45) M. D. Lechner, ed., *Refractive Indices of Pure Liquids and Binary Mixtures*, Landolt-Börnstein Vol. III/38B, Springer (1996).

(46) F. Allen, EM Industries (private communication).

(47) S. Ramdas and J. M. Thomas, *J. Chem. Soc. Faraday II* **72**, 1251 (1976).

(48) T. Hanemann, W. Haase, I. Svoboda and H. Fuess, *Liquid Crystals* **19**, 699 (1995).

(49) G. Celebre, M. Longeri, E. Sicilia and J. W. Emsley, *Liquid Crystals* **7**, 731 (1990).

(50) J. D. Jackson, *Classical Electrodynamics*, 2nd edition, Wiley, New York, NY (1975).

(51) C. D. Bain, P. B. Davies, T. H. Ong, R. N. Ward and M. A. Brown, *Langmuir* **7**, 1563 (1991).

Tables

Table 1: Fitting parameters χ_q, ω_q and Γ_q of SFG spectra for 5CT monolayer on water.

Mode	ω_q (cm^{-1})	Γ_q (cm^{-1})	$\chi_{q,\ SSP}$	$\chi_{q,\ PPP}$	$\chi_{q,\ SPS}$
d^+	2852	8.0	0.43 ± 0.23	.21 ± 0.36	-0.42 ± 0.41
r+	2878	8.7	5.18 ± 0.52	-1.52 ± 0.18	-0.97 ± 0.31
d^-	2917	10.0	0.67 ± 0.34	-0.80 ± 0.36	0.02 ± 0.76
r^+_{FR}	2943	10.0	4.19 ± 0.12	-5.23 ± 0.22	-0.51 ± 0.42
r^-	2959	10.6	1.50 ± 0.18	8.45 ± 0.41	-2.82 ± 0.26
CN stretch	2233	7.3	13.55 ± 1.30	-3.17 ± 0.43	5.35 ± 0.50

Table 2: Fitting parameters χ_q, ω_q and Γ_q of SFG spectra for a hexadecanol monolayer on water.

Mode	ω_q (cm^{-1})	Γ_q (cm^{-1})	$\chi_{q,\ SSP}$	$\chi_{q,\ PPP}$	$\chi_{q,\ SPS}$
d^+	2853	9.4	-1.2 ± 0.47	-0.01 ± 1.00	-0.50 ± 1.44
r+	2875	6.8	17.63 ± 1.40	-9.12 ± 0.90	-0.08 ± 1.50
d^-	2919	10.0	-0.01 ± 0.54	5.79 ± 3.69	-0.10 ± 0.85
r^+_{FR}	2936	7.8	14.35 ± 1.21	-8.71 ± 1.78	-0.72 ± 0.98
r^-	2959	9.0	-7.49 ± 2.75	15.63 ± 1.20	11.69 ± 1.63

Figure Captions

Figure 1. Chemical structure of 5CT.

Figure 2. Pressure-area isotherm for a 5CT monolayer on water.

Figure 3. SFG spectra for a 5CT monolayer on water in the CH stretch range. Circles, squares and triangles are the experimental data obtained with SSP, PPP and SPS polarizations, respectively. Solid lines are the fitting curves.

Figure 4. SFG spectra for a hexadecanol monolayer on water in the CH stretch range. Circles, squares and triangles are the experimental data obtained with SSP, PPP and SPS polarizations, respectively. Solid lines are the fitting curves.

Figure 5. SFG spectra for a 5CT monolayer on water in the CN stretch range. Circles, squares and triangles are the experimental data obtained with SSP, PPP and SPS polarizations, respectively. Solid lines are the fitting curves.

Figure 6. Slab model for calculation of local-field correction at the interface. The incident field E_0 is (a) parallel and (b) perpendicular to the interface.

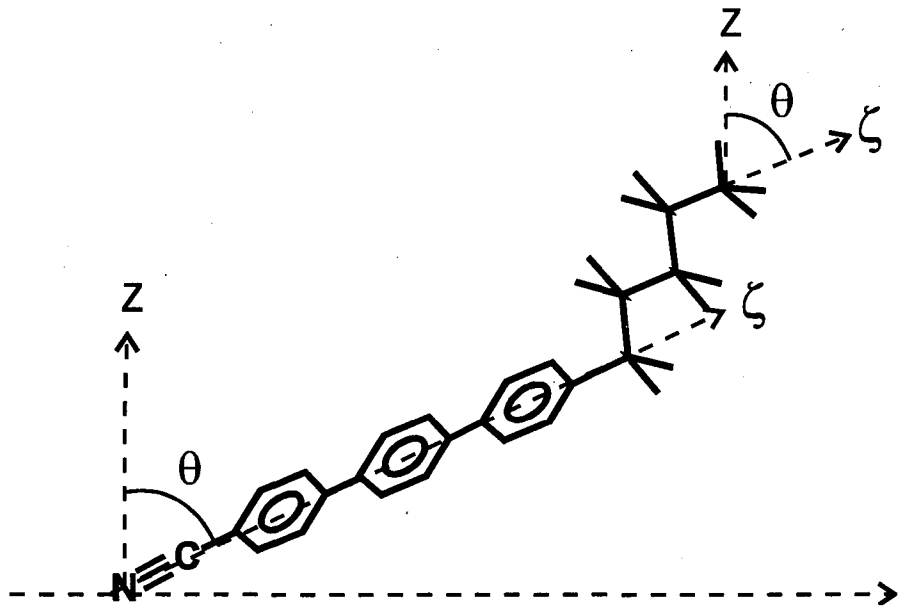

Figure 1

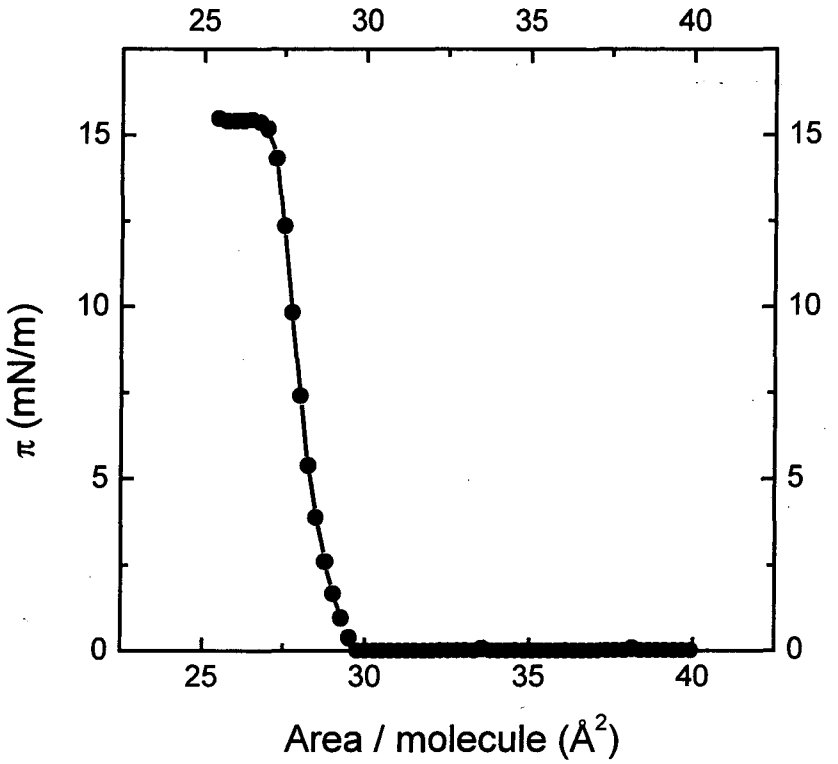

Figure 2

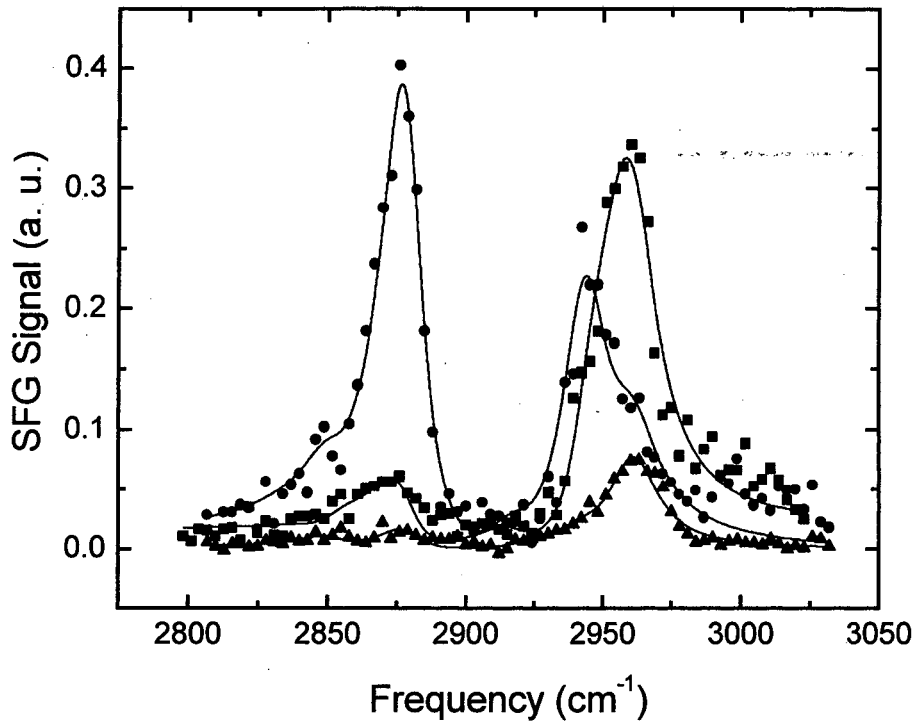
SFG Signal (a. u.)
0.0
0.1
0.2
0.3
0.4
2800
2850
2900
2950
3000
3050
Frequency (cm-1)

Figure 3

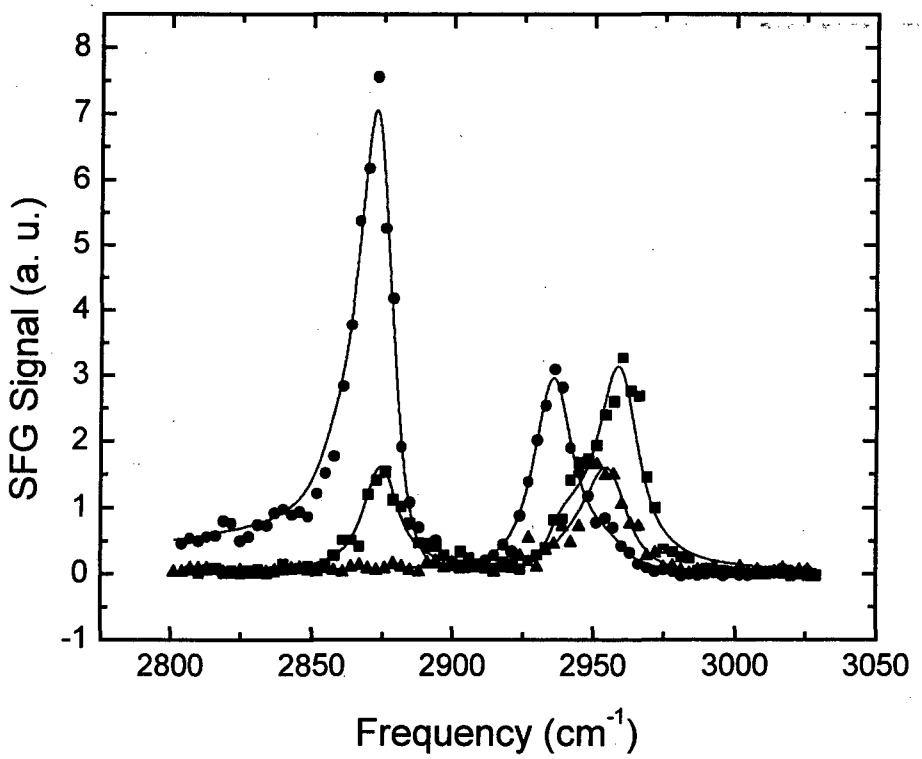
SFG Signal (a. u.)
8
7
6
5
4
3
2
1
0
-1
2800
2850
2900
2950
3000
3050
Frequency (cm-1)

Figure 4

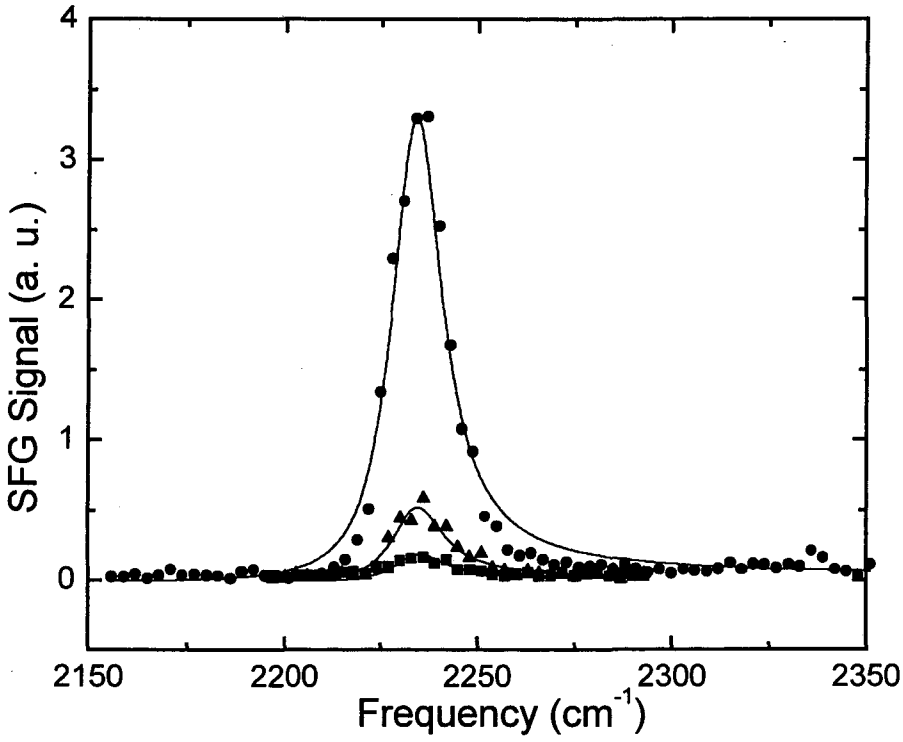

Figure 5

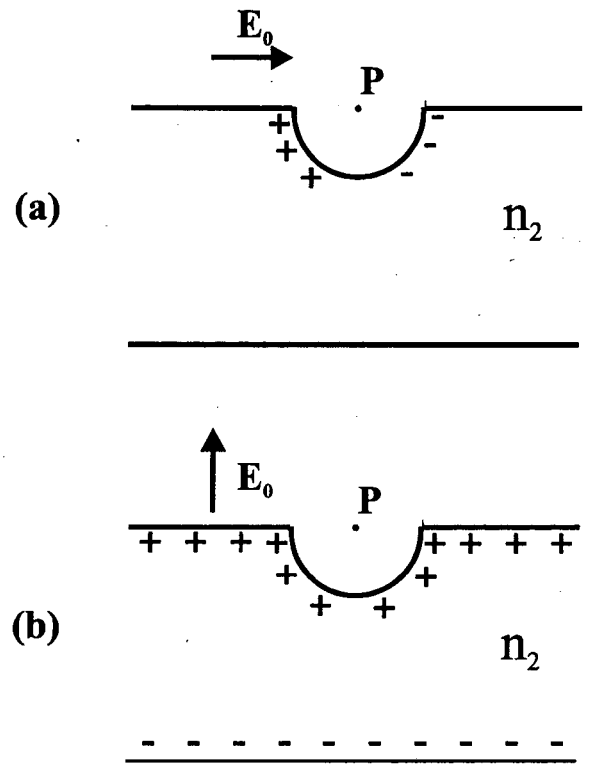

Figure 6

Chapter 6. Conformation of Surfactant Monolayers at Solid / Liquid Interfaces

A. Introduction

As we have mentioned in Chapter 1, adsorption of surfactants on various surfaces and interfaces plays an important role in a variety of technological processes, because of their ability to modify the interfacial properties of a substrate.[1,2] Detergency, emulsification, coatings, lubrication, mineral flotation, and oil recovery are just a few examples.[2-5]

They have therefore been studied extensively with many experimental techniques such as adsorption isotherms,[4,6-12] electrokinetic[4,6-11] and wetting[8,10,13,14] measurements, ellipsometry,[9,10] and calorimetry.[7,11,12] These techniques have provided some insights to the adsorption mechanisms, but only limited information about the structure of adsorbed films can be inferred from them. Recently, other techniques that can provide more microscopic information, such as neutron reflection,[15-17] nuclear magnetic resonance,[18,19] X-ray photoelectron spectroscopy,[20] infrared spectroscopy,[21,22] surface-enhanced Raman spectroscopy,[23-25] atomic force microscopy,[26] and the surface force apparatus[26-29] have been adopted to study the structure of monolayers and bilayers of many different surfactants, but so far several important questions related to orientation and conformation of surfactant molecules remain unanswered. More precisely, how the conformation of the surfactant alkyl chains would depend on the liquid environment surrounding them, or on the surface density and chain length of the adsorbed surfactant has hardly been studied experimentally. Several models for the configuration of adsorbed surfactants at

solid/liquid interfaces have been proposed, but direct experimental support is scarce.[18,20,30,31] In this Chapter we will address a few of these questions using SFG vibrational spectroscopy.

Our studies are also related to another important issue. In most commercial applications, surfactant solutions are composed of many ingredients in order to attain the desired properties. For instance, the addition of alkanes and alcohols to surfactant solutions has a profound influence on their bulk behavior[32-34] and adsorption properties.[35] The presence of ionic surfactants dramatically modifies the adsorption of non-ionic surfactants.[36,37] Addition of alcohols to cationic surfactant solutions may change the interaction between mica surfaces immersed in the solutions.[38] In microemulsions, the interaction of the oil phase with surfactant monolayers determines their stability.[39] Clearly, understanding the interactions among different surfactants in a mixture or between oil and surfactants is a fundamental problem that has far-reaching consequences in applications.

Towards this goal, many authors have studied co-adsorption of surfactants at solid/liquid interfaces using techniques like adsorption isotherms,[36,37,40] fluorescence probes,[41] ellipsometry[42] and sum-frequency generation.[43-46] They reveal strong synergistic effects in the adsorption of ionic/non-ionic surfactant mixtures. The interaction of surfactants with alkanes has been studied in microemulsions and monolayers at the air/water interface with techniques like surface tension[47-50] and neutron reflection measurements,[51] fluorescence microscopy,[49] small-angle neutron scattering[52] and X-ray reflectivity.[53,54] It was found that depending on the chain length, the interacting alkane could spread on the monolayer and form a macroscopic film on the air/water

interface or stay as a bulk phase (droplets) in equilibrium with a mixed monolayer of surfactant and alkane. The extent of alkane penetration in the monolayers depends on the surfactant density at the air/water interface. These results serve as models for the oil/water interfaces,[53] important for understanding of microemulsion formation and biological systems.[55] Despite all these advances, a detailed microscopic picture of the various interfaces is still lacking, or at most incomplete.

The interaction of liquids with self-assembled monolayers is also of fundamental importance in connection with wetting phenomena.[56-58] If a contacting liquid can alter the structure of the monolayers,[57,59,60] this will in turn affect the wetting properties of the interface by the liquid. It is known that compact monolayers are rather insensitive to the liquid environment,[56,61-64] due to limited penetration of solvent molecules and lack of available space for conformational defects. The conformation of loosely packed monolayers, on the other hand, is considerably more sensitive to the liquid environment around them,[65,66] and has a profound implication on the interpretation of contact angle measurements. In the case of long-chain alkanes, it has long been suggested that they can penetrate and affect the properties of loosely packed monolayers[67-69] or mixed monolayers of alkyl thiols with different chain lengths.[57,59,70] A very recent molecular dynamics simulation[71] shows that penetration of hexadecane into loosely packed monolayers with different chain lengths can induce conformational changes in the monolayers.

In this Chapter we use SFG vibrational spectroscopy to study the microscopic structure of surfactant monolayers interacting with various liquids, trying to address a few of the important issues mentioned above. We have prepared self-assembled

surfactant monolayers on fused silica with different chain lengths and surface densities. These monolayers were put in contact with various liquids of different characteristic intermolecular interactions, such as non-associated liquids (non-polar and polar liquids whose major intermolecular interactions are dipole and van der Waals interactions) or hydrogen-bonding liquids. We also consider long-chain alkanes and alcohols separately, since their structure is similar to surfactant molecules and they may have strong interactions with them (chain-chain interaction), as suggested by our studies in Chapter 3.

Our results show that the surfactant conformation is very sensitive to the liquid environment, and it also depends on various parameters such as monolayer surface density and surfactant chain length. When the monolayers are in contact with non-associated liquids, the chain conformation is slightly more disordered than at the solid/air interface, the effect becoming stronger as the polarity of the liquid increases. In the case of hydrogen-bonding liquids, the monolayer chains are driven towards more compact configurations, which are possible if the alkyl chains become highly disordered, by the hydrophobic effect.[66] In the case of alkanes, the van der Waals chain-chain interaction between alkanes and surfactant could straighten the initially disordered surfactant chains, if strong enough. Finally, the long-chain alcohols form an ordered hydrogen-bonding layer above the surfactant monolayer. Then as in the case of hydrogen-bonding liquids, the hydrophobic effect causes the surfactant chain conformation to become highly disordered. This situation can however be reversed by dilution of the long-chain alcohols in a non-polar solvent. Then the alcohol molecules can no longer be hydrogen-bonded to form a layer. They can now penetrate the surfactant monolayer and straighten the surfactant chains via the chain-chain interaction.

B. Experimental Details

The surfactant monolayers were prepared by self-assembly on infrared-grade fused quartz windows (Esco Products Inc). The windows were thoroughly cleaned in hot chromic acid for several hours and then extensively rinsed with purified water (resistivity higher than 18.0 MΩ·cm, Barnstead NanoPure II). The pH value of the final rinse was allowed to equilibrate to 5.6 – 5.8. The substrates were then dried in a stream of N_2 gas and placed in an oven at 120 °C for 1 hour in order to remove any remaining water layer. This cleaning procedure produces a fully hydroxylated quartz surface that becomes negatively charged in water with sufficiently high pH due to partial ionization of the surface silanol groups.[72,73]

Cyclohexane (C_6H_{12}), carbon tetrachloride (CCl_4), methanol (CH_3OH), and butanol ($CH_3(CH_2)_3OH$) were purchased from J. T. Baker; DCE (1,2-dichloroethane – $(CH_2Cl)_2$), anhydrous octanol ($CH_3(CH_2)_7OH$), and hexadecanol ($CH_3(CH_2)_{15}OH$) from Aldrich. All chemicals used had purities above 99% and were used as received, except hexadecanol which was recrystallized twice from acetone. The deuterated liquids were obtained from Cambridge Isotopes or Isotec and had isotope enrichments higher than 98%. Four different cationic surfactants were used: DOAC (dioctadecyl-dimethylammonium chloride – $(CH_3(CH_2)_{17})_2N^+(CH_3)_2Cl^-$), DDAC (didecyl-dimethylammonium chloride – $(CH_3(CH_2)_9)_2N^+(CH_3)_2Cl^-$), DBAB (dibutyl-dimethylammonium bromide – $(CH_3(CH_2)_3)_2N^+(CH_3)_2Cl^-$) and DMOAP (N-octadecyl-dimethyl[(3-trimethoxysilyl)propyl]ammonium chloride – $CH_3(CH_2)_{17}N^+(CH_3)_2(CH_2)_3Si(CH_3O)_3Cl^-$). Purified DOAC and DDAC were obtained

from KAO Corporation and used as received. DBAB was prepared by mixing N,N-dimethyl-N-butylamine and 1-bromobutane (both from Aldrich) in warm ethanol (~ 60 °C) for a few hours an then recrystallized three times from diethyl ether and acetone. DMOAP was purchased from United Chemical Technologies as a 50% solution in methanol and filtered (0.45 μm pore size) before use.

The self-assembly procedure of DOAC and DDAC monolayers is similar to the method described in Ref. 26. The cleaned substrates were first immersed in a heated (~ 60 °C) cyclohexane solution of the surfactants (C = 0.2 mM) for 30 minutes. They were then rinsed in warm cyclohexane for another 30 minutes and blow-dried with N_2 gas. The DBAB monolayer was prepared in a similar way, except that the cyclohexane solution was saturated with DBAB. The DMOAP monolayer was prepared by immersing the clean substrates in an aqueous solution[74] of the surfactant containing acetic acid (100:3:2 water : acetic acid : DMOAP, by volume) for 30 minutes. Afterwards, they were rinsed with pure water for about one minute, blow-dried with N_2, and then baked at 120 °C for 1 hour. All these samples could be stored in a vacuum desiccator under P_2O_5 for more than 2 months with no degradation. Figure 1 shows the schematic structures of DOAC and DMOAP molecules, and the corresponding adsorbates left on the fused quartz substrate by the self-assembly procedure. Both surfactants are adsorbed as positive ions interacting with the negatively charged quartz surface, but in the case of DMOAP its head-group becomes hydrolyzed and it also binds covalently to the quartz surface.[74] DDAC and DBAB are similar to DOAC, except for the different length of their alkyl chains (C_{10} and C_4, respectively, compared to C_{18} for DOAC).

The SFG measurements were performed in setup A, described in Chapter 2. The IR and visible beams were incident on the monolayer-covered fused quartz substrate from the air side and overlapped at the quartz/liquid interface. The liquid was contained in a cell made of Teflon that was thoroughly cleaned in chromic acid and extensively rinsed with ultrapure water. Some long-chain alcohols are solid at room temperature. In such cases, the cell was heated to several degrees above the melting point of the alcohol.

C. Characterization of Self-Assembled Monolayers

In most experiments, it is important to first determine the surface density of surfactant monolayers. For the DOAC monolayer, this was accomplished by comparing SFG spectra of a Langmuir film of various known surface densities at the air/water interface to that of the self-assembled monolayer.[75] There is however some complication. The SFG spectrum in the CH stretch range for a DOAC monolayer at the air/water interface is distorted by interference with the shoulder of a strong OH stretch peak of the water layer at the interface, as shown in Figure 2(a) for a DOAC surface density (N) of 2.5 chains/nm^2. This OH peak at ~ 3200 cm^{-1} comes from the well-ordered hydrogen bonding network of water at the interface, due to the strong surface electric field generated by the charged DOAC monolayer, as discussed in Section C.2 of Chapter 4. To obtain the SFG spectrum for the CH stretch modes only, we must subtract off the water contribution. We realize that the SFG spectrum can be approximated by (see Eq. (2.16))

$$S(\omega_2) \propto \left|\chi^{(2)}(\omega_2)\right|^2 = \left| \sum_q \frac{\chi_q}{\omega_2 - \omega_q + i\Gamma_q} + B + C\cdot\omega_2 \right|^2 \qquad (6.1)$$

where χ_q, ω_q and Γ_q are the amplitudes, frequencies and linewidths of the CH stretch modes, respectively, and B+C·ω represents the dispersive background contributed by water. The vibrational modes involved are the CH_2 and CH_3 symmetric stretches (d^+ and r^+, respectively) at ~ 2850 and ~ 2875 cm^{-1} and the CH_3 Fermi resonance and asymmetric stretch (r^+_{FR} and r^-, respectively) at ~ 2935 and ~ 2960 cm^{-1}. The pure DOAC spectrum can then be calculated from Eq. (6.1) by setting B = C = 0. A set of spectra for various surface densities of DOAC obtained this way is shown in Figure 2(b). Note that the CH_2 peak at 2850 cm^{-1} gradually disappears with increasing surface density and hence decreasing amount of gauche defects, similar to the case of a pentadecanoic acid Langmuir film discussed in Chapter 2.[76] A comparison of this set of spectra to spectra of DOAC at the quartz/air interface (Figures 3 (top spectrum), 16(a) and 19 (top spectrum)) shows that the DOAC surface density is between 2.5 and 3.0 chains/nm^2. We take it as 2.8±0.2 chains/nm^2. It should be noted from Figure 2(b) that in this surface density range the SFG spectrum is very sensitive to the chain density. Therefore, the variation of the SFG spectra of DOAC at the quartz/air interface (Figures 3 (top spectrum), 16(a) and 19 (top spectrum)) is due to a small (~ 10%) change in surface density. The surface densities of DDAC and DBAB monolayers are assumed to be the same as that of DOAC because the self-assembly mechanism is dominated by electrostatic interaction between the cationic surfactant and the negatively charged substrate. Hydrophobic contribution to adsorption should be negligible since a non-polar solvent was used in the self-assembly process. Therefore, the surface density of the surfactants should be rather insensitive to the chain length. Indeed, in Ref. 26, surfactant monolayers of various chain lengths

prepared in a similar way on mica substrates were found to have very similar surface densities.

DMOAP is a single-chain silane surfactant (chain length C_{18}) that forms chemisorbed monolayers on glass. The surface density of a DMOAP monolayer was estimated to be ~ 2.0 chains/nm^2 from a similar procedure (using a Langmuir film of a single chain surfactant as a reference[76]) and from its known head-group area.[74] Because of the lower chain density of the monolayers used herein (~ 2 to 3 chains/nm^2) when compared to fully packed monolayers such as alkylthiols on gold[56,59] or OTS[69] (octadecyltrichlorosilane) on glass (~ 5.0 chains/nm^2), they are considerably less hydrophobic than the latter. For example, the water advancing contact angle on a DOAC monolayer was about 66°, compared to ~ 110° for fully packed monolayers.

Figure 3 displays the SFG spectra for a DOAC monolayer at the quartz/air interface in the frequency range of CH stretch modes, taken with three input-output polarization combinations (SSP, SPS and PPP). The peak assignments are the same as those discussed above and also in Chapter 3. They closely resemble the spectra of a pentadecanoic acid Langmuir film[76] at a comparable surface density (see for example Figure 3(b) of Chapter 2) and are typical of monolayers where the alkyl chains contain a significant amount of gauche defects, as evidenced by the presence of the d^+ mode at ~ 2850 cm^{-1} with a strength comparable to the r^+ peak at ~ 2875 cm^{-1}. This is to be expected from the lower surface density of DOAC monolayers (~ 2.8 chains/nm^2) when compared to fully packed monolayers with typical chain densities of ~ 5.0 chains/nm^2. The ratio of peak strengths of the d^+ to the r^+ mode ($D = \chi_{d^+} / \chi_{r^+}$) is often used as a measure of the relative conformational order of alkyl chains, with this ratio decreasing as the amount of

gauche defects in the chains decreases.[43,44,46,77,78] It will be used in the next sections to aid our discussion of the conformational changes of surfactant monolayers. The other major peak in the spectra is the r^{+}_{FR} at ~ 2940 cm^{-1}, although it strongly overlaps with the nearby d^{-} and r^{-} peaks. The latter two peaks are rather weak in all polarization combinations, although the d^{-} is more pronounced in the SSP polarization and the r^{-} is stronger for SPS and PPP polarizations. The lack of significant features due to CH_3 stretch modes of the surfactant head-group has been noticed before,[79] and may be caused by an almost in-plane orientation of these groups. Very weak features at ~ 2810, 2900 and 2990 cm^{-1} may be due to them, although this assignment is not definite. We will now discuss the SFG spectra for a DOAC monolayer in contact with non-associated liquids.

D. Interaction of Surfactant Monolayers with Non-Associated Liquids

D.1 DOAC Monolayer in Contact with Non-Associated Liquids

In an earlier SFG study of a closely packed OTS monolayer on fused quartz, it was found that the conformation of the alkyl chains is hardly sensitive to different liquid environments; they are always straight.[62] This is true for liquids as different as CCl_4, hexadecane and water. This result is not so surprising since at the fully packed surface density, the chain-chain interaction between the surfactant molecules dominates and the penetration of solvent molecules between chains is unlikely. At lower chain densities, however, the liquid molecules are expected to penetrate and interact with the exposed chains. Therefore, the alkyl chains would be more sensitive to the liquid environment and could adopt a large variety of conformations. This is indeed true for a DOAC monolayer, as we will see in this Chapter.

Here we discuss the SFG spectra of surfactant monolayers at the quartz/liquid interfaces for the case of non-associated liquids. This distinction is made because, as will be shown later, associated liquids such as hydrogen-bonding liquids have a dramatic effect on the chain conformation. Some of the liquids used in this Chapter posses CH or OH groups, so that they would exhibit resonant peaks in the same frequency region of the surfactant chains and confuse the spectrum of the latter. This problem can be solved by using completely deuterated liquids, so that their vibrational frequencies are shifted outside the frequency range of the surfactant chains without significantly modifying the intermolecular interactions or the liquid structure.

The SFG spectra for a DOAC monolayer at the quartz/CCl_4 interface taken with three polarization combinations (SSP, PPP and SPS) are displayed in Figure 4. The SSP spectrum is quite similar to the one obtained at the quartz/air interface (Figure 3). However, the relative increase of the ratio between the d^+ and r^+ peak strengths (D, as defined above) does indicate that the presence of CCl_4 leads to a more disordered chain conformation. The SPS spectrum supports this conclusion, since distinct features present in the SPS spectrum of DOAC at quartz/air interface are no longer evident in the spectrum of DOAC at the quartz/CCl_4 interface. The poorer orientational order of chains with gauche defects generally leads to an overall reduction of the SFG spectrum as can be expected from Eq. (2.14). The PPP spectrum also shows a relative increase of contributions from CH_2 groups compared to CH_3 groups. However, the PPP spectrum is more difficult to interpret because it has mixed contributions from the three independent $\chi^{(2)}$ components (see Eq. (2.8)). This result contradicts the common idea that packing of

liquid molecules between low-coverage surfactant monolayers would favor more ordered chain conformations than at the quartz/air interface.[18,21,22]

In order to gain a better understanding of how effectively the polarity of the liquid makes the alkyl chains disordered, we have obtained the SFG spectra of DOAC monolayers at quartz interfaces in contact with two other non-associated polar liquids: deuterated chloroform ($CDCl_3$, dipole moment μ = 1.15 D) and deuterated 1,2-dichloroethane ($ClCD_2CD_2Cl$, dipole moment μ = 1.86 D). They are displayed in Figure 5, with the SSP spectrum of Figure 4 (in CCl_4) also shown for comparison. The spectra show how the overall SFG signal gradually decreases as the dipole moment of the liquid molecules increases. It appears that with increasing polarity of the opposing liquid, the alkyl chains possesses an increasing amount of gauche defects, leading to a reduction in the SFG spectral intensity from the orientational average.

To support this interpretation, we have taken the SFG spectra of DOAC monolayers on quartz in contact with various mixtures of CCl_4 and $CDCl_3$. They are shown in Figure 6. As the concentration of $CDCl_3$ is increased, it can be seen that the overall spectral intensity is gradually reduced, as expected from the previous results. However, we note that the ratio D of d^+ to r^+ peak strengths also increases as the $CDCl_3$ concentration increases, indicating that the chain conformation is indeed becoming more disordered as the liquid environment becomes increasingly polar. Of course, this interpretation assumes that the DOAC monolayer cannot be removed by any of the liquids used in our experiments. We will address this issue in Section E.4.

D.2 Simple Free-Energy Argument

Here we want to give a simple free-energy argument to qualitatively explain the effect of liquid environment on surfactant chain conformation. For simplicity, we assume the surfactant chain density is low enough so that chain-chain interaction can be neglected. We recognize that this is not realistic for the cases we have studied but hopefully it will not affect our qualitative understanding of the main physical mechanisms involved in determining the chain conformation. In any case, quantitative predictions can only be attained by full calculations with realistic models. With the chains being considered as isolated and our interest focussed on chain conformation, the simplified system we will consider is simply a single alkyl chain immersed in bulk liquid; the presence of the solid substrate or surfactant head-groups is also neglected. Let F = E - TS be the total free energy of the chain-solvent system, where T and S refer to temperature and entropy, respectively. The internal energy E has contributions from the energy to create gauche defects in the surfactant chains (E_S), from interaction between liquid molecules (E_L) and from interaction between liquid molecules and the surfactant chain (E_{SL})

$$E = E_S + E_L + E_{SL} \tag{6.2}.$$

We treat the surfactant chain as an alkane of same chain length composed of CH_2 groups with CH_3 terminations. We assume each CH_2 or CH_3 group has the same size as a surrounding solvent molecule. This is not unreasonable since typical diameters of solvent molecules ($CDCl_3$ and CCl_4) and CH_2 groups are approximately 5 to 6 Å.[80] We then consider a simple three-dimensional lattice model with each cell containing either a liquid molecule, referred as (2), or a segment (CH_2 or CH_3 group) of the alkane chain, referred as (1). The gauche defects in the chain are represented by 90° bends in one of the three

orthogonal planes of the 3D lattice. Consider the two simple configurations illustrated in Figure 7. Configuration (I) represents a C_{18} alkane in an extended all-trans conformation surrounded by liquid molecules, and configuration (II) is the same as (I) except that the alkane molecule in a more compact conformation. It should be noted that for clarity reasons only one plane of cells is displayed in Figure 7 and configuration (II) is contained in that plane only. The total internal energy for each configuration can be calculated by restricting to nearest-neighbors interactions. Three different (negative) types of interaction energies need to be taken into account: liquid-liquid interaction (E_{22}), segment-segment interaction (E_{11}) and liquid-segment interaction (E_{21}). The energies E_{ij} are assumed to be from van der Waals interaction between like or dislike molecules or pseudo-atoms. The (positive) energy necessary for creating one gauche defect in the chain is denoted E_d.

Configuration (I) can be characterized by the numbers of nearest neighbors between segments, between solvent molecules, and between segments and liquid molecules, denoted by $n_{11}^{(I)}$, $n_{22}^{(I)}$ and $n_{12}^{(I)}$, respectively. The total internal energy (Eq. (6.2)) is consequently

$$E^{(I)} = n_{11}^{(I)} E_{11} + n_{22}^{(I)} E_{22} + n_{12}^{(I)} E_{12} \qquad (6.3).$$

In the same way, configuration (II) is characterized by $n_{11}^{(II)}$, $n_{22}^{(II)}$ and $n_{12}^{(II)}$ and its total internal energy is

$$E^{(II)} = n_{11}^{(II)} E_{11} + n_{22}^{(II)} E_{22} + n_{12}^{(II)} E_{12} + n_d E_d \qquad (6.4)$$

where n_d is the number of gauche defects in the chain. With this simple model, we can understand the basic mechanism responsible for the liquid-induced chain disordering deduced from the SFG spectra in this Section. From Figure 7 we see that the energy

difference between configurations (I) and (II) is due to: (a) $n_{11}^{(II)} > n_{11}^{(I)}$, since the chain folds on itself; (b) $n_{22}^{(II)} > n_{22}^{(I)}$ and (c) $n_{12}^{(II)} < n_{12}^{(I)}$, since solvent molecules that were interacting with the chain are now in the bulk liquid; (d) n_d gauche defects created in configuration (I). As E_{ij} are negative and E_d is positive, relations (a) and (b) lead to lower energy for configuration (II), while (c) and (d) tend to increase E for configuration (II) with respect to (I). To see which contribution is dominant, we need to estimate the energies E_{ij}.

Consider first the case of an alkane chain surrounded by nonpolar CCl_4 molecules. The interaction energies E_{ij} take the following values, assuming an intermolecular distance of 5.7 Å:[80]

$$\begin{aligned} E_{11} &= -1.2\cdot10^{-22}\ \text{J} \qquad (CH_2\text{-}CH_2) \\ E_{22} &= -44.0\cdot10^{-22}\ \text{J} \qquad (CCl_4\text{-}CCl_4) \\ E_{12} &= -7.4\cdot10^{-22}\ \text{J} \qquad (CCl_4\text{-}CH_2) \end{aligned} \tag{6.5}$$

We see that the interaction between liquid molecules is almost one order of magnitude larger than any other interaction, since CCl_4 is more polarizable than a CH_2 group. Therefore we expect the term $n_{22}E_{22}$ in Eqs. (6.3) and (6.4) to be dominant over $n_{11}E_{11}$ and $n_{12}E_{12}$. This implies that more compact configurations like (II) lead to more negative interaction energies (E_{int}). The configurations that minimize the total internal energy will result from a balance between this lowering of interaction energy by compact conformations and the energy cost n_dE_d for creating n_d gauche defects. Since $E_d \cong 62.0\cdot10^{-22}$ J (for n-butane in the gas phase[81]), comparable to E_{22} in Eq. (6.5), we note that the equilibrium conformation should indeed be very sensitive to the strength of intermolecular interactions in the liquid. Figure 8 illustrates schematically the delicate

balance in the total internal energy for the system that leads to an equilibrium conformation in a liquid environment.

In the above estimate, only the internal energy of both configurations has been discussed. The entropic contribution to the free-energy is obviously important. There is an entropy increase due to the collapse from an extended chain conformation to a more compact one. This would further lower the free-energy of the compact conformations. There is also an entropic contribution from the liquid structure surrounding the alkyl chain. At the surface of a polar liquid, molecules may become orientated by the dipole-dipole interactions between them, which will lead to lower entropy at the surface than in the bulk. In general, polar liquids have lower surface entropy than nonpolar liquids. For example, the values for surface entropy of $CHCl_3$ and CCl_4 are 116 J/(K·m^2) and 139 J/(K·m^2), respectively, as calculated from data of reference.[82] If we extrapolate this surface behavior to molecules surrounding the alkyl chains, then for more extended conformations a larger number of polar molecules would be ordered around the chains and the entropy of the interfacial system would be lowered. On the other hand, a more compact conformation involves less ordered polar molecules and the entropy of the interfacial system would increase. Hence, a compact conformation is entropically favorable and the free energy of the system is additionally lowered by the entropy term.

With this simple model, we can now analyze qualitatively the effect of various liquids on surfactant chain conformation and compare the results to our experimental observations. In the case of non-associated liquids examined in this Section, we expect the intermolecular interaction (E_{22}) in the liquid to increase as its polarity increases, due to stronger dipole-dipole and dipole-induced-dipole interactions. By the free-energy

argument discussed above, this favors more compact conformations. Also, as discussed above, liquids with higher dipole moments should have lower interfacial entropy, further lowering the free energy for more compact conformations. This is what we have observed for the conformation of DOAC monolayers in contact with non-associated liquids.

This free-energy model also predicts that as the surfactant chains become shorter, the effect of liquids on chain conformation should become weaker. This is because as shorter chains fold, less liquid molecules surrounding the chains would go back to the bulk. Therefore, for a given number of defects, both the gain in interaction energy and the entropy increase from an all-trans conformation would be reduced, or in other words, the magnitude of E_{int} in Figure 8 would be reduce with respect to n_dE_d, leading to a smaller n_d at equilibrium. We shall examine this in the following.

D.3 Effect of Surfactant Chain Length

We have also studied DDAC and DBAB monolayers on fused quartz in contact with non-associated liquids, to investigate if the conformational changes would become less significant as the surfactant chains become shorter. The SFG spectra of monolayers with different chain lengths C_n (DBAB (n = 4), DDAC (n = 10) and DOAC (n = 18)) are shown in Figure 9. For monolayers adsorbed at the quartz/air interface (Figure 9(a)-(c)), the relative strength of the r^+ stretch (2875 cm^{-1}) to the d^+stretch (2850 cm^{-1}) increases with the decrease of chain length. This indicates that the shorter chains have less gauche defects, as expected if the chain-chain interaction is relatively unimportant (because of the lower surface density of these monolayers). Figure 9(d)-(f) displays the corresponding SFG spectra for these monolayers at the quartz/CCl_4 interface. The CH_2 peak (d^+) is

almost insignificant in the spectra of a DBAB monolayer in both air and CCl_4, whereas in the case of DOAC it is very pronounced, more so in CCl_4 than in air. A comparison of the two sets of spectra shows that the effect of CCl_4 on the surfactant chains gradually increases as the chain length increases, as expected from the free-energy arguments of Section D.2.

E. Interaction of Surfactant Monolayers with Hydrogen-Bonding Liquids

E.1 DOAC Monolayer in Contact with Hydrogen-Bonding Liquids

We now consider the effect of highly polar hydrogen-bonding liquids on the surfactant conformation. The liquids used were deuterated methanol (CD_3OD) and deuterated water (D_2O). The SFG spectra for a DOAC monolayer at the quartz/D_2O interface and at the quartz/CD_3OD interface taken with the SSP polarization combination are shown in Figure 10, together with the spectrum obtained at the quartz/CCl_4 interface for comparison. The former are at the noise level, with little discernible features. This is true for all three different input-output polarization combinations (SSP, SPS and PPP) as seen in Figure 11 for DOAC at the quartz/D_2O interface. Therefore, the vanishing SFG signal is not due to a certain selection rule related to a specific polarization combination. It must result from the existence of a near inversion symmetry for both CH_2 and CH_3 groups of the surfactant chains. This can happen if the chains become highly disordered, folded into a compact configuration (or "curled up"), so that the orientations of both CH_2 and CH_3 groups are almost random. The observation shows that hydrogen-bonding liquids have a much stronger effect on the chain conformation than non-associated liquids.

We have also taken the SFG spectra for a DOAC monolayer at the interfaces with a set of mixtures of CCl_4 and CD_3OD. As shown in Figure 12, all the peaks in the SSP spectrum attributed to the surfactant chains decrease drastically when the concentration of CD_3OD increases from 0 to 1% (in volume fraction). At 0.25%, all peaks in the SFG spectrum of DOAC have decreased significantly, and they nearly vanish at 1%. Among them, the r^+ peak at ~ 2875 cm^{-1} decreases the fastest, indicating a rapid deterioration of the orientational order of terminal CH_3 groups that results from increase in the amount of gauche defects in the chains. With the increasing CD_3OD concentration, the surfactant chains must have progressively folded into a compact form, i.e., the chains "curled up" leading to an isotropic-like configuration (on average) for the CH_2 and CH_3 groups, which then become SFG inactive.

The 1% volume fraction of CD_3OD in the above experiment certainly does not mean that the same concentration of CD_3OD is present at the interface. In fact, from the observed drastic effect of the mixtures on the chain conformation, one would expect a much higher surface concentration of methanol. To get a rough estimate of the methanol concentration at the interface, we took the SFG spectra of the DOAC monolayer at the interface of quartz with mixtures of CH_3OH and CCl_4. The observed spectra in the CH stretch range, shown in Figure 13, now come from both DOAC chains and CH_3OH adsorbed at the interface. As with deuterated methanol, the peaks due to DOAC observed at 0% concentration gradually decrease and become completely replaced by the CH stretch modes (r^+ and r^+_{FR} at ~ 2830 and 2950 cm^{-1}, respectively) of methanol[83] at a concentration of 1%. From a comparison of the peak strengths of the CH_3 symmetric stretch of methanol in the SFG spectra of the quartz/DOAC/mixture and air/methanol

interfaces, we found the surface concentration of methanol at the interface of the 1% methanol mixture to be ~ 40% (mole fraction). This value is likely to be underestimated because in the comparison it is assumed that the orientational distribution of methanol molecules at both interfaces is the same. Since the methanol molecules are solvating the curled up surfactant chains, they may have a broader orientational distribution than at the neat liquid surface.

These results show that the microscopic structure of the interfacial liquid plays a fundamental role in determining the conformation of the surfactant chains, since hydrogen-bonding liquids with polarity similar to DCE have a remarkably stronger effect on the surfactant alkyl chain conformation. This can be qualitatively understood by recalling the free-energy argument of Section D.2. Note that the energy for a hydrogen bond is of the order of - $5.4 \cdot 10^{-20}$ J,[84] about one order of magnitude stronger than E_{22} for CCl_4 given in Eq. (6.5). We expect that as the intermolecular interactions between liquid molecules become stronger (E_{22} more negative), the interaction energy E_{int} sketched in Figure 8 would become relatively more important than $n_d E_d$, therefore driving the chain conformation towards more compact configurations. This argument assumes that liquid molecules surrounding the surfactant chains must have broken hydrogen bonds. As we will discuss in Section E.5, this is not obvious *a priori*. However, we found experimentally that surface water molecules surrounding a DOAC monolayer indeed have dangling OH groups (see Section E.3).

E.2 Effect of Surfactant Chain Length

As seen in Section D.3 for the case of non-associated liquids, it is expected that as the surfactant chains become shorter the effects of the liquid environment on chain conformation should become less noticeable. To study this issue in the case of hydrogen-bonding liquids, we took the SFG spectra of DBAB and DDAC monolayers at the quartz/D_2O and quartz/CD_3OD interfaces. In all cases, the spectra vanish in the same way as for DOAC. Figure 14 shows the SFG spectra for a DBAB monolayer at the interfaces of quartz and mixtures of CCl_4 and CD_3OD. As in the case of DOAC, the spectrum decreases in intensity with increase of methanol concentration and nearly vanishes at about 1% volume fraction. The same result was obtained with DDAC.

These results are in contrast to the case of non-associated liquids, where the difference of chain conformations in air and liquid environments was indeed smaller for shorter surfactant chains. We attribute this contrast to the remarkably stronger intermolecular interactions involved in the case of hydrogen-bonding liquids. It is interesting to note that even chains as short as C_4 (4 carbons long, which can have at most three gauche defects) can lead to a vanishing SFG spectrum. This suggests that in the case of non-associated liquids, where we can still observe features in the SFG spectrum, the average number of gauche defects per chain is less than three.

E.3 Structure of Water in Contact with a DOAC Monolayer

Previous studies[86] have shown that a characteristic of hydrophobic surfaces is the existence of dangling OH groups (not hydrogen-bonded) for water molecules at the interface. Since the self-assembled surfactant monolayers used herein make the quartz surface hydrophobic, we expect the same to be true in our case. We have measured the

temperature dependence of the SFG spectrum of the quartz/DOAC/water interface. The result is displayed in Figure 15. It is seen that the spectral features in the 2800 to 3000 cm^{-1} range for the CH stretch modes of the surfactant chains are nearly absent and hardly depend on temperature. The broad spectral features between 3000 cm^{-1} and 3700 cm^{-1} come from the OH stretch modes of interfacial water molecules. As discussed in Chapter 4, the peaks at ~ 3200 cm^{-1} and ~ 3400 cm^{-1} can be attributed, respectively, to a more ordered ("ice-like") and less ordered hydrogen-bonding network of water molecules. A relatively narrower peak at ~ 3650 cm^{-1} is due to dangling OH groups at the interface.[85] These spectral features of water in Figure 15 do show temperature dependence. The peak at ~ 3400 cm^{-1} increases with increase of temperature while the peak at 3200 cm^{-1} decreases, and so does the overall spectral intensity. As discussed in Ref. 85, this corresponds to the fact that the ice-like hydrogen-bonding network that characterizes surface water structure becomes more disordered by thermal agitation at higher temperatures. No noticeable temperature dependence for the dangling OH peak at 3650 cm^{-1} is observed. These results will be discussed in more detail in Section E.5.

E.4 Dissolution of the Monolayers

The interpretation given in the preceding sections regarding disappearance of SFG signal from surfactant monolayers in contact with hydrogen-bonding liquids assumes that they are not dissolved by any of the liquids used. This is indeed what we found experimentally. When the samples were soaked in various solvents, including water, for periods longer than our data acquisition time (~ 30 min) and subsequently dried, the SFG spectrum from the monolayer in air was recovered almost to the level before the solvent

exposure. The case with water is depicted in Figure 16. It shows the spectra for a DOAC monolayer on quartz: (a) in air, freshly prepared, (b) immersed in water, and (c) blow-dried by N_2 gas after immersed in water and then stored it in a vacuum desiccator with P_2O_5 for a few days. While the spectrum of DOAC is completely suppressed in water, it recovers after the monolayer is dried, although the chain conformation is not as ordered as that of the freshly prepared sample, possibly because of incomplete drying.

Similar results were obtained with other solvents. For example, Figure 17(a) shows the spectra for a DOAC monolayer at the quartz/CCl_4 interface before and after it has been immersed in $CDCl_3$ for a few hours and rinsed with pure CCl_4. Although the intensity is significantly reduced after exposure to $CDCl_3$, it is nevertheless considerably stronger than the spectrum obtained in pure $CDCl_3$ (see Figure 5), indicating again that dissolution of the monolayer by the solvents cannot be responsible for the changes in the SFG spectra upon varying the liquid environment. This is also true for the short-chain surfactants like DBAB, as shown in Figure 17(b). The spectra of DBAB at the quartz/CCl_4 interface, before and after immersion in methanol and rinse with pure CCl_4, are almost identical. Therefore, any appreciable dissolution of the monolayers can be ruled out. In fact, removal of the surfactant monolayers from quartz can only be attained by cleaning with strongly oxidizing solutions ("piranha" solution, chromic acid) or by etching the substrate in a concentrated alkaline solution.

We have also observed disappearance the SFG spectrum of DMOAP monolayers in the same hydrogen-bonding solvents.[86] DMOAP is a silane that chemisorbs onto the quartz surface[74] and certainly cannot be dissolved in these solvents. The same effect has also been observed for loosely packed surfactant monolayers on different substrates

(quartz and mica). The SFG spectra of water in contact with a DOAC monolayer (Figure 15) also indicate that the surfactant molecules have not been dissolved away by water, since in this case the quartz surface should become hydrophilic and no peak at ~ 3650 cm^{-1}, corresponding to dangling OH groups, should be observed. These results clearly indicate that conformational disordering of alkyl chains in water and other hydrogen bonding solvents is responsible for the observations. This is expected to be a generic phenomenon although it becomes less important for densely packed monolayers due to limited solvent penetration into the monolayers.[61,62,63,64]

The vanishing SFG spectra of loosely packed surfactant monolayers in contact with hydrogen-bonding liquids is due to a considerable reduction in peak strength for the CH stretch modes of the alkyl chain, when compared to spectra taken at the quartz/air interface. To evaluate how much χ_q is reduced from air to the liquid environment, we have analyzed the SFG spectrum of a DMOAP monolayer at the quartz/air and quartz/H_2O interfaces. They were reported previously[86] but are reproduced in Figure 18, showing more detail in the CH stretch range. Figure 18(a) shows the SFG spectrum for a DMOAP monolayer at the quartz/air interface. The spectrum is dominated by the CH_2 symmetric stretch (d^+) at ~ 2850 cm^{-1} with the CH_3 symmetric stretch (r^+) as a weak shoulder at ~ 2875 cm^{-1}. Another broad peak around ~ 2930 cm^{-1} has contributions from r^+_{FR}, d^- and r^- at approximately 2935, 2920 and 2960 cm^{-1}, respectively. The large ratio of d^+ to r^+ peak strengths indicates that the chain conformation is quite disordered, as expected[57,62,65] from the low surface density of this monolayer (2.0 chains/nm^2). Figure 18(b) shows the spectrum of the DMOAP monolayer at the quartz/water interface. In this case, there is a considerable background signal from the nearby strong and broad OH-

stretch peak of interfacial water molecules (at around 3200 cm^{-1}), as in the case of DOAC Langmuir films discussed in Section C and shown in Figure 2. Interfering with this frequency-dependent background, there are however small but noticeable features that can be assigned to the same CH-stretch modes of the DMOAP spectrum at the quartz/air interface. Fitting the spectra of Figure 18(a) and (b) to Eqs. (2.16) and (6.1), respectively, we obtain the peak strengths for the CH stretches of DMOAP in air and immersed in water. We find that for the d^+ and r^+ modes, χ_q is reduced by a factor 4.5 and 1.5 in water environment as compared to the quartz/air interface, respectively. For a DOAC monolayer, the peak strengths in water are similar to the case of DMOAP, while the strengths at the quartz/air interface are considerably stronger. Therefore, in the case of a DOAC monolayer χ_q is reduced by a factor ~ 10 for both d^+ and r^+ modes when the chains go from air to water environment. The spectrum for a DMOAP monolayer at the quartz/water interface in the absence of a background from water (for instance, if water is replaced by D_2O) can be simulated from the fitting parameters by setting B and C to zero in Eq. (6.1). The simulated spectrum is shown in Figure 18(b) as a dashed line. It can be seen that without the background from water the signal is near our detection limit, which agrees with the observations in the DOAC monolayers in contact with D_2O.

E.5 Discussion

As discussed above, the dissolution of the monolayers can be ruled out. Therefore the only interpretation to the vanishing SFG spectra of surfactant monolayers in contact with hydrogen-bonding liquids is a drastic increase in conformational disorder of their alkyl chains. The hydrogen-bonding liquids clearly form a separate class of liquids due to

the particularly strong short-range interactions among molecules, which usually leads to their association in the liquid phase.

At first sight the results described in this Chapter may seem surprising. For example, previous experiments on the subject by infrared spectroscopy[21,22] have arrived at conclusions opposite to the ones inferred from our data. It was suggested that loosely packed surfactant monolayers have their chains straightened up in the presence of methanol or water. While the results may depend on chain density, we attribute the discrepancy to difficulty in interpretation of the results obtained by the technique. SFG spectroscopy has proven to be a very powerful tool for studying chain conformation because conformation changes often lead to significant changes in the spectra, allowing a more straightforward interpretation.

However, it has been long suggested that adsorbed surfactant chains may become curled up when immersed in hydrogen-bonding liquids.[30] More recently, a molecular dynamics simulation of a surfactant molecule in water showed some interesting features.[87] The conformation of a single anionic surfactant molecule (sodium dodecyl sulfate – $CH_3(CH_2)_{11}SO_4^-Na^+$) in water was found to undergo dramatic changes as a function of time. The alkyl chain conformation was found to be very dynamic, varying from an extended to a curled up configuration, and vice-versa, in the picosecond timescale.

Other well-studied phenomena can also be related to our observations. Surfactants adsorbed at a solid/liquid interface qualitatively resemble polymers grafted on a surface and immersed in a solvent, although the two have very different molecular sizes. The analogy provides us with some insights to the behavior of surfactant chains in solvents.

The effect of solvents on polymer conformation has been studied extensively,[88-90] but to our knowledge the same on surfactant chains has never been reported. It is known that the conformation of polymer chains immersed in a solvent depends strongly on the so-called quality of the solvent. For instance, when the interaction between the segment of the polymer chains and the solvent molecules is favorable ("good solvent"), the chains tend to expand further, whereas they tend to fold into more compact conformations when the interaction is unfavorable ("poor solvent"), in order to decrease the number of contacts between the chains and the solvent molecules.[91] This is exactly the idea behind the free-energy argument described in Section D.2. The model captures the essential physics that determines the chain conformation in a liquid environment, although it is obviously too simple for a quantitative description of the interfacial system. Now we want to extend that argument to the case of hydrogen-bonding liquids.

There are again two contributions to lower the free energy of the interfacial system when the chains fold into more compact conformations. First, the interaction energy between liquid molecules for the associated liquids is much stronger than in the case of non-associated liquids. Therefore, when the chains fold the number of solvent molecules interacting weakly with the alkyl chains may be reduced, leading to a decrease in the total energy E of the interfacial system. However, this may not be the dominant contribution. As will be discussed below, there is also a large entropy reduction associated with the ordering of solvent molecules around the alkyl chains. Therefore, it is very favorable to reduce the surface area of the chains exposed to the solvent (compact conformations), in order to maximize the total entropy S of the interfacial system.

The tetrahedral coordination of water molecules allows the formation of a 3-dimensional hydrogen-bonding network. In contrast, molecular dynamics simulations[92] have shown that alcohol molecules with a maximum of two hydrogen bonds per molecule can only form a 1-dimensional chain-like structure, as in the case of their crystalline phases.[93] Solvation of nonpolar, non-hydrogen-bonding solutes in these liquids may disrupt such hydrogen-bonded networks. Interactions between water and hydrophobic solutes and the energetic and structural response of water molecules to the hydrophobic solutes is generally known as hydrophobic effect and interaction,[94-100] and are often described in terms of the "iceberg formation model" proposed by Frank and Evans.[101] The main ideas of the model are outlined below.

The driving forces that determine the interfacial structure of hydrogen-bonding liquids around a hydrophobic guest are tendencies for the liquid to attain the maximum number of hydrogen bonds and to form a dense well-ordered layer in contact with the exposed hydrophobic surface. Depending on the size and shape of the hydrophobic guest, this cannot always be satisfied. For example, it has been demonstrated, both theoretically and experimentally,[85,102,103] that for the water surface layer adjoining an extended hydrophobic planar surface (like the air/water interface), sacrifice of one of the four possible H-bonds of each water molecule is required to minimize the total free-energy. Similar numerical calculations have shown that the molecular arrangement of water around a small hydrophobic solute is governed by the same principle. However, when the solute is not too large (a methane molecule, for example) it is possible for the water molecules to pack around the hydrophobic guest without giving up any of their H-bonds. In this case, water adopts the so-called "clathrate-like" structure[99,100] around the small

solute: a structure in which water molecules link to form a polygonal cage around the solute. This is due to the ability of tetrahedrally coordinated molecules to link and wrap around any small solute. The main consequence of this arrangement of the water molecules is that small hydrophobic entities will tend to aggregate in aqueous solution. Consider, for example, two small separated solutes. Each would induce an "ice-like" water structure around it (the "iceberg") that has lower entropy than the bulk water structure. This is energetically unfavorable; the free energy can be reduced by aggregating the two small solutes, since the surface area of the aggregate is smaller than the total surface area of the two separate solutes. This entropically driven "hydrophobic interaction" allows the aggregation to stabilize. For increasingly larger solutes and aggregates, a theoretical description of the transition from the clathrate-like structure to the ice-like hydrogen-bonding network at a flat hydrophobic wall is beginning to emerge,[104-106] although experimental work in this field is limited.[107]

Our experimental investigation on the conformation of surfactant alkyl chains immersed in hydrogen-bonding liquids brings some insights to the above-mentioned problem, since the surfactant chains are nonpolar hydrophobic entities of the intermediate size. Our experimental results show that similar to aggregation of small solutes, the hydrophobic effect causes the surfactant chains to collapse in order to reduce their surface area exposed to the surrounding liquid. The same free-energy argument used to qualitatively understand the effect of non-associated liquids is still valid. However, in the case of hydrogen-bonding liquids the entropy term in the free energy should be much more important. Thermodynamic measurements[101] together with theoretical calculations of Pratt and Chandler[108] on various alkanes in water show that the strength of the

hydrophobic interaction increases considerably with the chain length. According to the calculations, the chains assume a more compact conformation in water than in air and longer chains take on more compact conformations. Our experiment with hydrogen-bonding liquids yields essentially the same result for all surfactant chain lengths and the difference in the interfacial structure of the liquids (3D or 1D hydrogen-bonded network) does not seem to play a major role. This, however, could be due to a very rapid vanishing of the SFG signal from the chains as the number of defects increases, making it impossible to distinguish the degree of compactness of the chain conformation after it is below a certain limit. The experiments with DBAB described in Section E.2 suggest that this is indeed the case.

One may expect a weaker hydrophobic effect at higher temperature, as the hydrogen-bonding network of the liquid surrounding the chains becomes more disordered. In the case of water, the SFG spectra of Figure 15 do indeed show the evidence of a more disordered water surface structure at higher temperature, but no noticeable change can be seen in the spectral features of the surfactant chains. This is presumably because the effect of temperature is not strong enough to be detected in the limited range we have studied. The presence of the dangling OH peak of water in the spectra of Figure 15 indicates that the surfactant chains can indeed be regarded as hydrophobic entities of the intermediate size, around which the water molecules should form a hydrogen-bonding network intermediate between the one around a small hydrophobic solute and the one against an extended hydrophobic surface.

F. Interaction of Surfactant Monolayers with Alkanes

F.1 Interaction with Alkanes

In Section D.2, we have seen that in the case of non-associated liquids such as CCl_4, $CHCl_3$ and DCE, the interaction energies between liquid molecules is much larger than between liquid molecules and CH_2 groups or between two CH_2 groups. This allows us to neglect the latter two and conclude that compact chain conformations would become more favorable as the interaction among liquid molecules increases. An interesting question then arises: what happens if the liquid is non-associated, but the interaction among liquid molecules is comparable to liquid-CH_2 and CH_2-CH_2 interactions? Alkanes appear to be good examples, since they are composed of the same alkyl chains found in the surfactants. We therefore studied the interaction of various surfactant monolayers with alkanes.

Figure 19 shows a series of SFG spectra for a DOAC monolayer at the quartz/deuterated alkane interface. The top curve is the SFG spectrum for the DOAC monolayer in air, shown for comparison. The other curves in Figure 19 show SFG spectra for the DOAC monolayer in contact with various deuterated alkanes. The alkane chain length is indicated on each curve. The alkanes used were deuterated so that their vibrational modes are outside the frequency range of the surfactant chain modes; therefore, the spectra in Figure 19 reflect the conformational order of surfactant chains only.

To help the discussion of our results, the spectra have been fitted to Eq. (2.16). As discussed in Section E of Chapter 5, all fitting parameters are assumed to be real, since the laser wavelengths are away from electronic transitions. As mentioned earlier, the ratio of the peak strength of the CH_2 symmetric stretch to that of the CH_3 symmetric stretch

($D = \chi_{d^+} / \chi_{r^+}$) decreases as the amount of gauche defects in the chains decreases. In Figure 19, this ratio D is 0.70, 0.56 and 0.64 for a DOAC monolayer in contact with air, decane, and dodecane, respectively. The difference is not significant as it is within experimental uncertainty (~ 10%) due to sample-to-sample variations and inaccuracy of the fitting procedure. All we could say is that the surfactant conformation is not significantly changed by interaction with these alkanes. For alkane chain lengths of C_{14} and C_{16}, the DOAC spectrum exhibits hardly any trace of the d^+ mode at 2850 cm^{-1}: D is 0.16 in tetradecane and 0.07 in hexadecane, suggesting that the surfactant chains are nearly in the all-trans conformation. Apparently, the alkane molecules wedging into the surfactant monolayer now have a sufficiently long chain length to provide enough chain-chain interaction between alkane and surfactant molecules for the surfactant chains of length C_{18} to straighten up. The situation resembles the frozen surface monolayer of alkanes or fully packed Langmuir films, studied in Chapters 3 and 4, which have all-trans conformations due to the strong chain-chain interaction among surface molecules.

One may expect that for the surfactant chains to get straightened by sufficiently strong chain-chain interaction, both alkane and surfactant chains should be long enough. To verify this we repeated the same experiment as above but replacing DOAC by DDAC, which has a chain length of C_{10}. As mentioned earlier, DDAC is expected to have nearly the same surface chain density as DOAC. This is supported by their similar SFG spectra at the quartz/air interface shown in Figure 20(a) and (b), as it is known that the SFG spectra of surfactant monolayers depend strongly on surface density[75,76] but considerably less on alkyl chain length.[109] We found that none of the alkanes used in the experiment of Figure 19 was able to straighten the surfactant chains. As an example, the results for

DOAC and DDAC monolayers in contact with deuterated tetradecane (C_{14}) are shown in Figures 20(c) and 20(d), respectively. Note that while the chain conformations of the molecules in air are very similar, they are very different when interacting with tetradecane: the DOAC chains are straightened but the DDAC chains are not. (The ratio of d^+ and r^+ peak strengths D is 0.60, 0.86 and 0.99 for DDAC in contact with air, tetradecane and decane, respectively.) This shows that indeed *both* surfactant and alkane must have long enough chains to effect straightening of surfactant chains. For lack of surfactants with intermediate chain length, we can only conclude at present that the minimum chain length for the surfactant chains to observe the straightening effect is between C_{10} and C_{18}. It is interesting to note that the minimum alkane chain length for surface freezing to occur is C_{15} (see Chapter 3).

Another parameter of importance in this phenomenon must be the chain density of the surfactant monolayer.[67,68,110] We expect that for surfactant monolayers of too low a surface density, the chain-chain interaction between alkane and surfactant is also not strong enough to cause straightening of surfactant chains. To see whether this is true, we have obtained SFG spectra of DOAC and DMOAP monolayers in air and deuterated hexadecane, which are displayed in Figure 21. Both surfactants have the same chain length (C_{18}), but the chain density for the DMOAP monolayer (2.0 chains/nm^2) is about 70% of that for DOAC. The spectra in Figures 21(a) and 21(b) are for the DMOAP and DOAC monolayers in air, respectively. Because of the lower chain density, the DMOAP monolayer appears to have more gauche defects, as evidenced in the spectrum of Figure 21(a) by a larger ratio D of d^+ to r^+ peak strengths (see Section E.4). When the monolayers are immersed in deuterated hexadecane their spectra show markedly different

behaviors. The DMOAP spectrum (Figure 21(c)) is qualitatively similar to that in air. On the other hand, the DOAC spectrum (Figure 21(d)) undergoes a dramatic change with the disappearance of the CH_2 modes that implies straightening of surfactant chains. We then conclude that the minimum chain density of the surfactant monolayer for the chain straightening to happen in alkanes is between 2.0 and 2.8 chains/nm^2.

F.2 Discussion

Our results are directly relevant to the general use of contact angle wetting measurements to probe the structure of adsorbed monolayers.[57,59,111,112] Alkanes (especially hexadecane) are widely used as probe liquids in such experiments. We now know that when loosely packed monolayers are being probed, one must be careful in interpreting the results due to possibility of solvent penetration into the monolayer leading to its restructuring. This has long been suggested in connection to wetting experiments on incomplete monolayers,[67,68] where it appeared that hexadecane and tetradecane could penetrate the octadecylamine partial monolayers and make them highly oleophobic, resembling fully packed monolayers of alkyl chains. The solvent penetration had much less dramatic effects if the amine chain length was reduced to C_{12} or if solvents with bulky molecules were used. Also, if the amine monolayer had a surface density below ~ 40% of a full monolayer, oleophobicity was quickly lost. All these observations are in remarkable agreement with our spectroscopic results on the interactions of surfactant monolayers with alkanes.

The ability of alkanes to penetrate loosely-packed monolayers and restructure the interfacial layer has also been suggested more recently to explain wetting measurements

on partial surfactant monolayers[69] and mixed alkylthiol monolayers of different chain lengths.[59,70] Bain and Whitesides[59] have studied wetting on various mixed monolayers of C_{12} and C_{22} thiols on gold. They found that as the fraction of C_{12} chains on the surface was increased from 0 to about 0.5, the hexadecane contact angle varied from 46° to ~ 20°. This reduction in oleophobicity was attributed to the disorder of the exposed ends of the C_{22} chains above the compact C_{12} layer. Using decane instead of hexadecane, the drop in oleophobicity occurred more abruptly and at a larger fraction of C_{12} chains in the monolayer. They attributed this result to the fact that the length of a decane molecule fits nearly exactly into the vacancies left in the mixed monolayer by the replacement of C_{22} by C_{12}. With decane molecules penetrating the partial monolayer it would produce a fully packed layer of alkyl chains with mainly methyl groups in contact with the liquid. This would increase the oleophobicity in comparison to a disordered layer of alkyl chains. When the surface density of C_{22} chains became less than 80% of a monolayer, decane penetration could no longer sustain a fully packed ordered layer of alkyl chains and the oleophobicity started to drop. This observation is qualitatively consistent with our results although in our case the minimum surfactant and alkane chain lengths to render the formation of a fully packed monolayer of alkyl chains are longer than C_{10}. However, our result is related to a chain density of about 2.8 chains/nm^2 (56% of a full monolayer), and one expects that the minimum surfactant and alkane chain lengths for forming a fully packed monolayer via chain-chain interaction should depend on the surface density of vacancies in the surfactant monolayer.

One more recent experimental work reported in the literature can be directly related to our results. Allara *et. al.*[113] have studied the wetting behavior of self-assembled

alkoxy monolayers on SiO_2 with chain densities of 2.6 ± 0.3 chains/nm^2 and several different chain lengths. They found a hexadecane contact angle (θ_{HD}) of ~ 10° for chain lengths shorter than C_{15}, a rapid increase of θ_{HD} from C_{15} to C_{18}, and θ_{HD} ~ 36° for C_{18} or longer, but a water contact angle θ_W of ~ 100° for all chain lengths. Their interpretation was that a structural transition in the monolayers (*in air*) from a more disordered to a more ordered chain conformation had happened when the alkoxy chain length increased from C_{15} to C_{18}. Knowing our results, we can now have a better understanding of their observations. All alkoxy monolayers, regardless of their chain lengths, will have their chains curled up when exposed to water because of the hydrophobic effect.[66] They therefore look the same to water, thus giving rise to the same water contact angles. The observed conformational transition of the alkoxy monolayer in hexadecane with increasing alkoxy chain length can be understood from the possible change of chain conformation induced by chain-chain interaction with hexadecane. For alkoxy monolayers with chain lengths varying from C_{15} to C_{18}, the chain-chain interaction between alkoxy chains and hexadecane penetrating the monolayer must have become increasingly stronger and at C_{18} strong enough to induce straightening of the alkoxy chains. The mixed monolayer of alkane and alkoxy chains formed with C_{18} or longer would appear similar to a compact layer of alkyl chains (as monolayers of alkylthiols on gold or OTS on glass). Therefore, θ_{HD} should increase to a value close to what has been observed[59,113] for fully packed monolayers (~ 46°). If their wetting experiments were done with decane instead of hexadecane probably no such transition would be observed, knowing that decane has little effect on the surfactant chain conformation for this surfactant density.

The above work of Allara *et. al.*[113] has been complemented by molecular dynamics simulations.[71] The result shows that alkane penetration into the monolayer indeed can cause restructuring of the monolayer. However, although their simulation reproduces the observed change in the wetting behavior of hexadecane at the proper surfactant chain length, the physical picture deduced from the simulation is very different from what we have described: the hexadecane penetration into the surfactant monolayers is significant for surfactant chain lengths shorter than C_{15} and *reduced* considerably for longer ones. Only a small increase in ordering of the chain conformation appears for the *shorter* surfactant monolayers ($\leq C_{14}$) upon contact with hexadecane; conversion to a nearly all-trans conformation *is not observed* for any chain length. These predictions disagree with our experimental findings and are opposite to the picture we described earlier.

G. Interaction of Surfactant Monolayers with Long-Chain Alcohols

G.1 Interaction with Long-Chain Alcohols

In Section E we have studied the effect of hydrogen-bonding liquids on the chain conformation of loosely packed surfactant monolayers. We have seen that methanol is able to dramatically induce disorder in the surfactant chains because of the hydrophobic effect. The alkyl chains get "curled up" to reduce their exposed area to the liquid and minimize the number of broken hydrogen bonds at the interface. In light of our experiments with alkanes (Section F, above), some interesting questions arise. What would happen to the chain conformation of a surfactant monolayer immersed in a long-chain alcohol? Would the chain-chain interaction between alcohol and surfactant be

strong enough to overcome the hydrophobic effect and induce straightening of the surfactant chains? To answer these questions we have carried out SFG spectroscopic experiments with DOAC monolayers in contact with alcohols of different chain lengths. The results are presented in Figure 22. The spectra in Figure 22(a), obtained with three deuterated alcohols with very different chain lengths show hardly any visible peaks from the surfactant chains. Apparently, these alcohols had induced "curling up" of the surfactant chains as water or methanol would do. Again, this is presumably due to the hydrophobic effect: the alcohols would form a hydrogen-bonding interfacial layer with OH facing the surfactant chains, which in turn become "curled up" to minimize the area of exposure to the alcohol layer. The spectra in Figure 22(b) were obtained with regular (perprotonated) alcohols of the same length as those listed in Figure 22(a). They do show the characteristic CH_2 and CH_3 stretch peaks for alkyl chains. Since as in the case of deuterated alcohol no signal should be expected from the surfactant chains, the SFG spectra of Figure 22(b) must have come from oriented alcohol molecules at the interface. We note that the spectrum of hexadecanol shows pronounced CH_3 modes and almost no CH_2 mode, suggesting that hexadecanol at the interface had formed an ordered hydrogen-bonded layer with a nearly all-trans chain conformation. With decreasing alcohol chain lengths, the SFG spectra (not shown, except for C_8 and C_4), reveal that the alcohol layer of chain lengths C_5 to C_{12} at the interface has a considerable amount of gauche defects in their chains. For butanol (C_4) and propanol (C_3), the amount of defects is less because of their short chain lengths.

One can reduce the hydrophobic effect of alcohol at the interface by diluting the hexadecanol in a non-polar solvent, disrupting the interfacial hydrogen-bonded network.

Figure 23 shows the SFG spectra for a DOAC monolayer in contact with a 0.5 M solution of hexadecanol in carbon tetrachloride. Deuterated hexadecanol was used in Figure 23(a) and therefore the spectrum comes only from the DOAC monolayer. Instead of a vanishingly weak SFG trace as seen in Figure 22(a), the spectrum now exhibits distinct peaks characteristic of all-trans alkyl chains. Clearly, the alcohol chains must have wedged into the surfactant monolayer and the resultant chain-chain interaction has straightened the surfactant chains. This is only possible if the hydrogen-bonding network of alcohol is disrupted and the alcohol molecules individually penetrate the surfactant monolayer. To determine in this case the orientation of hexadecanol molecules adsorbed at the solution/DOAC interface we compare in Figure 23 the SFG spectra for this system using deuterated and regular alcohols in CCl_4. Both are dominated by CH_3 resonances although with regular alcohol, a shoulder due to the CH_2 d^+ mode at 2850 cm^{-1} can be seen. This indicates that both surfactant and alcohol chains at the interface are nearly all-trans, the latter being slightly disordered. The peak strengths of the CH_3 modes are however significantly stronger in the case of regular alcohol, allowing us to conclude that the alcohol chains must be oriented in the same direction as the surfactant chains. If they were oriented oppositely, their contribution to SFG would interfere destructively with that from the surfactant chains and the spectrum would be much weaker.

G.2 Discussion

As we mentioned earlier, the DOAC monolayers cannot be removed by alcohols or other common organic solvents. Therefore, the only interpretation for the vanishingly weak SFG spectrum of DOAC in contact with pure deuterated long-chain alcohols

(Figure 22(a)) is that the surfactant chains must have contained a large amount of gauche defects or, in other words, "curled up". This suggests that the situation is similar to what we have previously observed in the cases of water and methanol (Section E), in which the liquid molecules like to form a hydrogen-bonding network at the solid/liquid interface in order to minimize the number of broken hydrogen bonds at the interface. The surfactant chains in turn become "curled up" to reduce their exposed area to the liquid and minimize disruption to the hydrogen-bonded network at the interface. For this to happen, the alcohol molecules must adsorb at the interface with their OH groups forming a hydrogen-bonding network and facing the disordered surfactant monolayer. To show that this is indeed the case, we use the SFG spectra of DOAC taken with regular alcohols (Figure 22(b)). In this case, the SFG spectra comes only from oriented alcohol molecules at the interface, since Figure 22(a) already shows that the signal from DOAC is negligible when in contact with deuterated alcohols. For sufficiently long alcohol molecules, e.g. hexadecanol, the spectrum in Figure 22(b) indicates that the chain-chain interaction is strong enough to straighten their chains. Comparing this spectrum to that of DOAC in contact with deuterated hexadecane (Figure 19) allows us to determine the absolute orientation of the alcohol layer. This is done as follows. The SFG spectra of hexadecanol/DOAC (Figure 22(b)) and hexadecane/DOAC (Figure 19) interfaces can be fitted to Eq. (2.16). We found that in both cases the r^+ mode amplitude χ_{r^+} has the same sign as the nonresonant background χ_{NR}. This indicates that the CH_3 groups of alcohol molecules and DOAC in the two cases point in the same direction. Since the nearly all-trans DOAC chains must point away from the quartz substrate, we can conclude that alcohol molecules at the interface must also have their chains pointing away from the

substrate, and consequently OH groups facing the DOAC monolayer. Figure 24(a) shows a cartoon of the structure of the hexadecanol/DOAC interface inferred from our experiment.

One may argue that the alcohols at the interface should have their alkyl chains facing the hydrophobic surfactant monolayer. This is opposite to what we observed. In addition, this structure is also inconsistent with our spectra: if the alcohol chains faced and interacted with the DOAC monolayer, the situation would be similar to the case of DOAC in contact with alkanes discussed above. The chain-chain interaction should make the chains more ordered or straightened instead of curling up. The vanishing signals from DOAC in Figure 22(a) indicate that this is definitely not the case. While we have no detailed free energy calculation to support the structure sketched in Figure 24(a), we can make some plausible arguments. It is known, theoretically[114,115] and experimentally,[43,116-120] that chain molecules with an OH terminal tend to form an oriented hydrogen-bonding network at interfaces in order to minimize the number of broken hydrogen bonds. This is even possible with the OH terminals facing a hydrophobic medium. For example, both molecular dynamics simulations[114] and infrared spectroscopy[119] have shown that the OH-terminated alkylthiol molecules adsorbed on gold tend to have their OH terminals hydrogen-bonded together and form a highly ordered monolayer with the bonded OH groups facing the air or vacuum. The question is which orientation of the alcohol layer is energetically more favorable, one with OH terminal groups facing the surfactant monolayer or one with the alkyl chains facing the surfactant monolayer. In terms of chain-chain interactions, we expect the two configurations to be comparable. With the OH groups pointing towards the surfactant monolayer, however, there is an entropy gain

resulting from curling up of the surfactant chains. This configuration is then likely to have a lower free energy.

We now discuss the case of DOAC/hexadecanol-in-CCl_4. When hexadecanol is diluted in CCl_4, the fraction of associated alcohol molecules is reduced and the fraction of isolated alcohol molecules is increased.[121-123] The hydrophobic effect at the DOAC/liquid should be reduced due to disruption of the hydrogen-bonding network at the interface. Figure 23 clearly shows that both DOAC and hexadecanol at the interface now have their chains mostly in the all-trans conformation. Apparently individual alcohol molecules in solution can now adsorb at the interface, filling the empty sites in the surfactant monolayer. The hexadecanol chains are long enough to induce a straightening of the surfactant chains via the chain-chain interaction, as in the case of alkanes (Section F, above). A similar effect due to the co-adsorption of alcohol and soluble surfactants at a hydrophobic-solid/solution interface has been observed previously by SFG spectroscopy.[43,46]

As mentioned earlier, we can determine from the spectra in Figure 23 the relative orientation of the adsorbed alcohol molecules with respect to the DOAC monolayer. If the alkyl chains of both molecules are pointing away from the substrate, their CH_3 modes should contribute to the SFG signal constructively. On the other hand, if the adsorbed alcohols have their chains pointing towards the DOAC monolayer, the SFG signals from the CH_3 modes of alcohol and DOAC would interfere destructively. The spectra in Figure 23 show that the signal from the (alcohol + DOAC) layer (Figure 23(b)) is much stronger than that from the DOAC monolayer alone (Figure 23(a)), implying that the adsorbed alcohol molecules have the same orientation as the DOAC molecules. Fitting the spectra

in Figure 23 to Eq. (2.16) yielded the mode amplitudes χ_{r+}. We found that they have the same sign compared to the nonresonant background χ_{NR} and compared to χ_{r+} for the spectra of Figures 19 and 22(b). This means that in all these cases, the alkyl chains of DOAC and alcohol are pointing away from the substrate. Figure 24(b) shows a cartoon of the DOAC/hexadecane-in-CCl_4 interface as deduced from our data. This configuration should indeed be energetically favorable. In the bulk solution, alcohol molecules are surrounded by CCl_4 so that the solution is strongly hydrophobic. It is highly unfavorable to have alcohol molecules adsorbed with the OH groups facing the solution.

H. Summary

In summary, we have used sum-frequency vibrational spectroscopy to study the conformation of loosely packed self-assembled surfactant monolayers at solid/liquid interfaces. We found that, in contrast to fully packed monolayers, their chain conformation is very sensitive to the liquid environment. At the solid/air interface, the surfactant chains contain a significant amount of gauche defects, as expected from their lower surface density. When immersed in non-associated liquids such as carbon tetrachloride or chloroform, the chain conformation becomes more disordered, the effect being stronger for more polar liquids. It is also more pronounced for longer surfactant chains. For hydrogen-bonding liquids the effect is even stronger. The chains now appear to be highly disordered (there is no detectable SFG signal from the alkyl chains, as a result of near inversion symmetry).

These observations are interpreted in terms of a simple free-energy argument. If the intermolecular interaction between liquid molecules is much stronger than that

between liquid molecules and the alkyl chain or between chain segments, a more compact conformation is energetically favorable. This is because it would reduce the surface area of the chains exposed to the liquid to decrease the number of liquid molecules interacting with the chains. Compact conformations are also entropically favorable. In the case of water, this is the result of the well-known hydrophobic effect. Although the latter is known to have a distinct temperature dependence, we could not observe any changes in the SFG spectra of surfactant chains as the temperature was varied from 20 to 80 °C. It is likely that the changes are beyond our sensitivity. However, in contrast to the solvation of small nonpolar solutes by water, we found that water molecules surrounding the collapsed surfactant chains do have dangling OH groups. The interfacial water structure is intermediate between the one at a planar hydrophobic surface and the one around a small hydrophobic guest.

The situation is quite different if the surfactant monolayer interacts with liquids containing long hydrocarbon chains, such as n-alkanes and n-alcohols. In the case of alkanes, we found that if both alkane and surfactant molecules have sufficiently long chains (longer than about C_{14}), and the surfactant surface density is sufficiently high (higher than ~ 2.5 chains/nm^2), the penetration of alkane molecules into the surfactant monolayer can effectively eliminate the gauche defects initially present in the surfactant chains, due to a strong enough chain-chain interaction.

In the case of long-chain alcohols, they prefer to form a hydrogen-bonding network at the interface. Because of the hydrophobic effect, the surfactant chains become highly disordered ("curl up") to reduce their surface area exposed to the liquid alcohol. The surface alcohol molecules are well oriented; their chains are nearly all-trans if they

are long, thus forming a highly ordered layer above the highly disordered surfactant monolayer. However, diluting the alcohol in a non-polar solvent can disrupt the surface hydrogen-bonding network and the alcohol molecules can now wedge into the surfactant monolayer. They adsorb at the interface with the same chain orientation as the surfactant molecules, providing enough chain-chain interaction to transform both surfactant and alcohol chains into all-trans.

Although the set of data presented here is far from being complete enough for us to be able to draw detailed conclusions, we have obtained some rough ideas on how various liquids interact and affect the surfactant chain conformation at interfaces. While the work discussed in this Chapter is for self-assembled monolayers at solid/liquid interfaces, the general picture should be valid in other situations. For example, the effects of non-associated and hydrogen-bonding liquids on chain conformation should be similar in bulk solutions. Also, the interaction of long-chain molecules with surfactant monolayers at other interfaces, like air/liquid or liquid/liquid, may exhibit similar features to the ones discussed here. However, the quantitative parameters (critical chain length, critical surface chain density) could be different at these interfaces owing to the lateral mobility of the monolayers.

References

(1) G. D. Parfitt and C. H. Rochester, ed., *Adsorption from Solution at the Solid/Liquid Interface,* chaps. 3 and 6, Academic Press, New York (1983).

(2) D. R. Karsa, ed. *Industrial Applications of Surfactants II,* The Royal Society of Chemistry, Cambridge, UK (1990).

(3) R. Sharma, ed. *Surfactant Adsorption and Surface Solubilization,* ACS Symposium Series **615**, American Chemical Society, Washington, DC (1995).

(4) D. W. Fuerstenau and R. Herrera-Urbina, in *Cationic Surfactants, Physical Chemistry,* p. 407, D. N. Rubingh and P. M. Holland, eds, Surfactant Sci. Ser. **37**, M. Dekker, New York (1991).

(5) A. Adamson, *The Physical Chemistry of Surfaces,* 5th ed., chap. 13, Wiley-Interscience, New York (1990).

(6) B. J. Bijsterbosch, *J. Colloid Interface Sci.* **47**, 186 (1974).

(7) J. L. Trompette, J. Zajac, E. Keh, and S. Partyka, *Langmuir* **10**, 812 (1994).

(8) B. T. Ingram and R. H. Ottewill, in *Cationic Surfactants, Physical Chemistry,* p. 87, D. N. Rubingh and P. M. Holland, eds, Surfactant Sci. Ser. **37**, M. Dekker, New York (1991).

(9) P. Wängnerud and G. Olofsson, *J. Colloid Interface Sci.* **153**, 392 (1992).

(10) Z. M. Zorin, N. V. Churaev, N. E. Esipova, I. P. Sergeeva, V. D. Sobolev and E. K. Gasanov, *J. Colloid Interface Sci.* **152**, 170 (1992).

(11) S. Partyka, M. Lindheimer and B. Faucompre, *Colloids Surfaces A* **76**, 267 (1993).

(12) P. Wängnerud, D. Berling and G. Olofsson, *J. Colloid Interface Sci.* **169**, 365

(1995).

(13) Z. M. Zorin, V. P. Romanov and N. V. Churaev, *Colloid and Polymer Sci.* **267**, 968 (1979).

(14) E. A. Vogler, *Langmuir* **8**, 2013 (1992).

(15) W. R. Birch, M. A. Knewtson, S. Garoff, R. M. Suter and S. Satija, *Colloids Surfaces A* **89**, 145 (1994).

(16) A. R. Rennie, E. M. Lee, E. A. Simister and R. K. Thomas, *Langmuir* **6**, 1031 (1990).

(17) D. C. McDermott, J. McCarney, R. K. Thomas and A. R. Rennie, *J. Colloid Interface Sci.* **162**, 304 (1994).

(18) E. Söderlind and P. Stilbs, *Langmuir* **9**, 1678 (1993).

(19) E. Söderlind and P. Stilbs, *Langmuir* **9**, 2024 (1993).

(20) Y. L. Chen, S. Chen, C. Frank and J. Israelachvili, *J. of Colloid Interface Sci.* **153**, 244 (1992).

(21) L. C. Sander, J. C. Callis and L. R. Field, *Anal. Chem.* **55**, 1068 (1983).

(22) Y. I. Rabinovich, D. A. Guzonas and R. H. Yoon, *J. Colloid Interface Sci.* **155**, 221 (1993).

(23) A. L. Dendramis, E. W. Schwinn and R. P. Sperline, *Surface Science* **134**, 675 (1983).

(24) S. Sun, R. L. Birke and J. R. Lombardi, *J. Phys. Chem.* **94**, 2005 (1990).

(25) K. Suga, M. Bradley and J. F. Rusling, *Langmuir* **9**, 3063 (1993).

(26) Y. Tsao, S. X. Yang, D. F. Evans and H. Wennerström, *Langmuir* **7**, 3154 (1991).

(27) Y. L. E. Chen, M. L. Gee, C. A. Helm, J. N. Israelachvili and P. M. McGuiggan, *J. Phys. Chem.* **93**, 7057 (1989).

(28) J. L. Parker, V. V. Yaminsky and P. M. Claesson, *J. Phys. Chem.* **97**, 7706 (1993).

(29) M. W. Rutland and J. L. Parker, *Langmuir* **10**, 1110 (1994).

(30) H. Hemetsberger, P. Behrensmeyer, J. Henning and H. Ricken, *Chromatographia* **12**, 71 (1979).

(31) H. Rupprecht and T. Gu, *Colloid Polym. Sci.* **269**, 506 (1991).

(32) R. Zana, *Adv. Colloid Interface Sci.* **57**, 1 (1995).

(33) S. Reekmans, H. Luo, M. Van der Aurweraer and F. C. De Schryver, *Langmuir* **6**, 628 (1990).

(34) T. J. McIntosh, S. A. Simon and R. C. MacDonald, *Biochim. Biophys. Acta*, **597**, 445 (1980).

(35) F. Tiberg and J. Brinck, in *Surfactant Adsorption and Surface Solubilization,* R. Sharma, ed., ACS Symposium Series **615**, chap. 15, American Chemical Society, Washington, DC (1995).

(36) P. Somasundaran, E. Fu and Q. Xu, *Langmuir* **8**, 1065 (1992).

(37) M. L. Gonzáles Martin and C. H. Rochester, *J. Chem. Soc. Faraday Trans.* **88**, 873 (1992).

(38) R. H. Yoon and S. A. Ravishankar, *J. Colloid Interface Sci.* **179**, 391 (1996).

(39) M. Monduzzi, F. Caboi, F. Larché and U. Olsson, *Langmuir* **13**, 2184 (1997).

(40) T. R. Desai and S. G. Dixit, *J. Colloid Interface Sci.* **179**, 544 (1996).

(41) K. Esumi, T. Nagahama and K. Meguro, *Colloid Polym. Sci.* **269**, 1274 (1991).

(42) F. Tiberg, *J. Chem. Soc. Faraday Trans.* **92**, 531 (1996).

(43) C. D. Bain, P. B. Davies and R. N. Ward, *Langmuir* **10**, 2060 (1994).

(44) M. S. Johal, E. W.Usadi and P. B. Davies, *Faraday Discuss.* **104**, 231 (1996).

(45) M. S. Johal, R. N. Ward and P. B. Davies, *J. Phys. Chem.* **100**, 274 (1996).

(46) R. N. Ward, P. B. Davies and C. D. Bain, *J. Phys. Chem. B* **101**, 1594 (1997).

(47) R. Aveyard, B. P. Binks, P. D. I. Fletcher and J. R. MacNab, *Langmuir* **11**, 2515 (1995).

(48) R. Aveyard, B. P. Binks, P. Cooper and P. D. I. Fletcher, *Adv. Colloid Interface Sci.* **33**, 59 (1990).

(49) M. Thoma and H. Möhwald, *J. Colloid Interface Sci.* **162**, 340 (1994).

(50) H. D. Dörfler, C. Koth and W. Rettig, *J. Colloid Interface Sci.* **180**, 478 (1996).

(51) J. R. Lu, R. K.Thomas, B. P. Binks, P. D. I.; Fletcher and J. Penfold, *J. Phys. Chem.* **99**, 4113 (1995).

(52) J. Eastoe, K. J. Hetherington, D. Sharpe, J. Dong, R. K. Heenan and D. Steytler, *Langmuir* **12**, 3876 (1996).

(53) M. Thoma, M. Schwendler, H. Bates, C. A. Helm, T. Pfohl, H. Riegler and H. Möhwald, *Langmuir* **12**, 1722 (1996).

(54) G. Brezesinski, M. Thoma, B. Struth and H. Möhwald, *J. Phys. Chem.* **100**, 3126 (1996).

(55) R. Aveyard, P. Cooper and P. D. I. Fletcher, *J. Chem. Soc. Faraday Trans.* **86**, 3623 (1990).

(56) C. D. Bain and G. M. Whitesides, *J. Am. Chem. Soc.* **110**, 5897 (1988).

(57) S. V. Atre, B. Liedberg and D. L. Allara, *Langmuir* **11**, 3882 (1995).

(58) A. Ulman, S. D. Evans, Y. Shnidman, R. Sharma, J. E. Eilers and J. C. Chang, *J. Am. Chem. Soc.* **113**, 1499 (1991).

(59) C. D. Bain and G. M. Whitesides, *J. Am. Chem. Soc.* **111**, 7164 (1989).

(60) P. E. Laibinis, R. G. Nuzzo and G. M. Whitesides, *J. Phys. Chem.* **96**, 5097 (1992).

(61) J. Hautman and M. L. Klein, *Phys. Rev. Lett.* **67**, 1763 (1991).

(62) P. Guyot-Sionnest, R. Superfine, J. H. Hunt and Y. R. Shen, *Chem. Phys. Lett.* **144**, 1 (1988).

(63) T. H. Ong, P. B. Davies and C. D. Bain, *Langmuir* **9**, 1836 (1993).

(64) P. E. Laibinis, C. D. Bain, R. G. Nuzzo and G. M. Whitesides, *J. Phys. Chem.* **99**, 7663 (1995).

(65) J. Y. Huang, R. Superfine and Y. R. Shen, *Phys. Rev. A* **42**, 3660 (1990).

(66) P. B. Miranda, V. Pflumio, H. Saijo and Y. R. Shen, *Chem. Phys. Lett.* **264**, 387 (1997).

(67) L. S. Bartell and R. J. Ruch, *J. Phys. Chem.* **60**, 1231 (1956).

(68) L. S. Bartell and R. J. Ruch, *J. Phys. Chem.* **63**, 1045 (1959).

(69) R. Maoz and J. Sagiv, *J. Collloid Interface Sci.* **100**, 465 (1984).

(70) J. P. Folkers, P. E. Laibinis and G. M. Whitesides, *Langmuir* **8**, 1330 (1992).

(71) N. Kacker, S. K. Kumar and D. L. Allara, *Langmuir* **13**, 6366 (1997).

(72) R. K. Iler, *The Chemistry of Silica*, chap. 6, Wiley, New York (1979).

(73) S. Ong, X. Zhao and K. B. Eisenthal, *Chem. Phys. Lett.* **191**, 327 (1992).

(74) F. J. Kahn, *Appl. Phys. Lett.* **22**, 386 (1973).

(75) P. B. Miranda, V. Pflumio, H. Saijo and Y. R. Shen, *Thin Solid Films* **327-329**, 161 (1998).

(76) P. Guyot-Sionnest, J. H. Hunt and Y. R. Shen, *Phys. Rev. Lett.* **59**, 1597 (1987).

(77) M. S. Johal, E. W. Usadi and P. B. Davies, *J. Chem. Soc. Faraday Trans.* **92**, 573 (1996).

(78) J. C. Conboy, M. C. Messmer and G. L. Richmond, *J. Phys. Chem.* **100**, 7617 (1996).

(79) R. N. Ward, D. C. Duffy, P. B. Davies and C. D. Bain, *J. Phys. Chem.* **98**, 8536 (1994).

(80) J. N. Israelachvili, *Intermolecular and Surface Forces*, chaps. 5-8, Academic Press, New York, (1985).

(81) D. A. C. Compton, S. Montero and W. F. Murphy, *J. Phys. Chem.* **84**, 3587 (1980).

(82) O. R. Quayle, *Chem. Rev.* **53**, 439 (1953).

(83) R. Superfine, J. Y. Huang and Y. R. Shen, *Phys Rev. Lett.* **66**, 1066 (1991).

(84) G. A. Jeffrey, *An Introduction to Hydrogen Bonding*, chap. 2, Oxford University Press, Oxford, UK (1997).

(85) Q. Du, R. Superfine, E. Freysz and Y. R. Shen, *Phys. Rev. Lett.* **70**, 2313 (1993).

(86) Q. Du, E. Freysz and Y. R. Shen, *Science* **264**, 826 (1994).

(87) J. Shelley, K. Watanabe and M. L. Klein, *Int. J. Quantum Chem., Quantum Biology Symp.* **17**, 103 (1990).

(88) P. G. de Gennes, *Macromolecules* **13**, 1069 (1980).

(89) J. Lecourtier, R. Audebert and C. Quivoron, *Macromolecules* **12**, 141 (1979).

(90) M. D. Whitmore and J. Noolandi, *Macromolecules* **23**, 3321 (1990).

(91) P. J. Flory, *Principles of Polymer Chemistry*, Cornell University Press, Ithaca, (1953).

(92) W. L. Jorgensen, *J. Phys. Chem.* **90**, 1276 (1986).

(93) G. G. Shipley, in *The Physical Chemistry of Lipids*, D. M. Small, ed., chap. 5, Plenum, New York (1986).

(94) A. Pohorille and L. R. Pratt, *J. Am. Chem. Soc.* **112**, 5065 (1990).

(95) D. Smith and A. Haymet, *J. Chem. Phys.* **98**, 6445 (1993).

(96) M. E. Paulaitis, *Curr. Opin. Colloid Interface Sci.* **2**, 315 (1997).

(97) M. E. Paulaitis, S. Garde and H. S. Ashbaugh, *Curr. Opin. Colloid Interface Sci.* **1**, 376 (1996).

(98) T. Head-Gordon, *J. Am. Chem. Soc.* **117**, 501 (1995).

(99) T. Head-Gordon, *Proc. Natl. Acad. Sci. USA* **92**,8308 (1995).

(100) C. H. Bridgeman, A. D. Buckingham and N. T. Skipper, *Chem. Phys. Lett.* **253**, 209 (1996).

(101) H. Frank and M. Evans, *J. of Chem. Phys.* **13**, 507 (1945) and references therein.

(102) C. Y. Lee, J. A. McCammon and R. J. Rossky, *J. Chem. Phys.* **80**, 4448 (1984).

(103) R. M. Townsend and S. A. Rice, *J. Chem. Phys.* **94**, 2207 (1991).

(104) N. A. M. Besseling and J. Lyklema, *J. Phys. Chem. B* **101**, 7604 (1997).

(105) T. W. Arthur and A. D. J. Haymet, *J. Chem. Phys.* **109**, 7991 (1998).

(106) F. M. Floris, M. Selmi, A. Tani and J. Tomasi, *J. Chem. Phys.* **107**, 6353 (1997).

(107) A. Pertsemlidis, A. M. Saxena, A. K. Soper, T. Head-Gordon and R. M. Glaeser,

Proc. Natl. Acad. Sci. USA **93**, 10769 (1997).

(108) L.R. Pratt and D. Chandler, *J. Chem. Phys.* **67**, 3633 (1977) and references therein.

(109) G. R. Bell, S. Manning-Benson, C. D. Bain, *J. Phys. Chem. B* **102**, 218 (1998).

(110) W. C. Bigelow and L. O. Brockway, *J. Colloid Sci.* **11**, 60 (1956).

(111) F. M. Fowkes, ed., *Contact Angles, Wettability and Adhesion*, Advances in Chemistry **43**, American Chemical Society, Washington, DC (1964).

(112) C. D. Bain and G. M. Whitesides, *J. Am. Chem. Soc.* **110**, 6560 (1988).

(113) D. L. Allara, A. N. Parikh and E. Judge, *J. Chem. Phys.* **100**, 1761 (1994).

(114) J.; Hautman, J. P. Bareman, W. Mar and M. L. Klein, *J. Chem. Soc. Faraday Trans.* **87**, 2031 (1991).

(115) J. Gao and W. L. Jorgensen, *J. Phys. Chem.* **92**, 5813 (1988).

(116) C. D. Stanners, Q. Du, P. Cremer, R. P. Chin, G. A. Somorjai and Y. R. Shen, *Chem. Phys. Lett.* **232**, 407 (1995).

(117) A. Renault, J. F. Legrand, M. Goldmann and B. Berge, *J. Phys. II France* **3**, 761 (1993).

(118) M. Deutsch, X. Z. Wu, E. B. Sirota, S. K. Sinha, B. M. Ocko and O. M. Magnussen, *Europhys. Lett.* **30**, 283 (1995).

(119) L. Bertilsson and B. Liedberg, *Langmuir* **9**, 141 (1993).

(120) C. D. Bain and G. M. Whitesides, *J. Am. Chem. Soc.* **111**, 7155 (1989).

(121) R. Veldhuizen and S. W. de Leeuw, *J. Chem. Phys.* **105**, 2828 (1996).

(122) C. Brot, *J. Mol. Struct.* **250**, 253 (1991).

(123) A. N. Fletcher, *J. Phys. Chem.* **73**, 2217 (1969).

(124) Q. Du, E. Freysz and Y. R. Shen, *Phys. Rev. Lett.* **72**, 238 (1994).

Figure Captions

Figure 1. (a) Chemical structures of DOAC and DMOAP. (b) The corresponding species adsorbed on the quartz surface after the self-assembly process.

Figure 2. (a) SFG spectrum for a DOAC monolayer at the air/water interface with surface density of 2.5 chains/nm^2. The solid line is a fit using Eq. (6.1) and the dashed line is the DOAC spectrum calculated from Eq. (6.1) by setting B = C = 0. (b) SFG spectra of DOAC monolayers of different surface densities at the air/water interface calculated from Eq. (6.1) by setting B = C = 0. The surface densities (N in chains/nm^2) are indicated in each curve. The beam polarization combination is SSP.

Figure 3. SFG spectra for a DOAC monolayer at the quartz/air interface. The polarization combination is indicated in each graph.

Figure 4. SFG spectra for a DOAC monolayer at the quartz/CCl_4 interface. The polarization combination is indicated in each graph.

Figure 5. SFG spectra for a DOAC monolayer at various quartz/liquid interfaces: (●) quartz/CCl_4 interface; (▲) quartz/$CDCl_3$ interface; (○) quartz/DCE interface. The beam polarization combination is SSP.

Figure 6. SFG spectra for a DOAC monolayer at the quartz/{x CCl_4 + (1-x) $CDCl_3$} interface (x in volume fraction). (○) x = 1; (●) x = 0.9; (▽) x = 0.4; (▼) x = 0. The beam polarization combination is SSP.

Figure 7. (I) Representation of an all-trans C_{18} alkane molecule (filled circles correspond to CH_2 or CH_3 groups) surrounded by liquid molecules (empty circles) in a 3D lattice. Only solvent molecules interacting with the chain are shown. (II) Same alkane as in (I), but in a more compact conformation. The solvent molecules shown in the bulk were previously interacting with the chain in conformation (I). See text for details.

Figure 8. Schematic diagram representing the internal energy difference between configurations (I) and (II), $\Delta E \equiv E^{(II)} - E^{(I)}$, as a function of the average number of gauche defects in the chain (n_d). The dotted line is the contribution from gauche defects ($n_d E_d$) and the dashed line is the contribution from the interaction energies (E_{int}). $\Delta E = n_d E_d + E_{int}$.

Figure 9. SFG spectra for monolayers of double-chain surfactants with various chain lengths. Spectra (a) – (c) were taken at the quartz/air interface and (d) – (f) at the quartz/CCl_4 interface. (a) and (d) for a DBAB monolayer; (b) and (e) for a DDAC monolayer; (c) and (f) for a DOAC monolayer. The beam polarization combination is SSP.

Figure 10. SFG spectra for a DOAC monolayer at various quartz/liquid interfaces. (●) Quartz/CCl_4 interface; (▼) quartz/CD_3OD interface; (○) quartz/D_2O interface. The beam polarization combination is SSP.

Figure 11. SFG spectra for a DOAC monolayer at the quartz/D_2O interface. The polarization combination is indicated in each graph.

Figure 12. SFG spectra for a DOAC monolayer at the quartz/{(1-x) CCl_4 + x CD_3OD} interface (x in volume fraction). The bulk CD_3OD concentration is indicated in each graph, in % volume fraction. The beam polarization combination is SSP.

Figure 13. SFG spectra for a DOAC monolayer at the quartz/{(1-x) CCl_4 + x CH_3OH} interface. The bulk methanol concentration x (in % volume fraction) is indicated in each graph. The beam polarization combination is SSP.

Figure 14. SFG spectra for a DBAB monolayer at the quartz/{(1-x) CCl_4 + x CD_3OD} interface (x in volume fraction). The bulk CD_3OD concentration is (●) x = 0%; (▽) x = 0.25%; (▲) x = 0.50% and (○) x = 1.0%. The beam polarization combination is SSP.

Figure 15. SFG spectra for a DOAC monolayer at the quartz/water interface at various temperatures (indicated in each graph). The SFG spectrum for a clean quartz

/water interface at 20 °C (water pH = 8.0, from Ref. 124) is shown for comparison as empty circles. The beam polarization combination is SSP.

Figure 16. SFG spectra for a DOAC monolayer on quartz: (a) in air, freshly prepared, (b) immersed in water (D_2O), and (c) blow-dried by N_2 gas after being immersed in water and then stored in a vacuum desiccator with P_2O_5 for a few days. The beam polarization combination is SSP. The spectra have been separated vertically for clarity.

Figure 17. SFG spectra for (a) DOAC and (b) DBAB monolayers at the quartz/CCl_4 interface. The filled circles are spectra taken with freshly prepared samples. The empty circles are spectra for the same monolayers after they have been immersed in (a) $CDCl_3$ or (b) CD_3OD for a few hours and then rinsed with pure CCl_4. The beam polarization combination is SSP.

Figure 18. SFG spectra for a DMOAP monolayer at the (a) quartz/air and (b) quartz/water interfaces. The line in (a) simply connects data points. In (b), the solid line is a fit to Eq. (6.1) and the dashed line is the spectrum calculated from Eq. (6.1) by setting $B = C = 0$.

Figure 19. SFG spectra for a DOAC monolayer at the quartz/deuterated alkane interface. The alkane chain length is indicated on each curve. The spectrum for the DOAC monolayer at the quartz/air interface is shown for comparison (top

curve). The spectra have been separated vertically by 20 units. The solid line is a fit to Eq. (2.16). The beam polarization combination is SSP.

Figure 20. SFG spectra for (a) DOAC and (b) DDAC monolayers at the quartz/air interface and (c) DOAC and (d) DDAC monolayers at the quartz/deuterated tetradecane interface. The solid line is a fit to Eq. (2.16). The beam polarization combination is SSP.

Figure 21. SFG spectra for (a) DMOAP and (b) DOAC monolayer at the quartz/air interface, and (c) DMOAP and (d) DOAC monolayer at the quartz/deuterated hexadecane interface. The beam polarization combination is SSP.

Figure 22. SFG spectra for a DOAC monolayer at the quartz/alcohol interface: (a) with deuterated alcohols; (b) with regular alcohols. The chain length of the alcohols is indicated on each curve. The spectra have been separated vertically by 2 units in (a) and by 10 units in (b) for clarity. The solid line in the spectrum with regular hexadecanol in (b) is a fit to Eq. (2.16). The beam polarization combination is SSP.

Figure 23. SFG spectra for a DOAC monolayer at the quartz/hexadecanol solution interface: (a) with deuterated hexadecanol and (b) with regular hexadecanol. The solvent is CCl_4 and the alcohol concentration is 0.5 M. The solid line is a fit to Eq. (2.16). The beam polarization combination is SSP.

Figure 24. Schematics of the structures of: (a) quartz/DOAC/neat hexadecanol and (b) quartz/DOAC/0.5 M hexadecanol in CCl_4 interfaces. Chains are represented by solid lines, surfactant head-groups by $\oplus$ and CCl_4 molecules by empty circles.

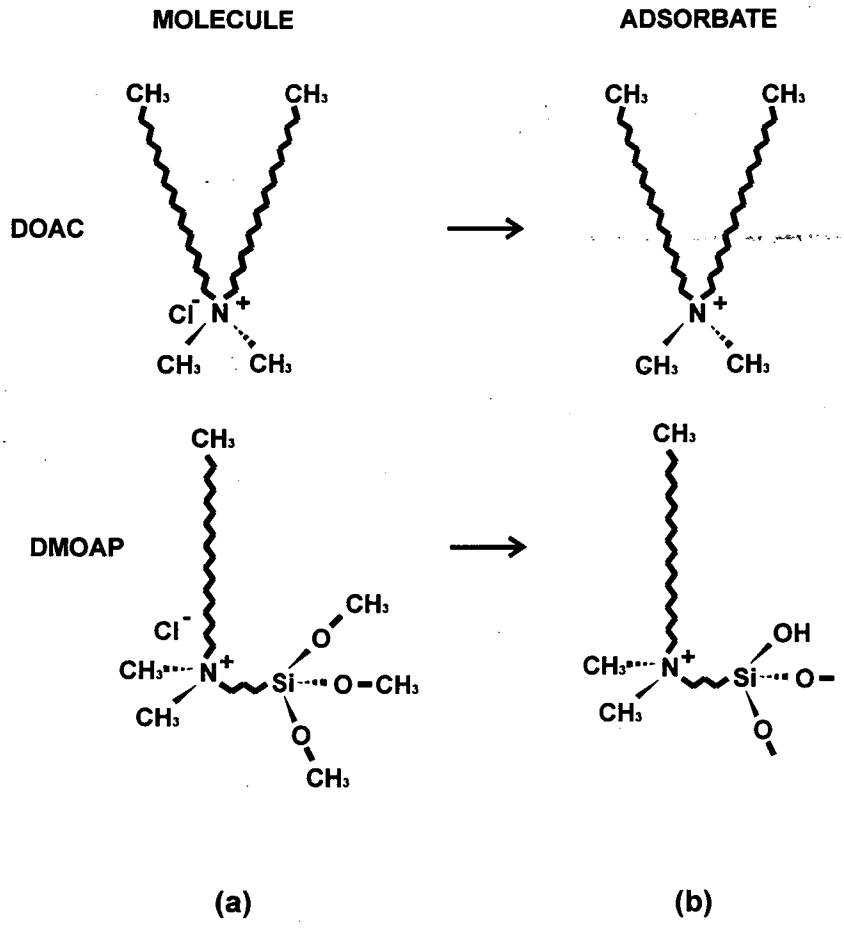

Figure 1

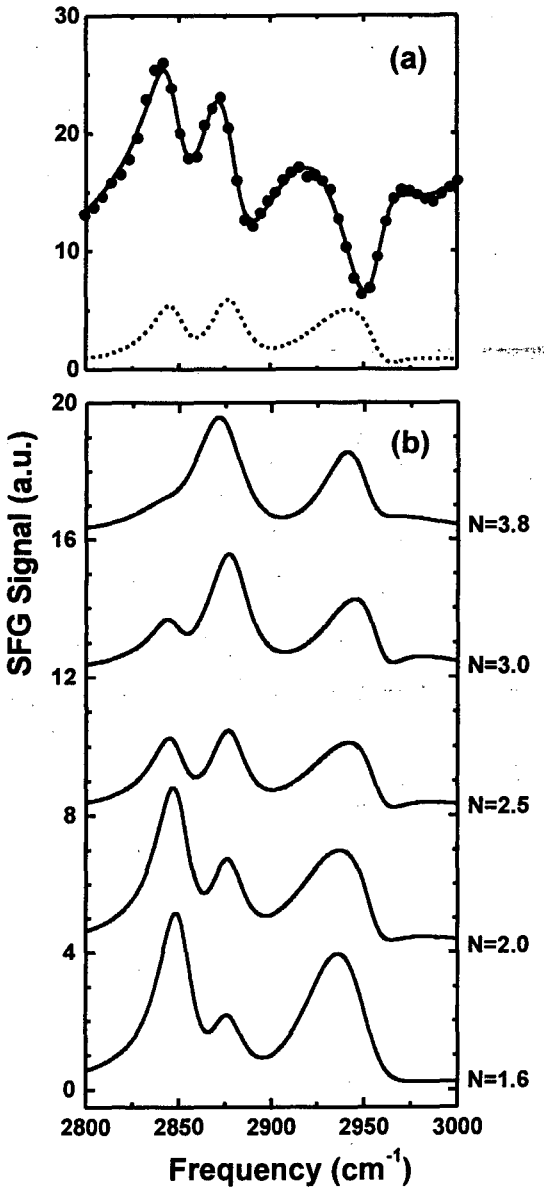
(a)
(b)
SFG Signal (a.u.)
Frequency (cm^{-1})
N=3.8
N=3.0
N=2.5
N=2.0
N=1.6
30
20
10
0
20
16
12
8
4
0
2800
2850
2900
2950
3000

Figure 2

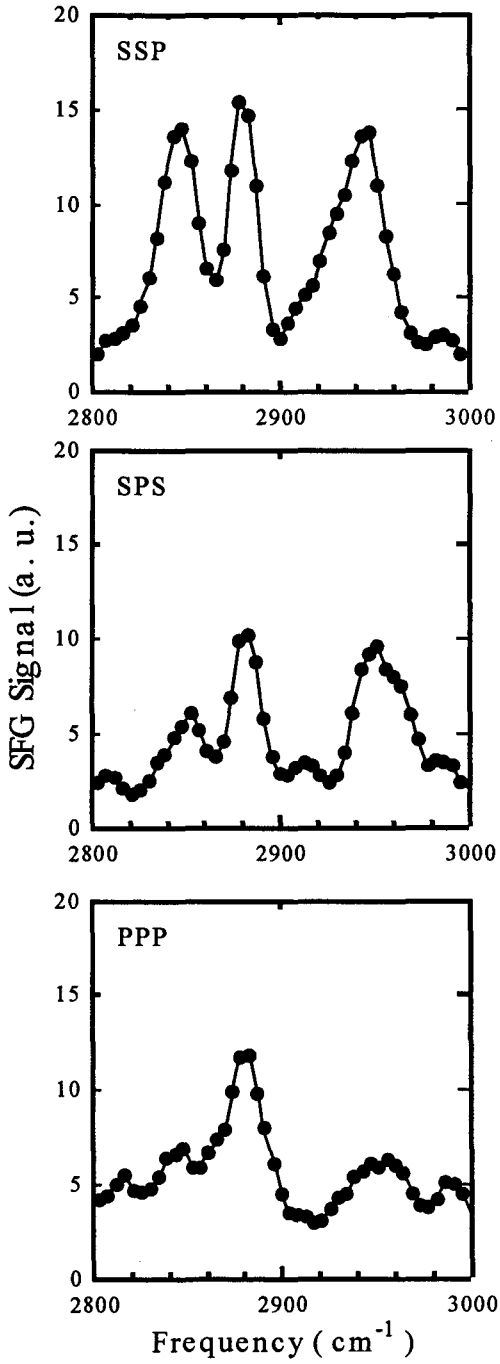
SSP
SPS
PPP
SFG Signal (a. u.)
Frequency (cm^{-1})
20
15
10
5
0
2800
2900
3000

Figure 3

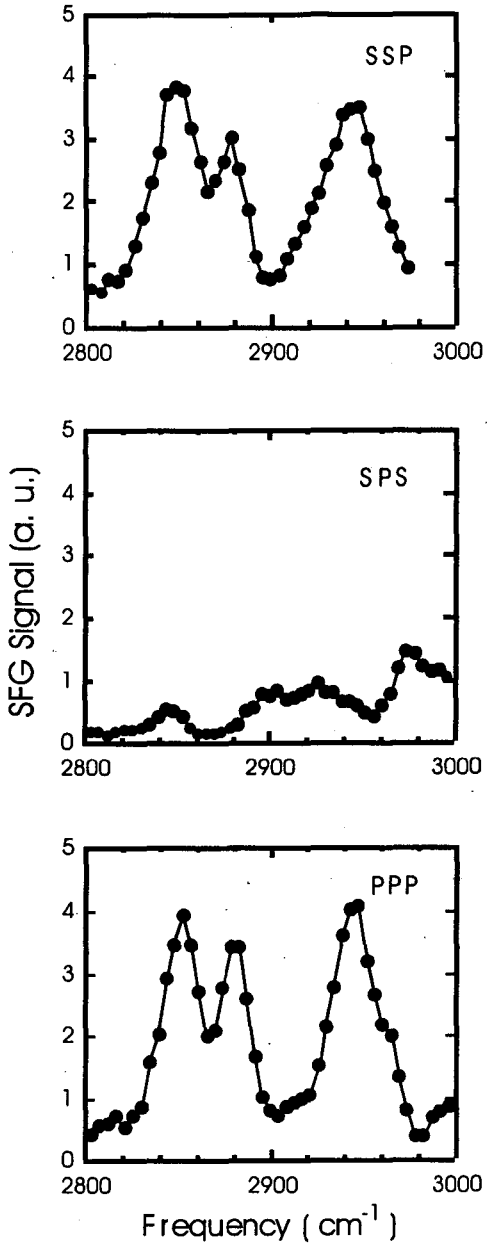
SSP
SPS
PPP
SFG Signal (a. u.)
Frequency (cm-1)
0
1
2
3
4
5
2800
2900
3000

Figure 4

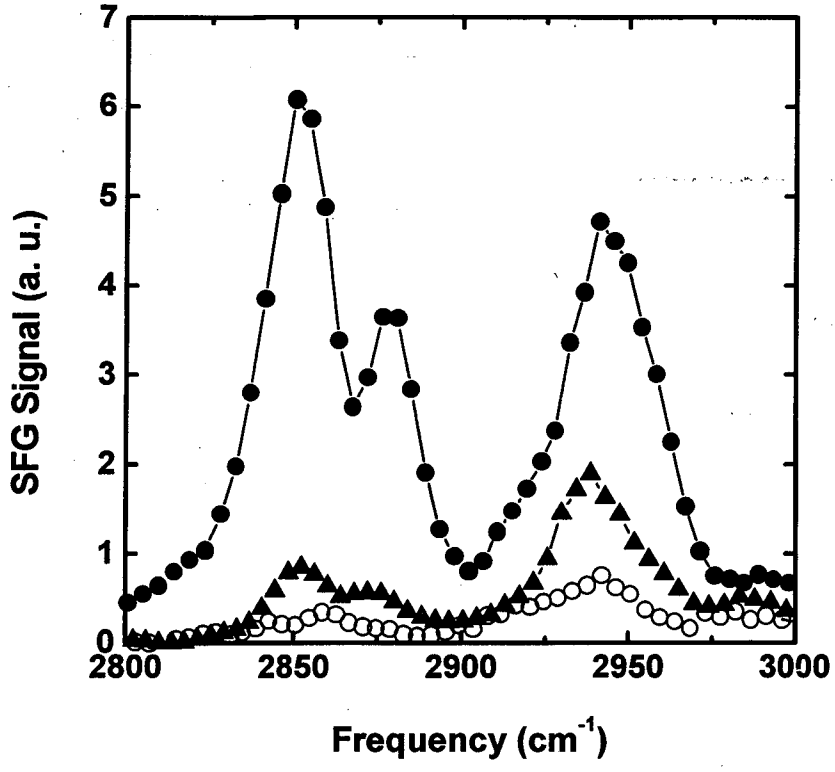
SFG Signal (a. u.)
Frequency (cm-1)
0
1
2
3
4
5
6
7
2800
2850
2900
2950
3000

Figure 5

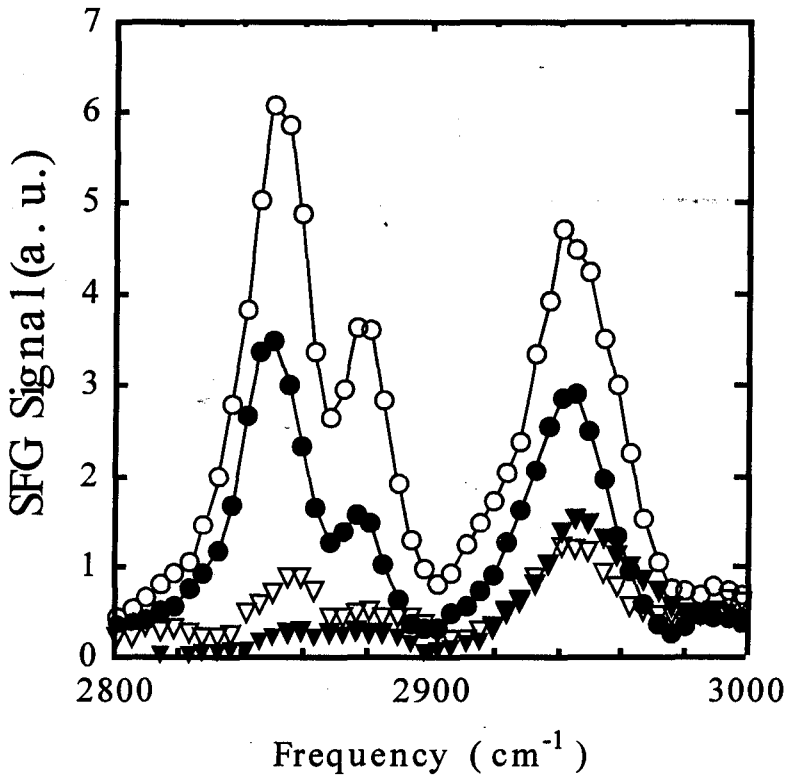

Figure 6

(Ⅰ)

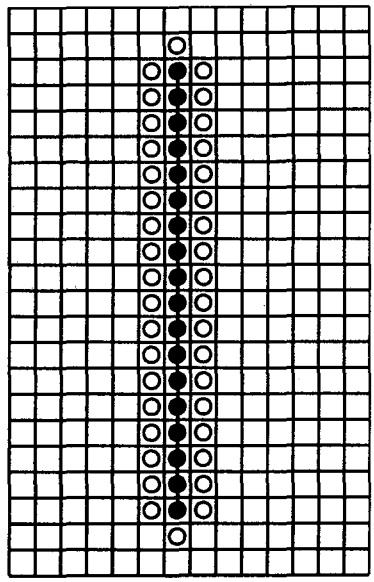

(Ⅱ)

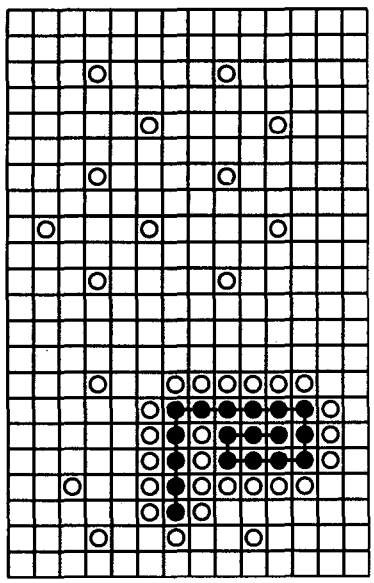

Figure 7

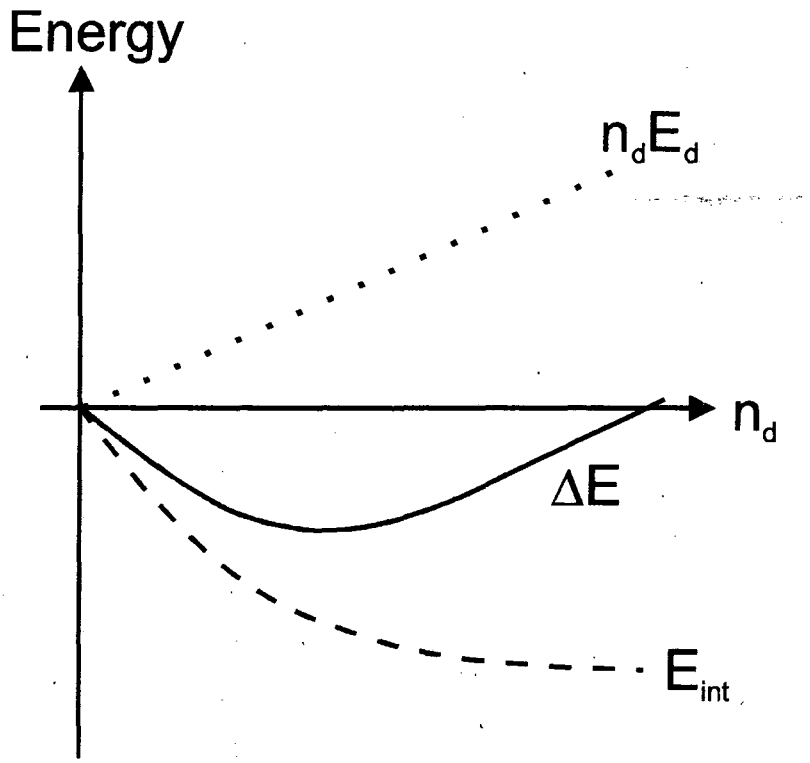

Figure 8

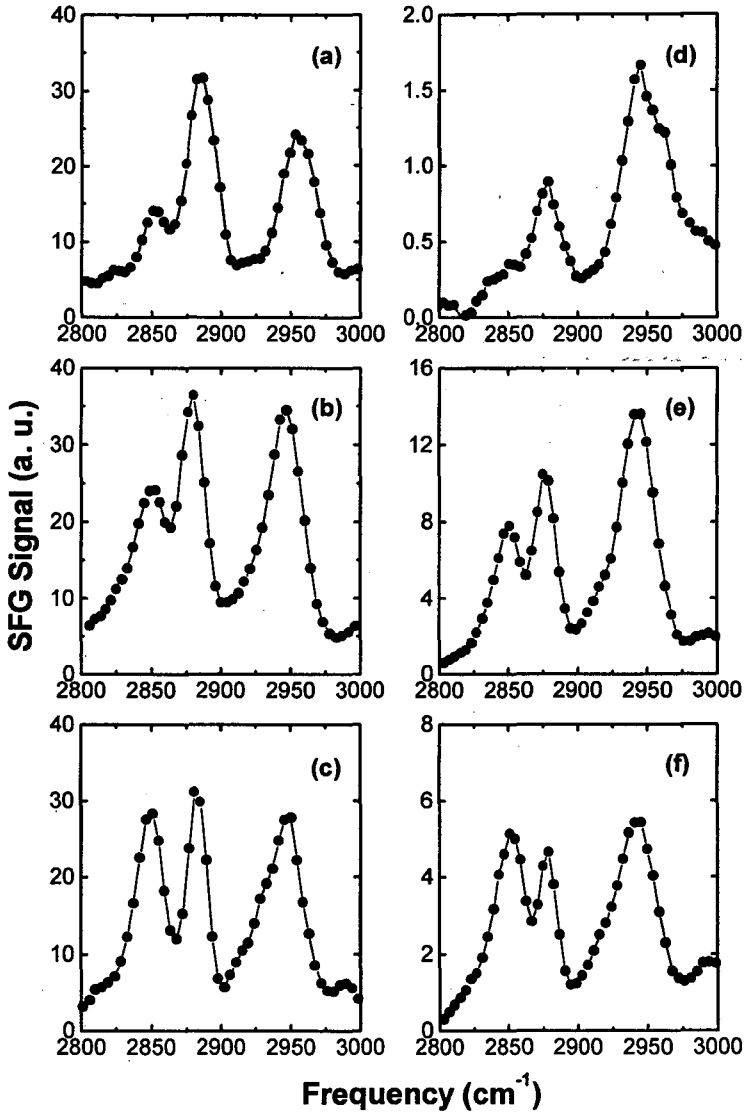

Figure 9

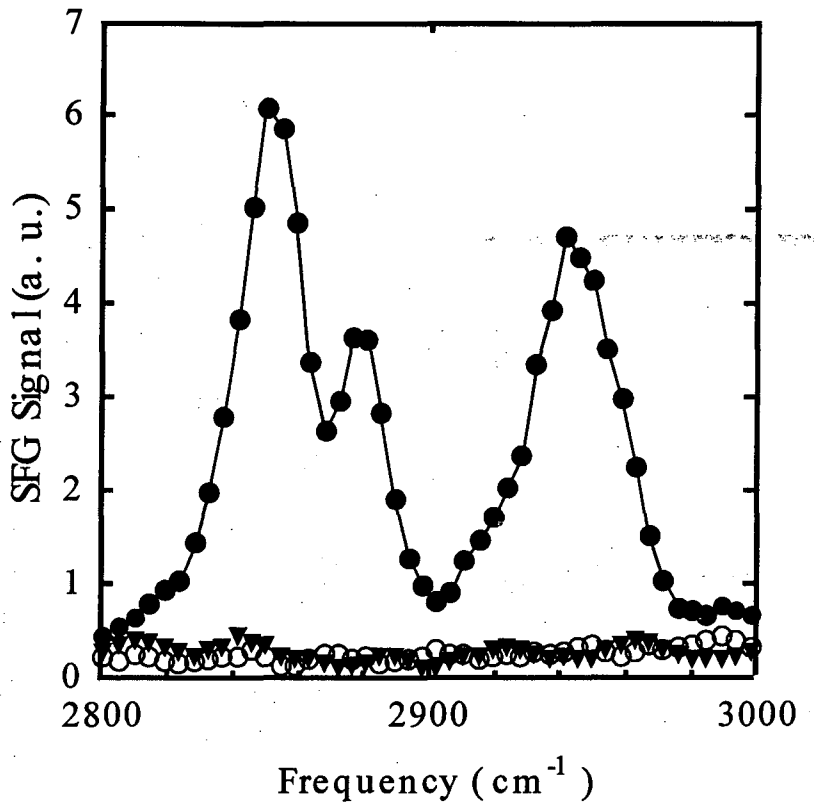

Figure 10

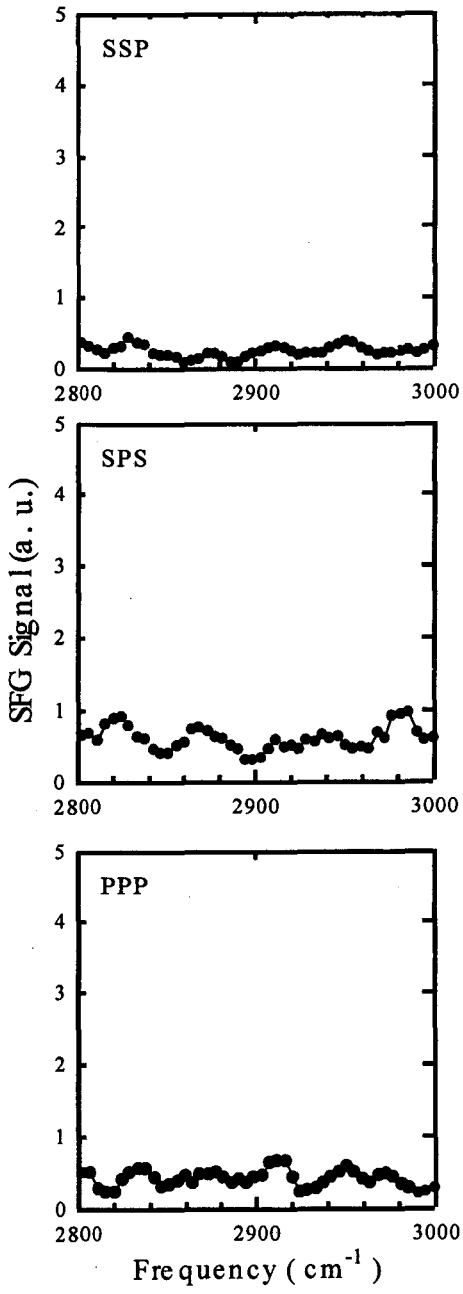
SSP
SPS
PPP
SFG Signal (a. u.)
Frequency (cm^{-1})
0
1
2
3
4
5
2800
2900
3000

Figure 11

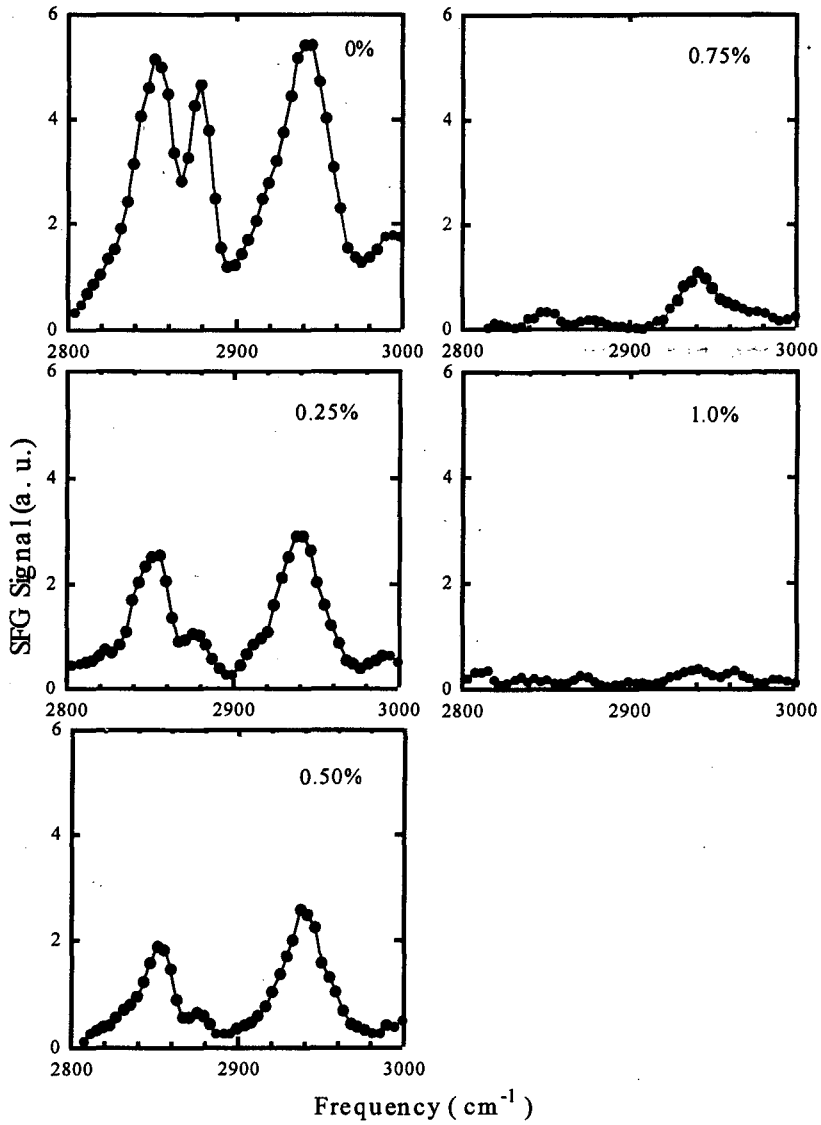
0%
0.75%
0.25%
1.0%
0.50%
SFG Signal (a. u.)
Frequency (cm^{-1})
2800
2900
3000
0
2
4
6

Figure 12

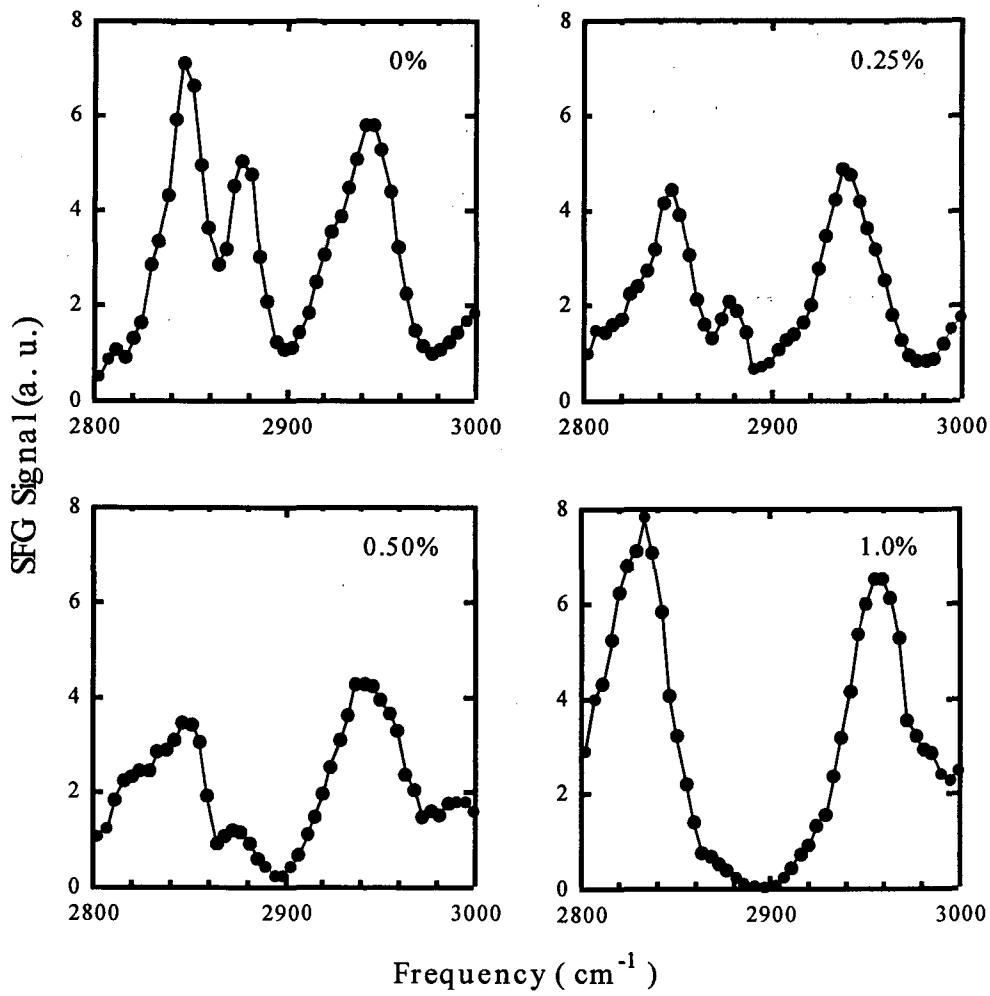

Figure 13

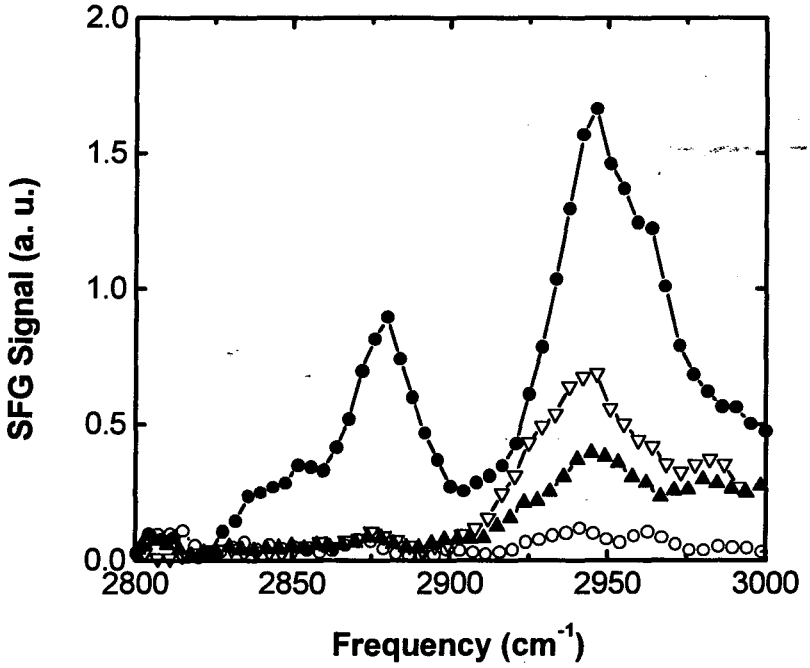
2.0
1.5
1.0
0.5
0.0
SFG Signal (a. u.)
2800
2850
2900
2950
3000
Frequency (cm-1)

Figure 14

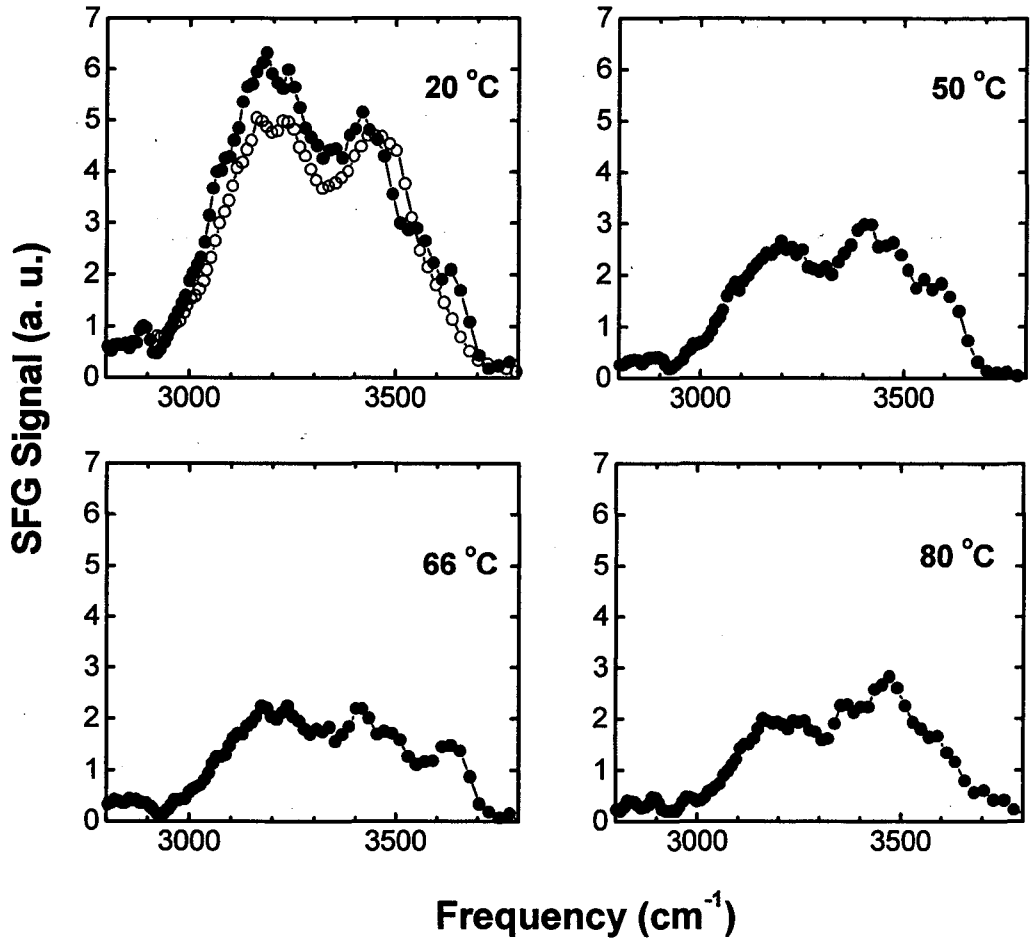

Figure 15

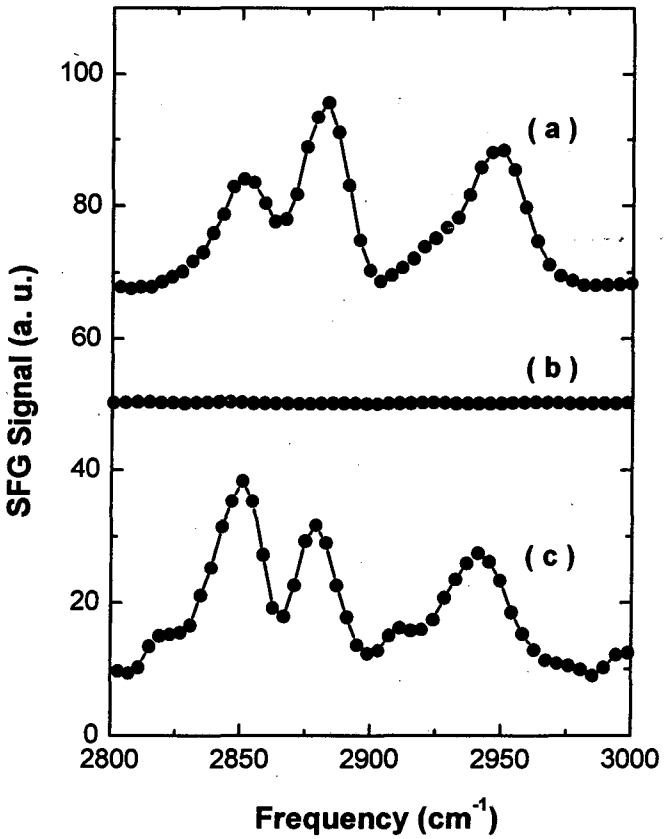
100
80
60
40
20
0
2800
2850
2900
2950
3000
SFG Signal (a. u.)
Frequency (cm-1)
(a)
(b)
(c)

Figure 16

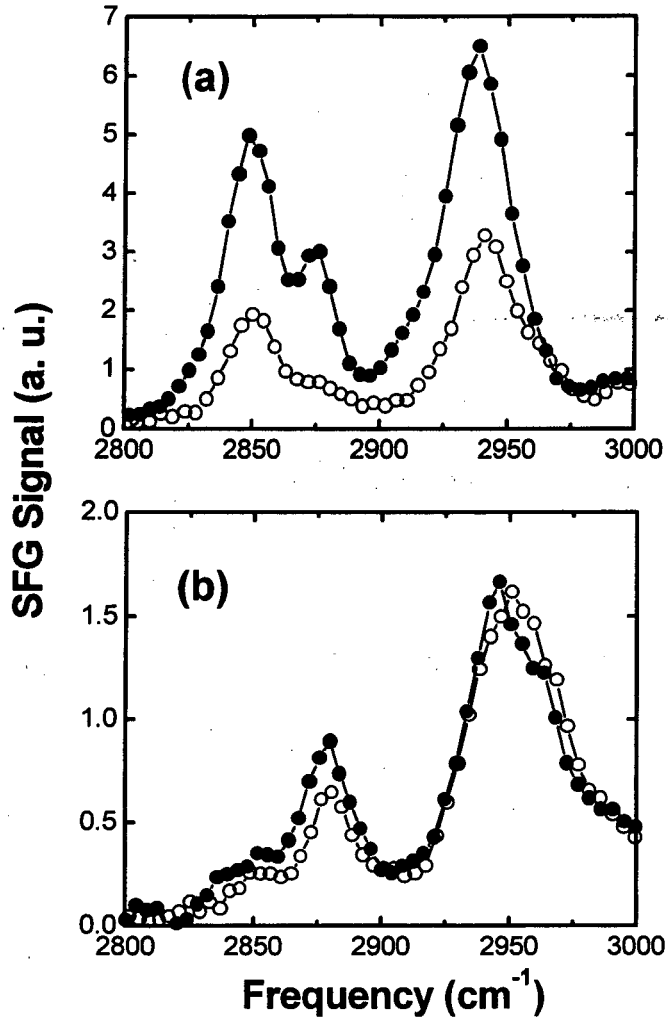
(a)
(b)
SFG Signal (a. u.)
Frequency (cm^{-1})
0
1
2
3
4
5
6
7
0.0
0.5
1.0
1.5
2.0
2800
2850
2900
2950
3000

Figure 17

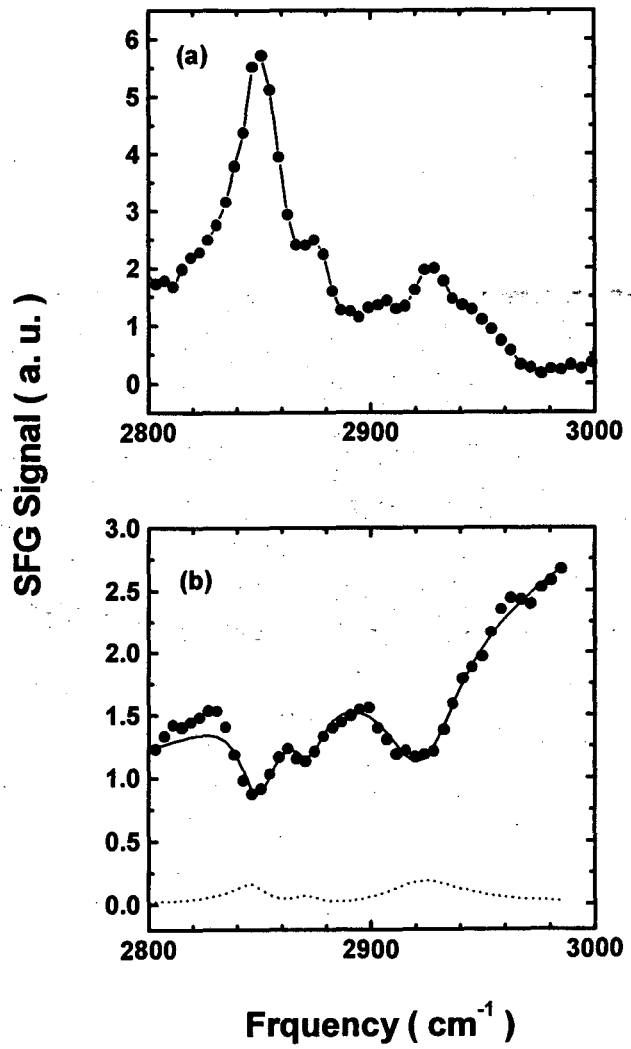

Figure 18

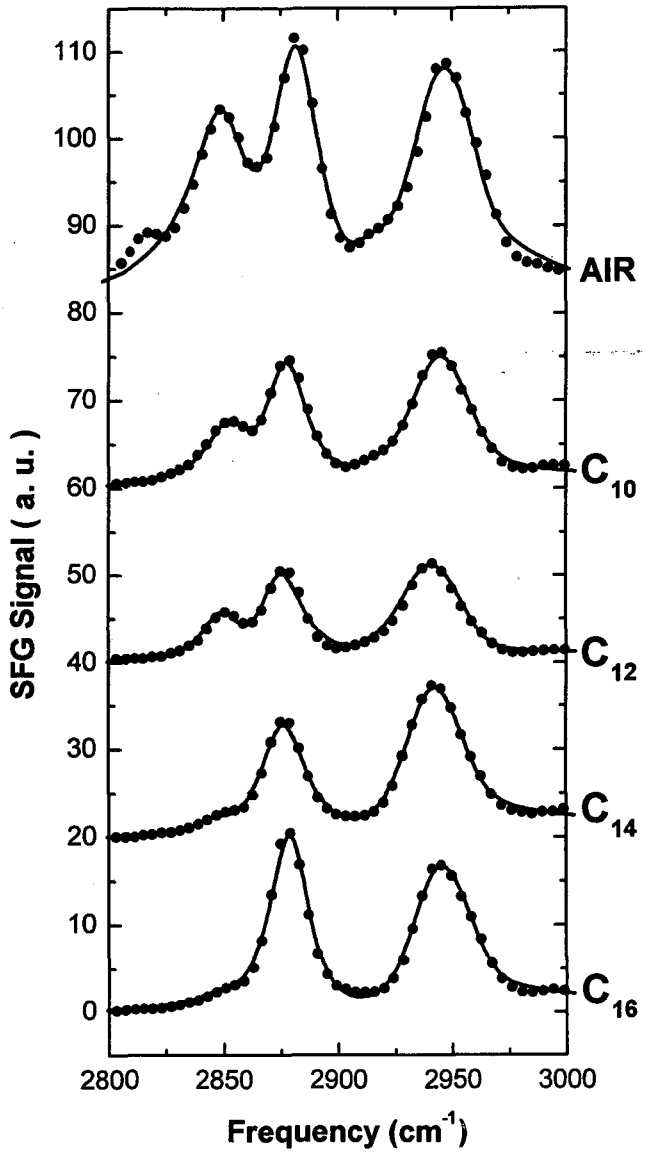
SFG Signal (a. u.)
Frequency (cm-1)
AIR
C10
C12
C14
C16
110
100
90
80
70
60
50
40
30
20
10
0
2800
2850
2900
2950
3000

Figure 19

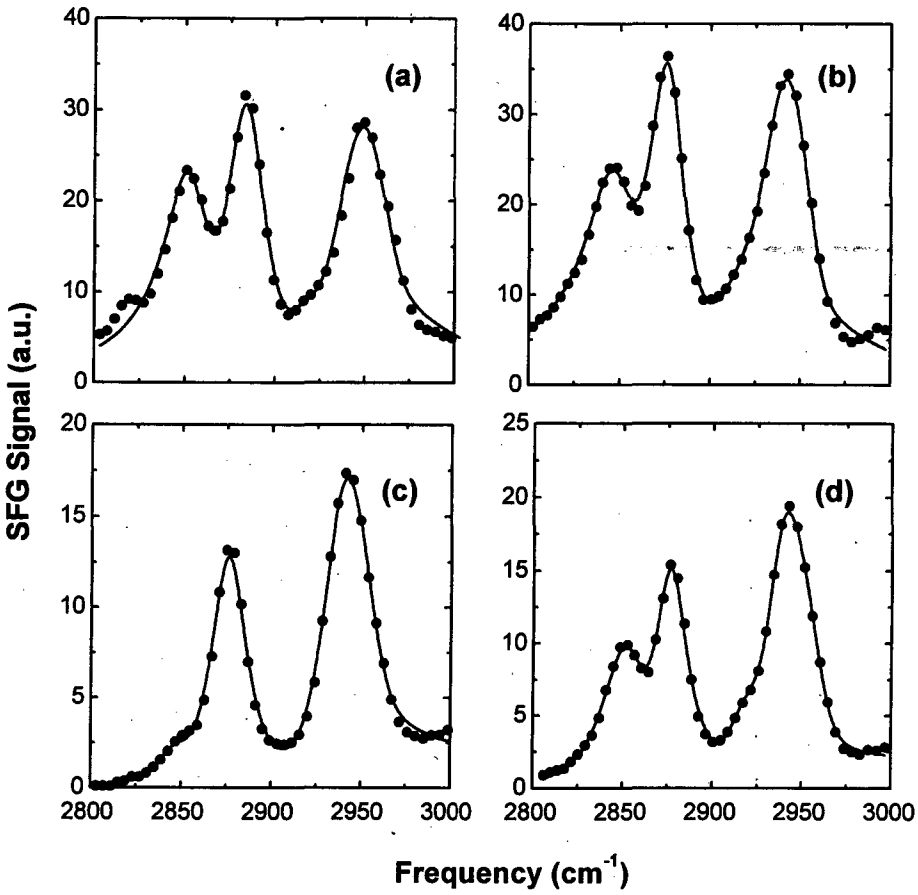
(a)
(b)
(c)
(d)
SFG Signal (a.u.)
Frequency (cm-1)
0
10
20
30
40
5
15
25
2800
2850
2900
2950
3000

Figure 20

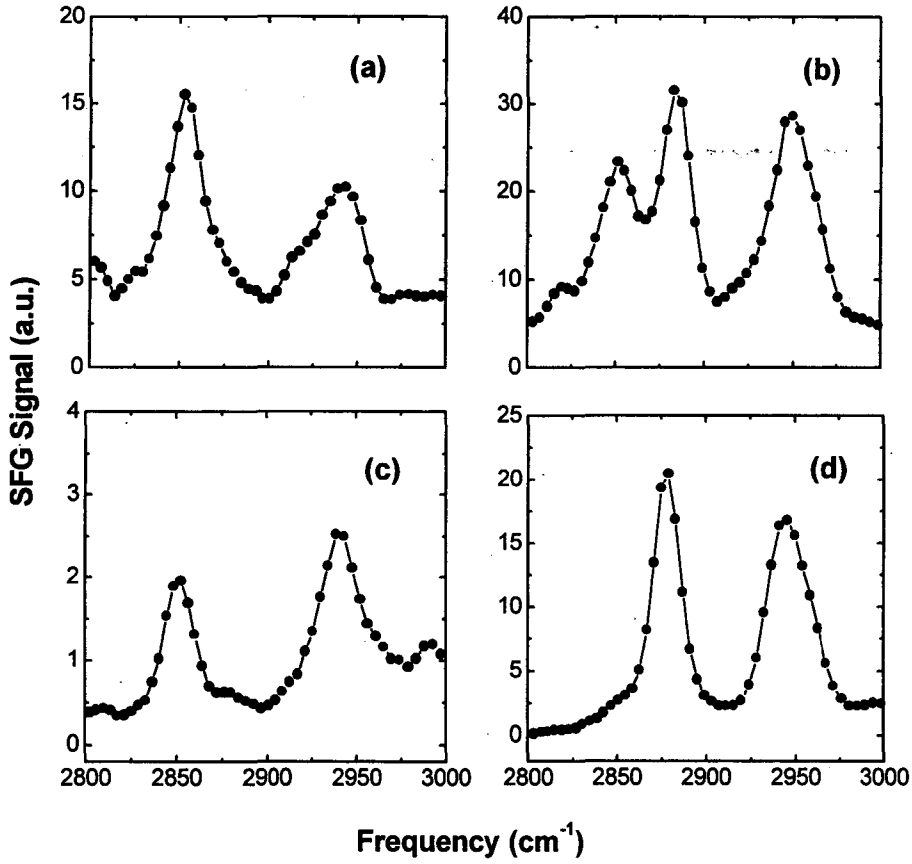

Figure 21

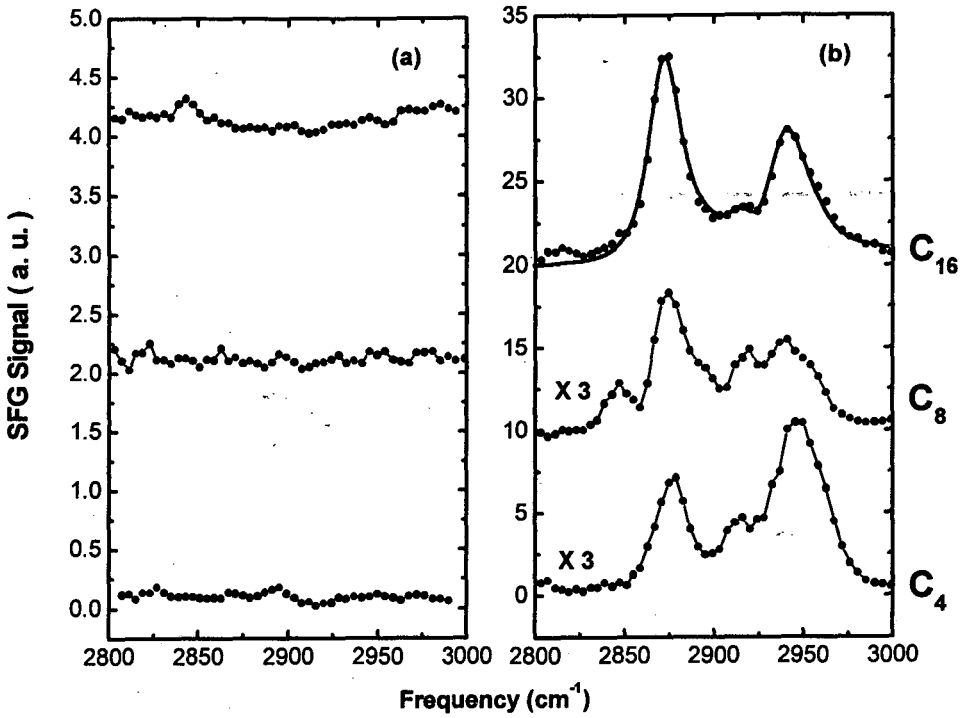

Figure 22

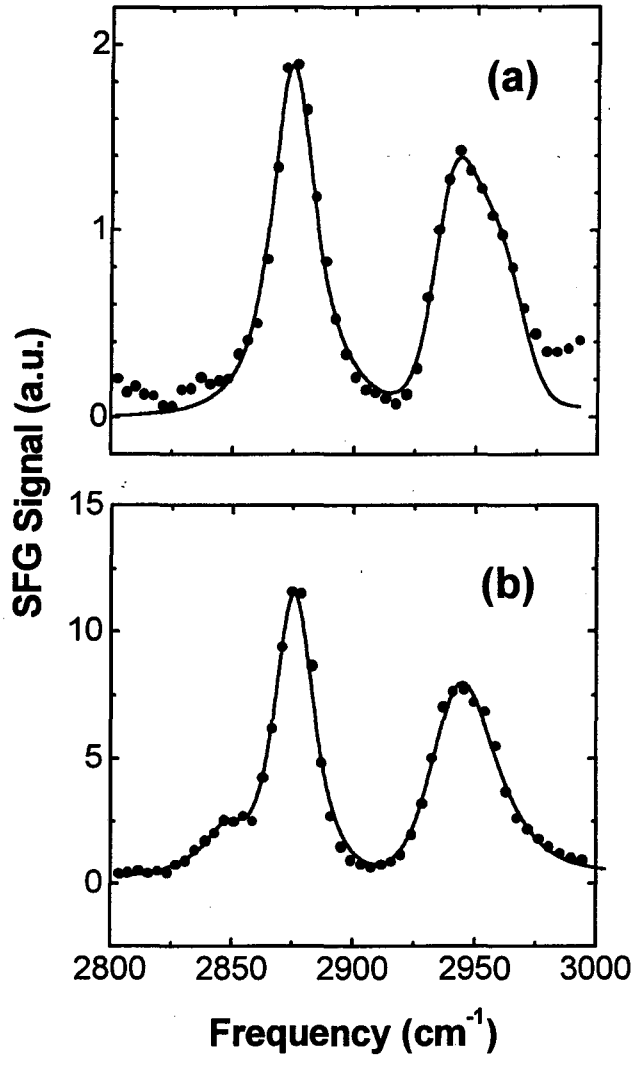
(a)
(b)
SFG Signal (a.u.)
Frequency (cm-1)
2
1
0
15
10
5
0
2800
2850
2900
2950
3000

Figure 23

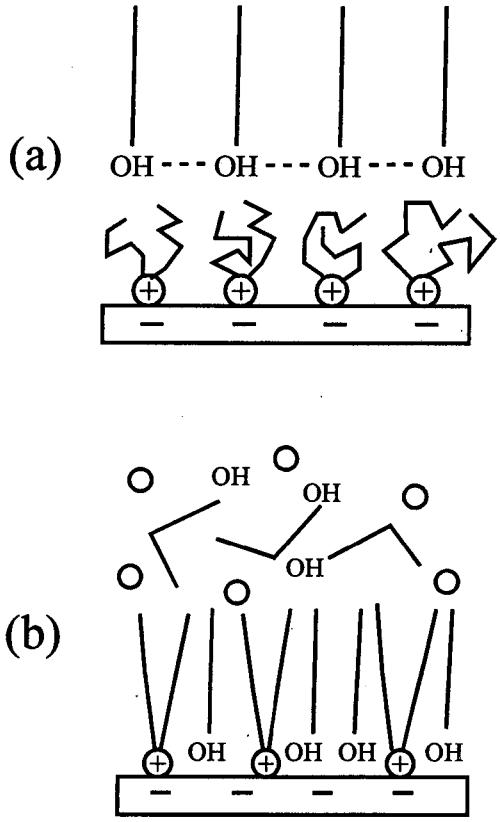

Figure 24

Chapter 7. Conclusion

In this Thesis, we have used sum-frequency vibrational spectroscopy (SFG) to study a variety of surfactant monolayers at both liquid/vapor and solid/liquid interfaces. Among the unique features of SFG spectroscopy, surface specificity and sensitivity to chain conformation were extensively utilized throughout this work. Surface crystallization of liquid alkanes and of alcohol monolayers at the air/water interface were studied in Chapter 3. In both cases the phase transition is driven by the strong chain-chain interaction and the crystalline monolayers have similar structures, with the chains in all-trans conformation and oriented nearly normal to the surface. We found, however, that above the transition temperature the monolayers have remarkably different structures: the alkane molecules have a considerable amount of gauche defects in their chains, while the alcohol monolayer is nearly all-trans even in the liquid phase. This contrast is due to hydrogen-bonding interaction of the alcohol Langmuir film with the water subphase that leads to increased surface ordering with respect to liquid alkanes.

The surfactant-water interaction is probed in more detail in Chapter 4 by studying the water surface structure underneath a Langmuir film. In the case of alcohol monolayers, the monolayer crystalline structure is nearly matched to the ice structure, leading to an epitaxial interaction that induces an ice-like ordering in the surface water layer. In contrast, fatty acid Langmuir films were found to induce considerable disorder in the water surface structure. However, the fatty acid monolayers can become ionized at high pH values of water. The resulting surface field can induce an ordered hydrogen-bonding network of water molecules at the interface as well as some structural changes in

the fatty acid head-group. We can anticipate extension of this investigation to other more complicated systems, such as biologically relevant lipid monolayers.

In Chapter 5, we showed that a combination of the second-order nonlinear optical processes of SFG and SHG can be used to map out completely the orientations of different parts of a molecule at an interface. We used a 5CT Langmuir film as an example. Complications due to the local-field correction at the interface and the related effective refractive index for the interfacial layer have been addressed.

Chapter 6 described our studies of self-assembled surfactant monolayers at solid/liquid interfaces. It was shown that the chain conformation of monolayers adsorbed at the solid/liquid interface is highly dependent on the monolayer surface density and on the nature of liquid-liquid and liquid-surfactant intermolecular interactions. Fully packed monolayers are well ordered in any environment due to strong surfactant-surfactant interactions and limited liquid penetration into the monolayer. In contrast, loosely packed monolayers were found to be very sensitive to the liquid environment. Non-polar liquids cause a mild increase in the surfactant conformational disorder, while polar liquids induce significant disordering. Hydrogen-bonding liquids are most effective in creating highly disordered chain conformations because of the hydrophobic effect. These results were qualitatively interpreted in terms of the interfacial free energy. The case of liquids composed of long-chain molecules is particularly interesting, since the chain-chain interaction between liquid and surfactant molecules becomes as important as the interaction among liquid molecules. When immersed in long-chain alkanes, the chain-chain interaction was found to be sufficiently strong to make the surfactant chains nearly all-trans (highly ordered chain conformation). In the case of long-chain alcohols,

competition between the hydrophobic effect and the chain-chain interaction was observed. These studies could be extended to surfactant monolayers at other interfaces, such as liquid/liquid and liquid/vapor interface. Extension to study the conformation of surfactants adsorbed on the surface of colloidal particles is also possible. This would permit a direct comparison of the structures of surfactant monolayers adsorbed on a flat, optically smooth surface, and on a highly curved surface of colloidal particles or nanocrystals.

As a general concluding remark, we note that there are many other research areas SFG vibrational spectroscopy has hardly explored. For example, SFG microscopy is yet to be developed. Both far-field[1-4] and near-field[5,6] imaging of interfaces by SHG have been demonstrated. With SFG, microscopic imaging of selective molecular species at an interface would become possible. Also, as can be noticed from our discussion in Chapter 2, the relation between alkyl chain conformation and features in the SFG spectra of CH stretch modes is rather qualitative. The lack of quantitative understanding of the observed spectra is a serious drawback. The knowledge about surfactant orientation and chain conformation at various interfaces would be greatly improved if how the CH_2 and CH_3 peaks in the spectrum vary with chain conformation can be quantitatively understood. Finally, recent developments in the generation of high power infrared pulses at longer wavelengths[7] allow the extension of SFG vibrational spectroscopy to lower frequency vibrations, and therefore, a more complete study of an interfacial structure would become feasible. For example, in the case of alkyl chains, C-C stretches and CH_2 waging modes are known to be very sensitive to chain conformation in infrared and Raman spectra[8,9]

and the same should be also true in SFG spectra. Also, unsaturated chains with C=C bonds have hardly been studied by SFG.

References

(1) I. I. Suni and E. G. Seebauer, *J. Chem. Phys.* **100**, 6772 (1994).

(2) M. Flörsheimer, C. Radüge, H. Salmen, M. Bösch, R. Terbrack and H. Fuchs, *Thin Solid Films* **285**, 659 (1996).

(3) L. Smilowitz, Q. X. Jia, X. Yang, D. Q. Li, D. McBranch and S. J. Buelow, *J. Appl. Phys.* **81**, 2051 (1997).

(4) J. Vydra and M. Eich, *Appl. Phys. Lett.* **72**, 275 (1998).

(5) I. I. Smolyaninov, A. V. Zayats and C. C. Davis, *Phys. Rev. B* **56**, 9290 (1997).

(6) I. I. Smolyaninov, A. V. Zayats and C. C. Davis, *Opt. Lett.* **22**, 1592 (1997).

(7) A. Dhirani and P. Guyot-Sionnest, *Opt. Lett.* **20**, 1104 (1995).

(8) G. Zerbi and M. Del Zoppo, *J. Chem. Soc. Faraday Trans.* **88**, 1835 (1992).

(9) D. A. Cates, H. L. Strauss and R. G. Snyder, *J. Phys. Chem.* **98**, 4482 (1994).

Appendix: Divergence of the SFG output beam

In designing an SFG detection system, it is often desirable to have the output beam lightly convergent, so that spatial filtering of the beam with pinholes is facilitated. To accomplish this, it is necessary to understand what governs the output beam divergence. We can gain some intuition by considering the case of SHG, where the reflected input and output beams are collinear. In such case, we expect that if the input beam is converging towards the sample with the waist beyond the sample, both the reflected input and output beams should focus at some point above the sample after reflection. Conversely, if the input beam is focussed before the sample, then both reflected input and output beams should be diverging from the sample. In the case of SFG the situation is similar, except that the divergence should depend more strongly on the visible input (ω_1) and weakly on the infrared input (ω_2), since the wavevector of the IR beam is much smaller than the visible (see Eq. (2.4)). However, if the convergence of the IR input is much stronger than the visible (e.g., the visible is a collimated beam while the IR is tightly focussed), then the IR beam will dictate the divergence of the output beam.

To make this more quantitative, we have calculated the divergence of the reflected SFG output for a given input geometry. Described here are only the essential steps of the calculation. We begin by assuming that both inputs are gaussian beams, given by[1]

$$\vec{E}(\vec{r},t) \propto u(\vec{r},t)\,\hat{e}\,e^{i(\vec{k}\cdot\vec{r}-\omega t)} \tag{8.1}$$

with

$$u(\vec{r},t) = \frac{e^{ikz}}{q(z)}\, e^{\,ik\frac{\left(x^2+y^2\right)}{2q(z)}} \quad , \qquad q(z) = \frac{\pi w^2}{i\lambda} + z \tag{8.2}$$

where ω, k and w are the frequency, wavevector ($k = 2\pi/\lambda$) and waist of the gaussian beam. The z-direction is the propagation direction and the beam waist is at z = 0. Following Ref. 1, we expand the input gaussian beams in terms of plane waves

$$u(\vec{r},t) = \frac{1}{(2\pi)^2}\iint U(k_x,k_y)\, e^{ik_z z}\, e^{i(k_x x + k_y y)} dk_x dk_y \tag{8.3}$$

where

$$k_z = \sqrt{k^2 - k_x^2 - k_y^2} \cong k - \frac{k_x^2 + k_y^2}{2k} \tag{8.4}$$

and

$$U(k_x,k_y) = i\,\lambda\, e^{-\frac{w^2}{4}\left(k_x^2+k_y^2\right)} \tag{8.5}$$

In Eq. (8.4) the paraxial approximation was used ($|k_x|$, $|k_y| << |k_z|$). The input geometry for the i^{th} beam is defined by the input angle β_i, the location (l_i) and size (w_i) of the beam waist (see Figure 1). Note that l_i is positive (negative) if the input beam is focussed beyond (before) the sample. The output beam will then consist of a superposition of plane waves. Each of these plane waves will have an amplitude A_3 determined by

$$A_3(k_{x1},\, k_{y1}, k_{x2},\, k_{y2}) = const \cdot A_1(k_{x1},\, k_{y1})\, A_2(k_{x2},\, k_{y2}) \tag{8.6}$$

where A_1 and A_2 are the amplitudes for the input components. We have assumed that the coefficient coupling the three waves with amplitudes A_1, A_2 and A_3 is independent of the k vectors. The direction of each output component is determined by matching of the input and output wavevector components in the surface plane. The output beam is then

obtained by integration of $A_3(k_{x1}, k_{y1}, k_{x2}, k_{y2})$ over $\vec{k}_1$ and $\vec{k}_2$. The calculation is straightforward but tedious and the result is (apart from a phase factor)

$$u_3(\vec{r},t) \propto \left[B_8 B_6 \left(B_1 - \frac{B_2^2}{B_6} \right) \left(B_4 - \frac{B_5^2}{B_8} \right) \right]^{-1/2} \exp\left\{ -\frac{1}{4} \left[\frac{y^2}{B_8} + \frac{B_7^2}{B_6} + \frac{\left(B_3 - \frac{B_2 B_7}{B_6} \right)^2}{\left(B_1 - \frac{B_2^2}{B_6} \right)} + \frac{y^2 \left(1 - \frac{B_5}{B_8} \right)^2}{\left(B_4 - \frac{B_5^2}{B_8} \right)} \right] \right\}$$

where (8.7)

$$B_1 = \alpha_1 + i \left(-\frac{x \sin\beta_1}{2k_1 \cos\beta_3} + \frac{(z\cos\beta_3 + x\sin\beta_3)\cos^2\beta_1}{2k_3 \cos^3\beta_3} \right)$$

$$B_2 = i (z\cos\beta_3 + x\sin\beta_3) \frac{\cos\beta_1 \cos\beta_2}{2k_3 \cos^3\beta_3}$$

$$B_3 = -x \frac{\cos\beta_1}{\cos\beta_3}$$

$$B_4 = \alpha_1 + i \left(-\frac{x \sin\beta_1}{2k_1 \cos\beta_3} + \frac{z\cos\beta_3 + x\sin\beta_3}{2k_3 \cos\beta_3} \right)$$

$$B_5 = i \frac{z\cos\beta_3 + x\sin\beta_3}{2k_3 \cos\beta_3}$$

$$B_6 = \alpha_2 + i \left(-\frac{x \sin\beta_2}{2k_2 \cos\beta_3} + \frac{(z\cos\beta_3 + x\sin\beta_3)\cos^2\beta_2}{2k_3 \cos^3\beta_3} \right)$$

$$B_7 = -x \frac{\cos\beta_2}{\cos\beta_3}$$

$$B_8 = \alpha_2 + i \left(-\frac{x \sin\beta_2}{2k_2 \cos\beta_3} + \frac{z\cos\beta_3 + x\sin\beta_3}{2k_3 \cos\beta_3} \right) \quad (8.8)$$

and

$$\alpha_1 \equiv \frac{w_1^2}{4} - i\frac{l_1}{2k_1} \quad , \quad \alpha_2 \equiv \frac{w_2^2}{4} - i\frac{l_2}{2k_2} \quad (8.9).$$

In Eqs. (8.7) to (8.9), the coordinate system is such that z is along the direction of the output beam in the reflected direction and the origin is at the sample position (see Figure 2). It is interesting to note that while the two inputs are gaussian beams, the output

described by Eqs. (8.7) to (8.9) is generally *not* a gaussian beam. It can be shown, however, that for *normal incidence* ($\beta_1 = \beta_2 = 0$) Eqs. (8.7) to (8.9) reduce to a gaussian beam of waist size (w_3) and position (l_3) given by

$$w_3^2 = w_1^2 w_2^2 \frac{w_1^2 + w_2^2 + 4\left[\left(\frac{l_1}{k_1 w_1}\right)^2 + \left(\frac{l_2}{k_2 w_2}\right)^2\right]}{\left(w_1^2 + w_2^2\right)^2 + 4\left(\frac{l_1}{k_1} + \frac{l_2}{k_2}\right)^2} \tag{8.10}$$

$$l_3 = l_1 l_2 \frac{k_3}{k_1 k_2} \frac{\frac{k_2 w_2^4}{l_2} + \frac{k_1 w_1^4}{l_1} + 4\left(\frac{l_1}{k_1} + \frac{l_2}{k_2}\right)}{\left(w_1^2 + w_2^2\right)^2 + 4\left(\frac{l_1}{k_1} + \frac{l_2}{k_2}\right)^2} \tag{8.11}$$

To illustrate this calculation, two representative examples are shown in Figures 3 and 4. The surfaces plotted are the beam cross section (defined as the contour line were the intensity drops by $1/e^2$ from the value on the z-axis) as the beam propagates away from the sample. In the numerical example shown in Figures 3 and 4, both input beams overlap at the surface with diameters of ~ 1 mm with incidence angles $\beta_1 = 45°$ and $\beta_2 = 57°$. The visible beam (ω_1) is at 532 nm and is lightly focussed by a lens (f = 100 cm) with the waist 25 cm beyond the sample. In Figure 3, the IR beam at wavelength of 3 μm is focussed (f = 10 cm) with the waist located 2 cm (a) beyond and (b) before the sample. In Figure 4, the IR beam at wavelength of 6 μm is focussed (f = 20 cm) with the waist located 4 cm (a) beyond and (b) before the sample. From these examples we see that if both input beams have their waist beyond the sample (Figures 3(a) and 4(a)), the SFG output is also convergent (and more so than the visible input). However, if the visible is converging (waist beyond the sample) and the IR is diverging (waist before the sample),

the output may be converging as in Figure 4(b) if the IR beam has a long wavelength (small wavevector) and is lightly focussed. On the other hand, if the IR input wavevector is large and the beam is tightly focussed (waist before the sample), the SFG output may become divergent despite the visible input being convergent, as in Figure 3(b). It may also be noticeable in Figures 3 and 4 that, in general, the SFG output is astigmatic, with different divergences in the x and y directions.

References

(1) A. E. Siegman, *Lasers*, chap. 16, University Science Books, Mill Valley, CA (1986).

Figure Captions

Figure 1. Parameters defining the input geometry for a gaussian beam. (X, Y, Z) is the lab frame, with Z along the surface normal and X in the incidence plane. The input beams have incidence angles β_i and overlap at the origin of (X, Y, Z). The gaussian beam waist of size w_i is located at the origin of (x, y, z), at a distance l_i from the sample position.

Figure 2. Geometry defining the output beam. (x, y, z) is the reference frame for the SFG output beam, which is reflected at an angle β_3 and has a waist of size w_3 located a distance l_3 from the sample position.

Figure 3. Calculated SFG beam profile for an input geometry with the visible focussed 25 cm beyond the sample with waist size 63 μm (w_1) and the IR beam ($\lambda = 3$ μm) focussed 2 cm (a) beyond and (b) before the sample, with waist size 17 μm. All units in the graph are in mm.

Figure 4. Calculated SFG beam profile for an input geometry with the visible focussed 25 cm beyond the sample with waist size 63 μm and the IR beam ($\lambda = 6$ μm) focussed 4 cm (a) beyond and (b) before the sample, with waist size 76 μm. All units in the graph are in mm.

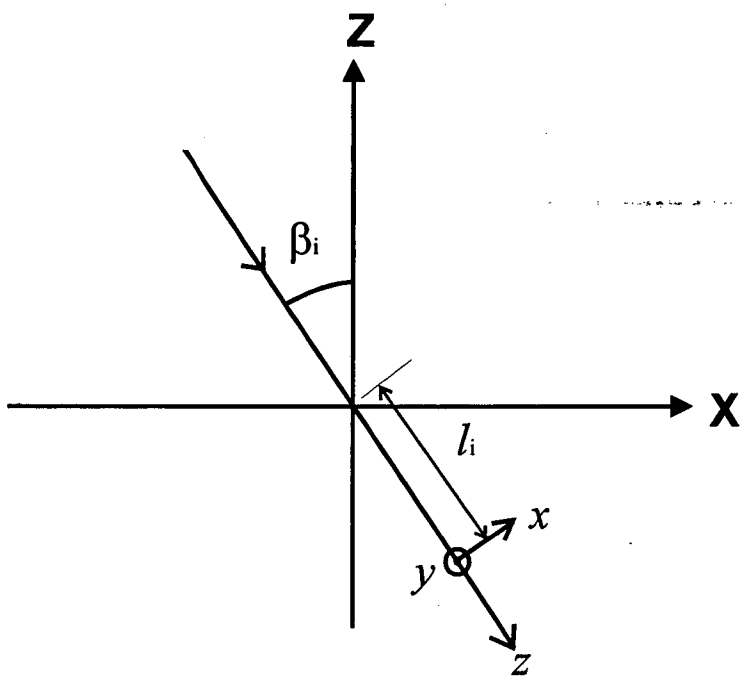

Figure 1

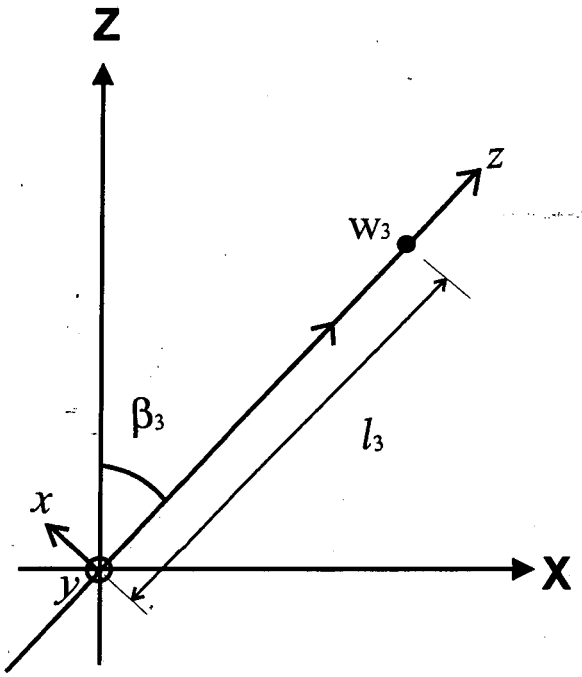

Figure 2

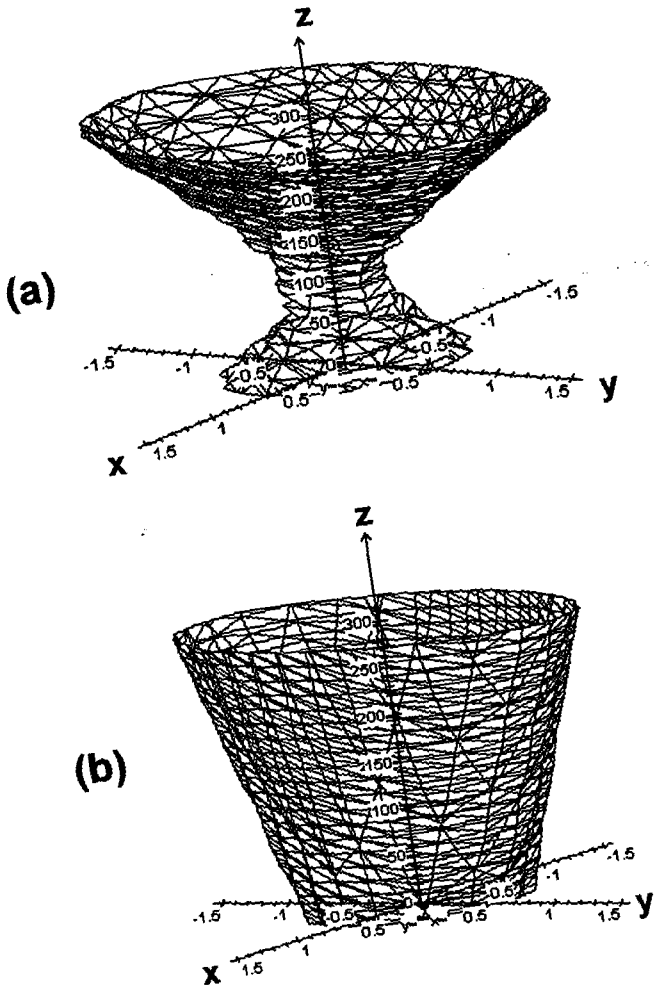
(a)
z
300
250
200
150
100
50
0
-1.5
-1
-0.5
0.5
1
1.5
x
y
(b)
z
300
250
200
150
100
50
0
-1.5
-1
-0.5
0.5
1
1.5
x
y

Figure 3

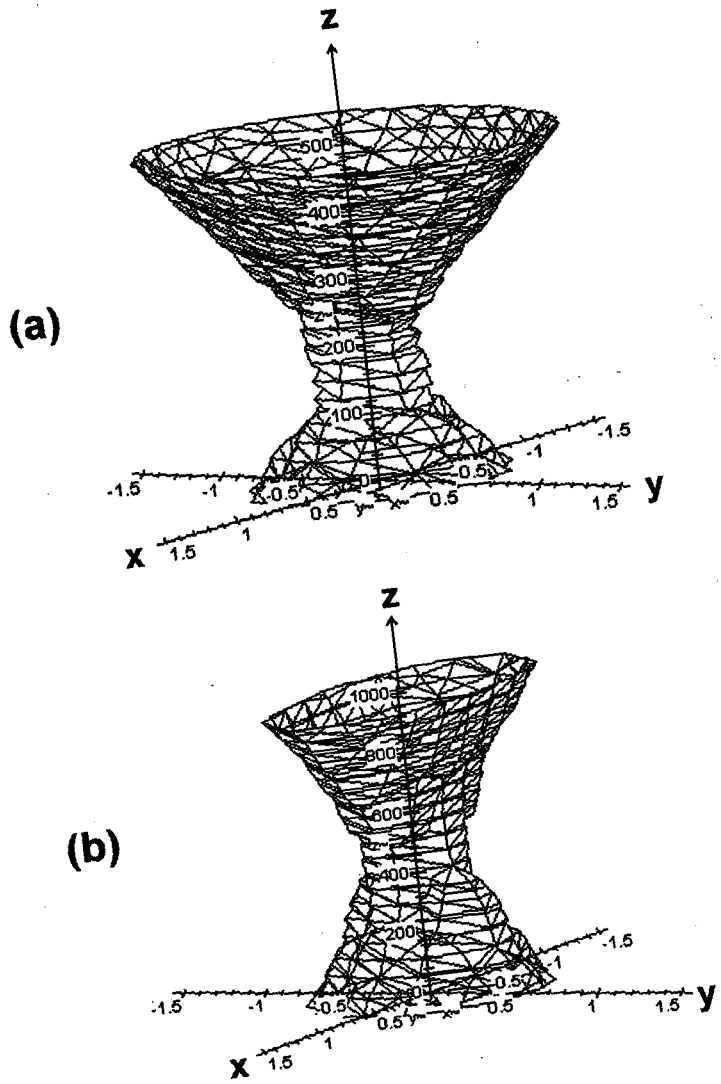
(a)
z
500
400
300
200
100
-1.5
-1
-0.5
0
0.5
1
1.5
y
x
(b)
z
1000
800
600
400
200
-1.5
-1
-0.5
0
0.5
1
1.5
y
x

Figure 4

ERNEST ORLANDO LAWRENCE BERKELEY NATIONAL LABORATORY
ONE CYCLOTRON ROAD | BERKELEY, CALIFORNIA 94720

Prepared for the U.S. Department of Energy under Contract No. DE-AC03-76SF00098